





This is to certify that the  
dissertation entitled

Z-SOURCE INVERTER BASED POWER CONDITIONING  
SYSTEMS FOR PV POWER GENERATION

presented by

Yi Huang

has been accepted towards fulfillment  
of the requirements for the

Doctoral degree in Electrical Engineering

  
Major Professor's Signature

Dec. 4, 2009  
Date

**PLACE IN RETURN BOX** to remove this checkout from your record.  
**TO AVOID FINES** return on or before date due.  
**MAY BE RECALLED** with earlier due date if requested.

DATE DUE	DATE DUE	DATE DUE
FEB 12 2011		

**Z-SOURCE INVERTER BASED POWERCONDITIONING  
SYSTEMS FOR PV POWER GENERATION**

**By**

**Yi Huang**

**A DISSERTATION**

**Submitted to  
Michigan State University  
in partial fulfillment of the requirements  
for the degree of**

**DOCTOR OF PHILOSOPHY**

**Electrical Engineering**

**2009**

# **ABSTRACT**

## **Z-SOURCE INVERTER BASED POWER CONDITIONING SYSTEMS FOR PV POWER GENERATION**

By

Yi Huang

The world's energy demand is increasing quickly. As photovoltaic system is one of the most promising alternative energy sources in DG. The power electronics converters based PCS in the PV system now becomes the key point in cost reduction.

The main tasks for inverter are draw the power out and injected a sinusoidal current to the grid. To competitive with other power sources, the most effective way is to develop inexpensive and reliable inverters. The aim of this thesis is therefore to develop new topologies and control strategies for PV system.

This thesis presented a new power conditioning system based on Z-Source inverter for renewable energy sources. The PV system performance depends not only on temperatures and irradiations, but also on maximum power tracking function of PV inverter. So it is important to verify the inverter system too. To help verifying the inverter system, a dc-dc converter based PV simulator was proposed and implemented. Also, both the stand-alone split-phase PV system and grid-connected three-phase PV system were proposed and analyzed. The simulation and experiment results were shown to verify the proposed system.

With unique X shape network, the Z-Source inverter can realize buck and boost function without additional dc-dc converter. For grid-connect action, the proposed harmonic injected unity power factor current control which also employed modified P&O MPPT method are suitable for PV power applications. By utilizing the Z-Source inverter, the volume, the cost, and the switching device count are minimized. Because of the single stage operation, the efficiency of the system can be greatly improved. The reliability can be enhanced greatly due to the shoot through states. With all these advanced features, the Z-Source inverter based PCS is very promising for renewable energy applications.

To my mother, father, and husband.

## ACKNOWLEDGEMENTS

Foremost, I am heartily thankful to my advisor, Dr. Fang. Z. Peng, who has supported me throughout my thesis with his patience and knowledge. I attribute the level of my Ph.D degree to his encouragement and effort and without him this thesis would not have been completed. One simply could not wish for a better advisor. This dissertation comes from numerous discussions with him, under his keen insight and guidance. I would also like to thank all my committee members, Dr. Strangas, Dr. Schlueter, and Dr. Promislow. Their insightful comments and suggestions have enhanced the technical soundness of this dissertation. I am grateful to my friends and colleagues from the Power Electronics and Motor Drive Laboratory. I would like to express my appreciation to Yuan, Dr. Lee, Miaosen, Richard, Lihua, Wei, Joe, Dong, Honnyong, Dr. Yoo, and all the lab mates in the Power Electronics Lab.

My thanks go to my family, especially my husband and my parents. Without their years of encouragement and continuous support, I would not have reached this point.

# TABLE OF CONTENTS

<b>LIST OF TABLES.....</b>	<b>ix</b>
<b>LIST OF FIGURES.....</b>	<b>x</b>
<b>CHAPTER 1. INTRODUCTION.....</b>	<b>1</b>
1. 1. BACKGROUND .....	1
1. 2. DISTRIBUTED GENERATION AND PHOTOVOLTAIC GENERATIONS.....	2
1. 3. POWER CONDITIONING SYSTEM.....	3
1. 4. OUTLINE OF THE THESIS .....	4
<b>CHAPTER 2. PHOTOVOLTAIC SYSTEMS.....</b>	<b>6</b>
2. 1. INTRODUCTION .....	6
2.1.1 History of Photovoltaics and new trends.....	6
2.1.2 Basics of Photovoltaics.....	8
2. 2. TYPES OF PHOTOVOLTAIC SYSTEMS [15-18].....	11
2. 3. INVERTERS IN PHOTOVOLTAIC SYSTEM .....	14
2. 3. 1 Introduction .....	14
2. 3. 2 Types of Inverters.....	16
<b>CHAPTER 3. SUMMARY OF PREVIOUS TOPOLOGIES .....</b>	<b>18</b>
3. 1. INTRODUCTION .....	18
3. 2. PV INVERTER STATUS [15-19] .....	19
3. 3. PV INVERTER BY POWER STAGE [20-38].....	20
3. 3 .1 Introduction .....	20
3. 3 .2 Single-stage Inverters .....	22
3.3.2.1. Four switch topologies.....	22
3.3.2.2. Six switch topologies.....	25
3. 3 .3 Multi-stage Inverters.....	26
3. 4. INDUSTRIAL PV INVERTER [37-53] .....	33
3. 4. 1 Introduction .....	33
3. 4. 2 Manufacture PV Inverter .....	33
<b>CHAPTER 4. Z-SOURCE INVERTER BASED POWER CONDITIONING SYSTEM FOR STAND-ALONE SYSTEM.....</b>	<b>47</b>
4. 1. INTRODUCTION.....	47
4. 2. THE BASICS OF PCS FOR RESIDENTIAL USE.....	48
4. 3. THE PROPOSED Z-SOURCE INVERTER SYSTEM.....	52

4. 4. CONTROL AND OPERATION PRINCIPLE.....	54
4. 5. DESIGN GUIDELINE.....	57
4. 6. SIMULATION AND EXPERIMENT RESULTS.....	59
4.7. SUMMARY.....	78
<b>CHAPTER 5. PV SIMULATOR SYSTEM .....</b>	<b>79</b>
5.1. INTRODUCTION.....	79
5.2. PREVIOUS PV SIMULATOR.....	80
5.3. PROPOSED PV SIMULATOR.....	84
5. 3 .1 Mathematical modeling of PV cell.....	84
5. 3 .2 Control strategies.....	87
5. 3 .3 Hardware designs.....	93
5. 3 .4 Experiment results.....	94
5.4. SUMMARY.....	99
<b>CHAPTER 6. GRID-CONNECTED Z-SOURCE INVERTER WITH PV SIMULATOR SYSTEM .....</b>	<b>101</b>
6.1. INTRODUCTION.....	101
6. 1 .1 Background.....	101
6.2. PROPOSED GRID-CONNECTED Z-SOURCE INVERTER SYSTEM.....	102
6.3. CONTROL ISSUES.....	105
6. 3 .1 General issues.....	105
6. 3 .2 Voltage control and current control.....	106
6. 3 .3 Modulation methods.....	106
6. 3 .4 MPPT methods.....	109
6. 3 .5 Synchronization in grid-connected applications.....	112
6.3.5.1. Synchronization methods.....	112
6.4. PROPOSED PLL SYNCHRONIZATION.....	114
6. 4 .1 Proposed PLL synchronization.....	114
6. 4 .2 Proposed harmonic injected feed-forward control.....	115
6.4.2.1. Third harmonic injection.....	116
6.4.2.2. Current control loop.....	126
6. 4 .3 Modified P&O MPPT control.....	132
6.5. HARDWARE AND SOFTWARE.....	136
6. 5 .1 Hardware of system setup.....	136
6. 5 .2 Hardware of control unit.....	138
6. 5 .3 Software implementation.....	140
6.6. SIMULATION AND EXPERIMENT RESULTS.....	146
6.7. PCS REQUIREMENTS AND STANDARDS.....	156
6.8. CONCLUSIONS.....	158
<b>CHAPTER 7. CONCLUSIONS .....</b>	<b>159</b>

7.1. SUMMARY OF CIRCUIT TOPOLOGIES AND THEIR SUITED APPLICATIONS ..... 159

7.2. CONCLUSIONS ..... 162

7.3. CONTRIBUTIONS ..... 163

7.4. RECOMMENDED FUTURE WORKS ..... 164

**APPENDICES.....165**

A.1. HARMONIC DISTORTION FACTOR OF THE CURRENT RIPPLE..... 165

A.2. SOME EXPERIMENT HARDWARES..... 168

A.3. FUNCTIONAL BLOCK DIAGRAM OF 2407A DSP CONTROLLER ..... 170

**REFERENCES .....172**

## **LIST OF TABLES**

Table 3.1: Manufacture PV inverters (Xantrex, Ballard, Beacon,Phoenixtex power.....	44
Table 3.2: Manufacture PV inverters (Fronius, studer, sma).....	45
Table 3.3: Manufacture PV inverters (Magnetek, PV Powered, Solectria, Xantrex).....	46
Table 5.1: The PV array parameters (SM-60 Module).....	86
Table 6.1: shoot-through interval, boost factor and voltage gain of three boost control methods.....	117
Table 7.1: Summary of central, string, and module integrated inverter.....	160
Table 7.2: Summary of the inverter topologies.....	161

## LIST OF FIGURES

Figure 1.1: Major types of power electronics devices.....	2
Figure 2.1: Evolution of the solar electrical capacities till 2030 [14].....	7
Figure 2.2: I-V characteristics with constant temperature.....	9
Figure 2.3: P-V characteristics with constant temperatur.....	9
Figure 2.4: I-V characteristics with constant irradiation.....	10
Figure 2.5: P-V characteristics with constant irradiation.....	10
Figure 2.6: Maximum power point tracking.....	11
Figure 2.7: An Off-grid PV system.....	12
Figure 2.8: A grid-connected PV system.....	13
Figure 2.9: A hybrid PV system.....	14
Figure 3.1: Line-frequency transformer.....	20
Figure 3.2: High-frequency transformer 1.....	20
Figure 3.3: High-frequency transformer 2.....	21
Figure 3.4: Centralized and decentralized inverter topologies [21].....	21
Figure 3.5: A single stage inverter.....	22
Figure 3.6: Four-switch boost inverter by Cáceres and Barbi [22].....	23

Figure 3.7: Four switch buck boost inverter by Vazquez et al [23].....	24
Figure 3.8: Four switch buck boost inverter by Kasa et al [24].....	24
Figure 3.9: Four switch isolated bidirectional buck boost inverter by Kjær and Blaabjerg [25].....	24
Figure 3.10: Four switch resonant buck boost inverter by Wang [26].....	25
Figure 3.11: Six switch buck boost inverter by Kusakawa et al [28].....	25
Figure 3.12: Dual power processing inverter.....	26
Figure 3.13: Two stage boost inverter [29].....	27
Figure 3.14: Two stage nonisolated buck boost inverter by Saha and Sundarsingh [30].....	28
Figure 3.15: Two stage isolated buck boost inverter by Saha and Sundarsingh [30]...	28
Figure 3.16: Buck-boost inverter by Funabiki et al [31].....	28
Figure 3.17: A flyback inverter with enhanced power decoupling by Shimizu [32]...	29
Figure 3.18: Multi-stage boost inverter with pseudo-dc-link.....	30
Figure 3.19: Multi-stage boost inverter by GEC [33].....	30
Figure 3.20: Bidirectional dc-ac-ac converter by Beristáin et al [40].....	31
Figure 3.21: Cascaded inverter system [54].....	32
Figure 3.22: Xantrex PV series topology [42].....	34

Figure 3.23: Ecostar Power Converters [44].....	35
Figure 3.24: Smart power M5 power system [45].....	36
Figure 3.25: Sunville inverter topology [46].....	37
Figure 3.26: FRONIUS IG 2000-LV [47].....	38
Figure 3.27: AJ series inverter [48].....	39
Figure 3.28: Sunny Boy 1100U inverter [49].....	40
Figure 3.29: Sunny Central [49].....	40
Figure 3.30: AURORA isolated outdoor model : PVI 2000-I-OUTD-US [51].....	41
Figure 3.31: Starinverter PCS [52].....	42
Figure 3.32: PVI13KW inverter system [53].....	43
Figure 4.1: The traditional PV systems.....	49
Figure 4.2: Direct PV inverter systems for $\pm 120$ V split phase residential power.....	50
Figure 4.3: The six-switch inverter control scheme.....	51
Figure 4.4: The proposed PCS for stand-alone PV system.....	53
Figure 4.5: Sketch map of the simple boost control.....	55
Figure 4.6: Typical V-I and P-V characteristics.....	60
Figure 4.7: V-I characteristics under different conditions.....	61

Figure 4.8: A 10 kW Z-Source inverter prototype.....	62
Figure 4.9: Simulation results of case 1 under the conditions of $1000 \text{ W/m}^2$ , $60^\circ\text{C}$ , and $V_{pv}=230 \text{ V}$ .....	64
Figure 4.10: Experimental results of case 1 under the conditions of $1000 \text{ W/m}^2$ , $60^\circ\text{C}$ , and $V_{pv}=230 \text{ V}$ .....	67
Figure 4.11: Simulation results of case 2 under the conditions of $250 \text{ W/m}^2$ , $0^\circ\text{C}$ , and $V_{pv}=450 \text{ V}$ .....	71
Figure 4.12: Experimental results of case 2 under the conditions of $250 \text{ W/m}^2$ , $0^\circ\text{C}$ , and $V_{pv}=450 \text{ V}$ .....	74
Figure 5.1: Typical PV module curves.....	80
Figure 5.2: PV simulator concept [5].....	81
Figure 5.3: Block diagram of the PV generator simulator circuit [63].....	82
Figure 5.4: The circuit of the simulator with a light emission unit [65].....	83
Figure 5.5: An equivalent circuit of a PV cell.....	84
Figure 5.6: The output characteristic of the SM-60 module.....	86
Figure 5.7: The PV simulator output characteristics.....	87
Figure 5.8: Proposed PV simulator and its control strategy.....	89
Figure 5.9: Analysis of voltage control.....	91

Figure 5.10: Combined voltage and current control divisions.....	92
Figure 5.11: PV simulator for resistor load conditions.....	94
Figure 5.12: Load current change.....	95
Figure 5.13: Solar irradiation change around load $R= 18.5 \text{ ohm}$ .....	97
Figure 5.14: Solar irradiation change around load $R= 18.5 \text{ ohm}$ .....	98
Figure 6.1: Traditional medium power stage grid-connected PV inverter system....	103
Figure 6.2: Grid-connected Z-Source PV inverter system configuration.....	104
Figure 6.3: SPWM method.....	108
Figure 6.4: Hysteresis current control.....	109
Figure 6.5: P&O MPPT method.....	110
Figure 6.6: INC MPPT method.....	111
Figure 6.7: PLL control loop.....	113
Figure 6.8: Zero crossing PLL.....	114
Figure 6.9: Phase detection methods.....	115
Figure 6.10: One-sixth of the fundamental injected.....	116
Figure 6.11: Third harmonic injected maximum constant boost.....	118
Figure 6.12: The relation between the voltage gain and modulation index.....	120

<b>Figure 6.13: Z-Source inverter operation modes.....</b>	<b>121</b>
<b>Figure 6.14: Relationship of the harmonic factor and modulation index with different PWM.....</b>	<b>123</b>
<b>Figure 6.15: Relationship of the harmonic factor with modulation index and dc bus voltage with and without harmonic injection.....</b>	<b>124</b>
<b>Figure 6.16: Grid-connected three phase Z-Source inverter system.....</b>	<b>127</b>
<b>Figure 6.17: Block diagram of control loop.....</b>	<b>128</b>
<b>Figure 6.18: Open loop bode plot.....</b>	<b>130</b>
<b>Figure 6.19: PI correction bode plot.....</b>	<b>131</b>
<b>Figure 6.20: Close loop system bode plot.....</b>	<b>131</b>
<b>Figure 6.21: PV I-V and constant power curve.....</b>	<b>133</b>
<b>Figure 6.22: PV I-V and constant power curve analysis.....</b>	<b>134</b>
<b>Figure 6.23: The block diagram of the MPPT control.....</b>	<b>135</b>
<b>Figure 6.24: The modified P&amp;O MPPT method.....</b>	<b>136</b>
<b>Figure 6.25: Universal DSP 2407A board.....</b>	<b>139</b>
<b>Figure 6.26: Control Unit diagrams.....</b>	<b>140</b>
<b>Figure 6.27: Interrupt handler flow chart.....</b>	<b>142</b>
<b>Figure 6.28: Flowchart of DSP code.....</b>	<b>143</b>

Figure 6.29: CPLD control block.....	145
Figure 6.30: PV output characteristic during irradiation change.....	147
Figure 6.31: The grid connected z-source inverter output current.....	148
Figure 6.32: The grid line to line voltage and z-source inverter line to line voltage.	149
Figure 6.33: The experiment results of power curve changed with voltage.....	149
Figure 6.34: Simulation results of $V_{pv}$ is around 400 V.....	151
Figure 6.35: Experiment results of $V_{pv}$ is around 400 V.....	152
Figure 6.36: Simulation results of $V_{pv}$ is around 330 V.....	153
Figure 6.37: Experiment results of $V_{pv}$ is around 330 V.....	154
Figure 6.38: Simulation results of $V_{pv}$ is around 230 V.....	155
Figure 6.39: Experiment results of $V_{pv}$ is around 230 V.....	156
Figure A.1: Ripple current for two phase legs of three-phase inverter.....	165
Figure A.2: PV simulator.....	168
Figure A.3: Z-Source inverter.....	168
Figure A.4: Part of grid-connected Z-Source inverter with PV simulator system.....	169
Figure A.5: Functional block diagram of 2407A DSP board.....	170

# CHAPTER 1. INTRODUCTION

## 1. 1. Background

When the energy crisis in the seventies was going on, photovoltaic became more and more popular as a substitute for fossil energy source. The worldwide improving environment awareness and the needs of the growing population in developing countries have increased the interest in photovoltaics as a long term, inexhaustible, environmentally friendly and reliable energy technology. Photovoltaic sources are well established in the alternative energy market. Also it is growing an average rate of 26% per annum [98].

In the photovoltaic systems, power electronics converters are the key enable parts. Energy is transferred from the PV, through power electronics converter, then finally to the load or grid. The power electronics converter will regulate the power and voltage, also realize maximum utilization of the energy from the PV. With the rapid improvement in material science, the cost of photovoltaic cell has dropped tremendously in last two decades, while as the price for the converter used in PV system remains almost the same. Thus, to lower the cost and at the same time achieve the best performance of the power electronics converter in the PV system now becomes the key issue for applications of PV system.

Generally, by substitute old power processors with Power Electronics converters will help a lot in system efficiency and dynamic response. The earliest power electronics can be dated back to 1948, from which Bardeen, Bratain, and Schockley invented the silicon transistor at Bell Telephone Laboratories. Since then, many new power semiconductor devices have been invented and evolved for control of power and energy. Figure 1.1 shows the rating and application range of major devices used in power conversions. For PV system, IGBTs and GTOs are most commonly used devices because of the voltage and current ratings.

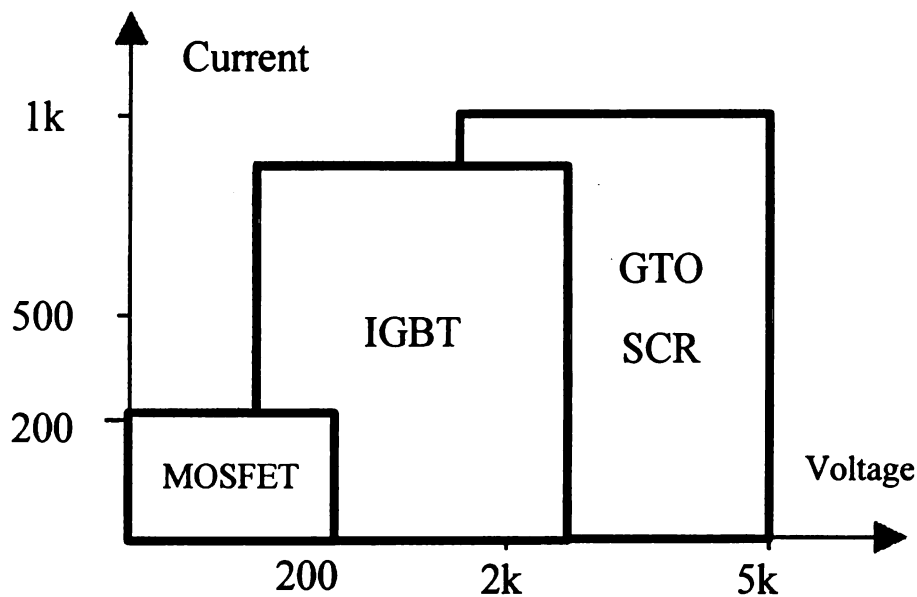


Figure 1.1: Major types of power electronics devices [19].

## 1. 2. Distributed Generation And Photovoltaic Generations

Based on above introduction, the extension of distributed generation (DG) is widely used to avoid the energy exhaustible from only the fossil fuel supply. Distributed generation, also called on-site generation, generates electricity from many small energy

sources typically in the range of 3 kW to 10,000 kW. With the widely used distributed generation system, consumers and power utilities can get much more benefits. Distributed generation can give more varied energy options, increase generation and transmission efficiency, and improve power quality and system stability, etc. The types of DG include Gas Turbines, Reciprocating Engines, Microturbines, and as well as the "green powers", such as fuel cell, wind turbine and photovoltaic (PV).

Among those green powers, photovoltaic has its unique advantages than other sources. Since the generation of electricity is directly from the sun, no fuel is needed. The production of electricity by the photovoltaic process is clean and produces no carbon dioxide or other toxic fumes. That's non-polluting energy. The PV system has a high reliability with at least 20 years of service time. The operating costs is low, because there is no moving parts, the PV cells need little upkeep. Photovoltaic system also has a good modularity due to their portability and sizebility. Usually photovoltaic system is near the point where the electricity is used, thus the wires connection can be reduced and the same to the construction time, the total construction costs can be reduced. Based from [101], the PV panel production cost is \$0.99 to 2.00/W (2007) plus installation and supporting equipment unless the installation is Do it yourself (DIY) bring the cost to \$6.50 to 7.50 (2007). As the price of PV cell itself is still decreasing, the PV system is very promising for DG.

### 1. 3. Power Conditioning System

In nowadays distribution systems, many different types of DG from under 10 kW to tens of megawatts generation are located around communities and industrial facilities.

When the power source of the DG does not meet the grid or load requirements, power converter is required to bridge between the source and load to act as the Power Conditioners.

Generally, a Power Conditioner for PV system will need to meet the following requirements:

- 1) Power conditioner system can process power conversion from dc voltage into ac voltage with the required frequency. The dc voltage can be higher or lower than the ac voltage.

- 2) The power quality must satisfy the low total harmonic distortion (THD), voltage and frequency deviation requirement.

- 3) Power conditioner system has protection for electric power systems, and some also can have anti-islanding protection and electrical isolation if necessary.

## 1. 4. Outline Of The Thesis

The goal of this thesis is mainly to research power conditioning system for PV. The previous topologies for PV inverter system were summarized and compared. In addition, a novel Z-Source power conditioning system is proposed for split phase stand alone PV system; also, the grid-connected three-phase Z-Source inverter system is proposed and analyzed. For test purpose, the dc-dc converter based PV simulator system is proposed and built. The outline of each chapter is listed as the following:

Chapter 2: Introduces the Photovoltaic system as the background for the whole thesis.

Chapter 3: Reviews the inverter topologies for photovoltaic power conditioning

system. Compares of those topologies are presented. The advantages and disadvantages for different topologies are also summarized.

Chapter 4: Proposes a novel Z-Source power conditioning system for split-phase stand alone residential photovoltaic system. The design and control is analyzed. The simulation and experiment results are presented to verify that.

Chapter 5: Proposed a dc-dc converter based PV simulator for Z-Source inverter system for test purpose. A new combined voltage and current control method is proposed and tested. The experiment results are shown for prove.

Chapter 6: Proposed a grid-connected three-phase Z-Source inverter with PV simulator system. The design and control is proposed and discussed in detail. The simulation and experiment results are shown to verify the proposed system and control strategies.

Chapter 7: Summarizes the inverter topologies, and makes a conclusion for the whole thesis. The contribution of the whole thesis is listed, and the future work is also recommended.

# CHAPTER 2. PHOTOVOLTAIC SYSTEMS

## 2. 1. Introduction

### 2.1.1 History Of Photovoltaics And New Trends

Renewable energy sources derive their energy from existing flows of energy, from on-going natural processes, such as sunshine, wind, flowing water, and geothermal heat flows. Now the most feasible alternative energy sources include solar power, fuel cell, and wind.

The energy available at the surface of the sun is  $60,000 \text{ kW} / \text{m}^2$ , where the sun's radiation at the top of the earth's atmosphere is only about  $1.4 \text{ kW} / \text{m}^2$ . After it passes through the atmosphere, about 80 trillion kW of solar radiation energy is available globally. This is about 13,000 times the present world energy use [100].

The history of PV's dates back to the early 19th. In 1839, Edmund Becquerel, a French experimental physicist, discovered the photovoltaic effect while experimenting with an electrolytic cell made up of two metal electrodes [12]. In the early 1950's, the Czochralski meter was developed for producing highly pure crystalline silicon. In 1954 Bell Telephone Laboratories produced a silicon PV cell with a 4% efficiency and later achieved 11% efficiency. Then with the development of the semiconductor technology and PV module manufactory, now photovoltaic has a wide range of applications.

From the US PV roadmap [13], the goal of the industry is to meet 10% of US peak electricity generation capacity by 2030. Figure 2.1 shows the different projections of the Japanese, US and EPIA roadmaps [14]. PV generation shows promising in the near future.

Now there are several major market players in US. For BP-solar, it was the number two to sell 58 MW in 2001. Then there is shell solar, shell solar sold 44.4 MW in 2001. And shell solar will invest 0.5 to 1 billion dollar in solar photovoltaics and wind energy from 2001 to 2006. Astropower sold 26 MW in 2001. And there are also ASE-Americas, United Solar Systems, Evergreen Solar, etc [14].

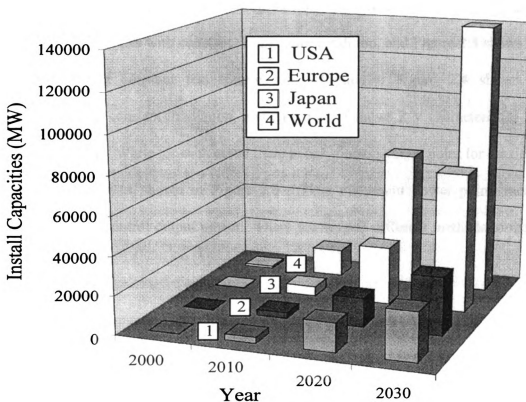


Figure 2.1: Evolution of the solar electrical capacities till 2030 [14].

*(Sources: Japanese, US and EPIA Roadmap)*

## 2.1.2 Basics Of Photovoltaics

The basic element of PV system is PV cell. PV cell can produce electricity due to quantum-mechanical process. Usually a PV cell consists of a p-n junction formed in a semiconductor material similar to a diode. If light is incident on a PV cell, current will flow when an electrical load is connected.

The characteristics of a PV cell are nonlinear. They depend on solar irradiation and cell temperature. For most crystalline silicon solar cells the reductions in voltage with increasing temperature is around  $0.50 \text{ \%}/^{\circ}\text{C}$ , though the rate for the highest-efficiency crystalline silicon cells is around  $0.35 \text{ \%}/^{\circ}\text{C}$ . Averagely, the rate for amorphous silicon solar cells is  $0.20\text{-}0.30 \text{ \%}/^{\circ}\text{C}$ , depending on how the cell is made [99]. Figure 2.2 shows I-V characteristics with constant temperature condition, and Figure 2.3 shows P-V characteristics with constant temperature too. Similarly, Figure 2.4 shows I-V characteristics with constant irradiation, while Figure 2.5 shows P-V characteristics with constant irradiation. While for each curve there is only one operation point for maximum utilization of power as shown in Figure 2.6. Thus maximum power point tracking (MPPT) is used to control output power. There are several different methods to realize MPPT.

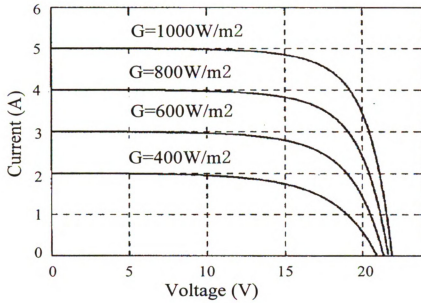


Figure 2.2: I-V characteristics with constant temperature.

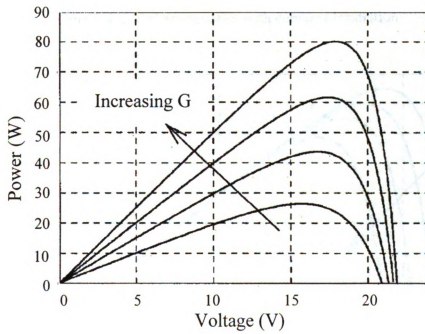


Figure 2.3: P-V characteristics with constant temperature.

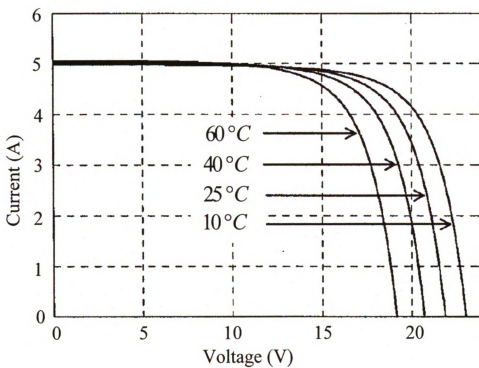


Figure 2.4: I-V characteristics with constant irradiation.

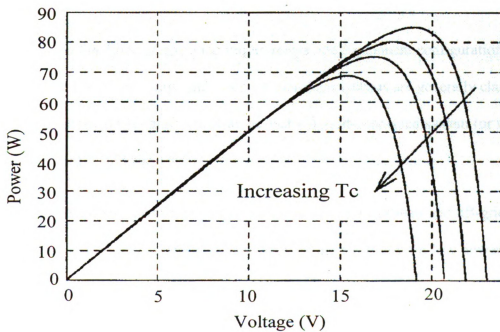


Figure 2.5: P-V characteristics with constant irradiation.

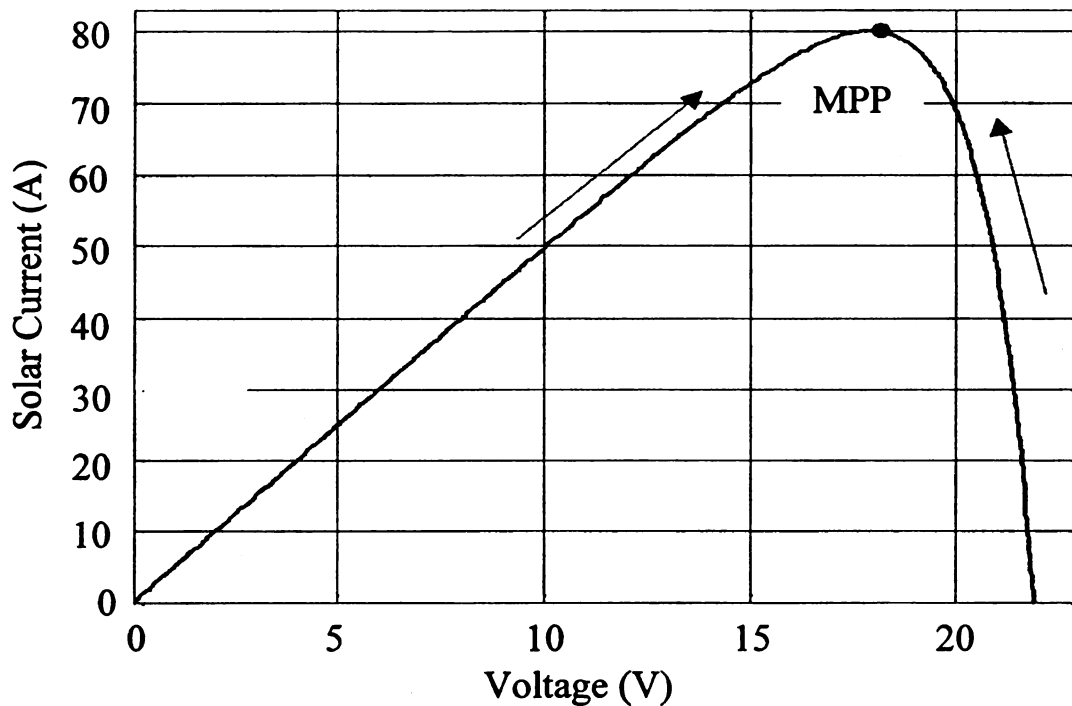


Figure 2.6: Maximum power point tracking.

## 2. 2. Types Of Photovoltaic Systems [15-18]

According to the different operation requirements, the component configurations, and ways to connect the power source and loads, photovoltaic systems are generally classified to three types: off-grid system (or stand-alone system), grid-connected system (or utility-interactive system), and hybrid system.

Off-grid systems can also be classified to off-grid domestic system and off-grid non-domestic system. Off-grid domestic systems provide the electricity for low power loads (such as lighting), which used by households and villages that are not connected to the utility grid. Systems of this type have been widely used to satisfy the energy demands of off-grid communities. The system size is usually around 1 kW. Off-grid non-domestic

systems provide power for a wide range of applications, such as water pumping, telecommunication, etc. Figure 2.7 shows the general off grid structure of PV system. In this system, a energy storage device, such as a battery pack, is usually required to supply transient power at the peak load.

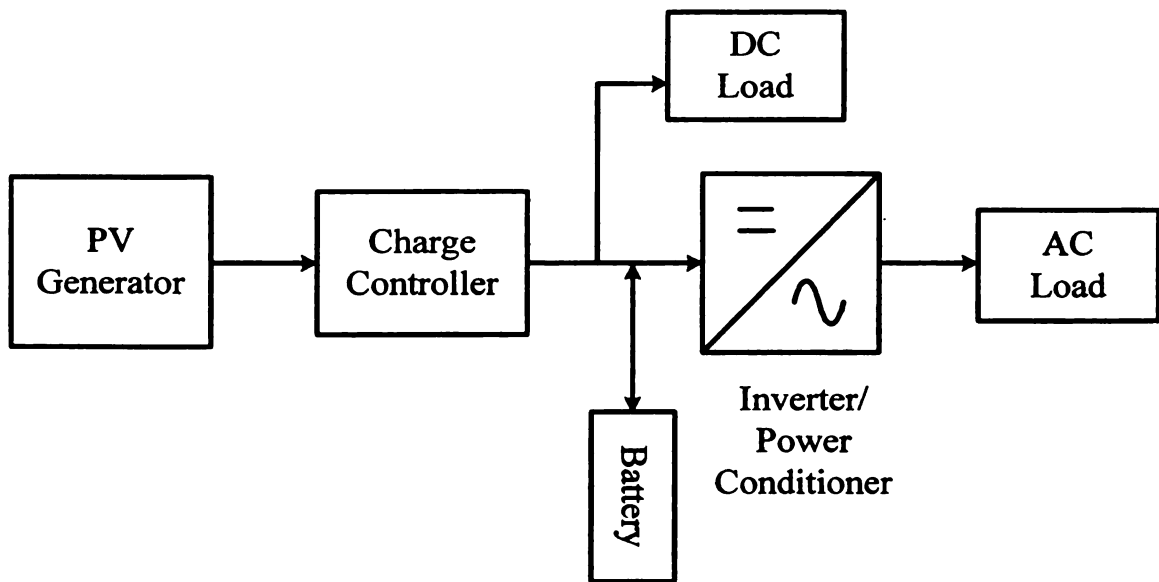


Figure 2.7: An Off-grid PV system.

Similarly, grid-connected systems can be classified to grid-connected distributed system and grid-connected centralized system. Grid-connected distributed systems provide electricity to a building or other loads that are connected to the utility grid. These systems are widely used and account for most of the installed PV capacity. Generally system capacity varies from 1 kW to 100 kW for different requirements. When on-site generation exceeds the need of loads, the excess energy can be fed back to the utility grid. With grid connected PV system, the distribution loss can be reduced because the systems are installed at the point of user. Since no extra land is required for

PV systems, costs for mounting systems can be reduced. One distinguish feature of PV system is that PV array can be used as roofing material as BIPV (building integrated PV).

Compared with off-grid installation, grid connected PV systems cost less because the energy storage is generally not required. Figure 2.8 shows the grid connected structure of PV system.

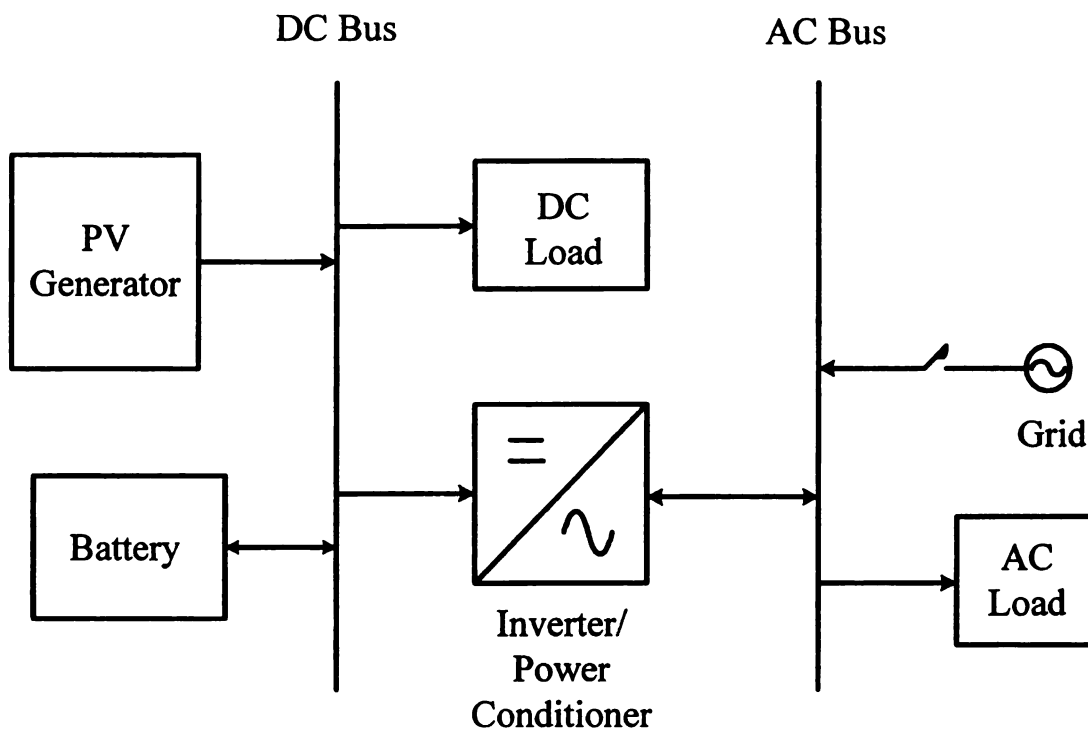


Figure 2.8: A grid-connected PV system.

Besides the aforementioned two types of PV systems, there is an alternative solution which is called as Hybrid PV system as shown in Figure 2.9. The hybrid system can either works as a stand alone system or a grid connected system. It provides the end user more options as the penalty of higher cost. Hybrid systems can be classified to three types: series hybrid system, switched hybrid energy system, and parallel hybrid energy system. Usually hybrid PV systems contain at least one other generation source such as

wind turbine, which is not a utility. Those systems can provide continuous power whether the PV can provide enough power or not.

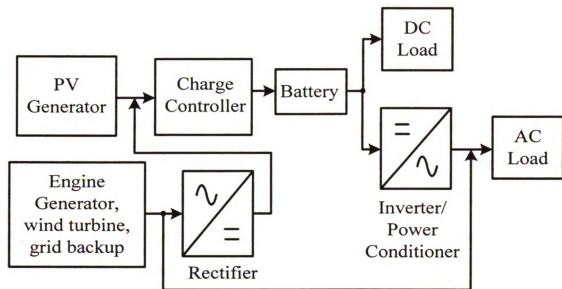


Figure 2.9: A hybrid PV system.

## 2. 3. Inverters In Photovoltaic System

### 2.3.1 Introduction

Inverter is an electronic device that converts dc electricity to ac electricity. Because solar panels and batteries can only generate and store dc electricity, while the appliances people used from the utility grid need ac electricity, the inverter is the key part in the power processing unit in PV systems.

Power Electronics inverters convert dc electricity to ac electricity by switching mechanisms to break the continuous current into pulses. Nowadays, inverters can be made small enough to along with laptop for working on the road, and large enough to

send megawatts of renewable energy into the utility grid. Different inverter has different configuration, power output quality and expected service life.

The PV inverter is a costly and complex component of PV systems that convert dc power to ac power from the PV modules. Inverter mean time to first failure (MTFF) is around five years [19]. To minimize inverter cost and at the same time improve inverter performance and reliability is the primary goal of PV manufactures. Since the inverter is not only used in the PV system, but also used for other Distributed Energy Resources (DER), such as wind, fuel cells, etc. The inverter requirements are similar that universal designs with replaceable modules are the best solutions for a 'next generation' inverter [19]. For all the residential grid-connected DG types, the inverter should be able to convert between 2 and 10 kW of dc power, prevent islanding, reduce radio frequency interference, provide the low harmonic distortion, and optionally provide backup power. Therefore, the residential grid-connected inverters for solar, wind, and fuel cells can be nearly identical.

Inverter technology is the key technology to have reliable and safety operation of PV system. It is also required to generate high quality power to ac utility system with reasonable cost. By means of high frequency switching of semiconductor devices with Pulse Width Modulation-PWM methods, high efficiency conversion with high power factor and low harmonic distortion power can be achieved. The remaining problem is the cost.

In a PV system, the inverter has to realize the following functions:

1. convert dc power to ac power usable by most business and household devices

2. modify the voltage and current output from the PV array
3. converter the ac power to the specific voltage and frequency range of utility network
4. safeguard the utility network system and its personnel from possible harm during repairs
5. prevent damage to the PV array and other component during unusual operating conditions

Major design considerations for inverters include their capacity, voltage rating and battery capability. In addition, the high operating voltage minimizes transmission losses.

### 2.3.2 Types Of Inverters

As described before, there are various types of inverter configuration. Self commutated voltage type inverter is employed in all inverters with a capacity of 1 kW or under, and up to 100 kW.

The self commutated inverter has more advantages than the line commutated inverter. The self commutated inverter can freely control the voltage and current waveform at ac side, and adjust power factor and suppress the harmonic, and highly resistant to the system disturbance. Therefore, most inverters for distributed power sources such as photovoltaic generation now employ a self commutated inverter.

The self commutated inverter can be classified to voltage and current types. The voltage type is a system in which the dc side is a voltage source and the voltage waveform of the constant amplitude and variable width can be obtained at the ac side. The current type is a system in which the dc side is the current source and the current

waveform of the constant amplitude and variable width can be obtained at the ac side. In the case of photovoltaic power generation, the PV output is dc voltage, so the voltage type inverter is employed.

Both the voltage control and the current control can be performed to the voltage type inverter. The current control scheme is used more popular because a high power factor can be obtained with simple control, and transient current suppression is possible during disturbances, such as voltage changes in the utility power system. For the output ac voltage control, general PWM control can be utilized.

# **CHAPTER 3. SUMMARY OF PREVIOUS WORK**

## **3. 1. Introduction**

For growing PV market, there is a lot of occupation for grid-connected applications. And around 95% are used for AstroPower domestic residential business [20]. Now the residential system power rating ranges from 1.6-9.6 kW. And customer can also choose 2.4, 3.6, 4.8, 7.2 kW sizes due to their requirements. For commercial system, the power rating can be 10-300 kW or more.

Grid-connected PV system has the advantage of more effective utilization of generated power. According to [20], PV grid-connected inverter systems have good performance, including high conversion efficiency and power factor exceeding 90% for wide operating range, while at the same time maintaining current harmonics THD less than 5%.

With the development of power electronics devices and the corresponding technologies, the cost and size of PV inverter reduced a lot recently. The progress of circuit design of inverter and control methods also helps a lot. The control circuit also provides protection functions like the maximum power point tracking.

### 3. 2. PV Inverter Status [15-19]

In a PV system, the PV array output voltage cannot be applied to the load directly in common. Thus the inverter is needed to process that. It is very important to make the power meet the specific demand of the equipment.

There are various inverter employed in the PV system. Now for the PV inverter, the input voltage is higher than ever, some up to 600 V. The single unit costs around \$0.6-\$1.0/watt. The inverter efficiency is around 85% in average. The system becomes easier to install with higher dc voltage input.

Inverter can be operated for normal fluctuations of voltage and frequency at the utility grid side. The standard voltage and frequency for a single phase circuit is 120/240 V and 60 Hz in US, for a three phase circuit is 480 V and 60 Hz. For the standard values, the inverter can operate substantially without any problems within the tolerance of 10% and -15% for the voltage, and  $\pm 0.4$  to 1% for the frequency.

The operable dc voltage range is determined by the rated power of the inverter, rated voltage of the ac utility grid system. For a capacity of 1 kW or below, the operable dc voltage ranges from 14-25 V, 27-50 V, 45-100 V, 48-120 V, and 55-110 V. In addition, for a capacity of 1 kW to 10 kW, the operable dc voltage ranges from 40-95 V, 72-145 V, 75-225 V, 100-350 V, 125-375 V, 139-400V, 230-450 V, 250-600 V, and 450-800 V.

The harmonic current from the inverter is very small, because the PWM control scheme is used as the output waveform control of the inverter. Thus fewer problems arise.

The developments of PV system need more requirements for the inverter. For the future application, inverters maybe need utility interactive and stand alone capability, more reliability, longer life cycle, and lower failure probability.

### 3. 3. PV Inverter By Power Stage [20-38]

#### 3.3.1 Introduction

Some power conditioning systems employ transformers in the topologies. Figure 3.1 shows that a line-frequency transformer (LFT) is located between the grid and inverter. This transformer can avoid the injection of dc current into the grid. Figure 3.2 shows that a high-frequency transformer is located in an HF-link grid-connected ac-ac converter. Figure 3.3 shows that a high-frequency transformer is located in a dc-link PV-module-connected dc-dc converter.

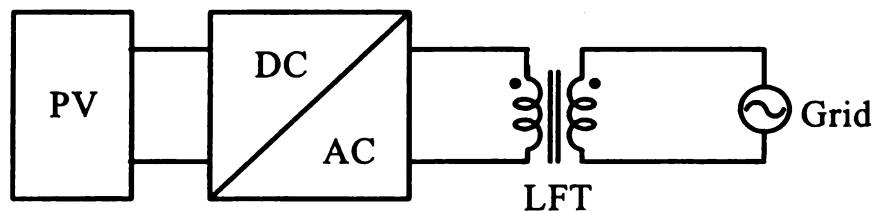


Figure 3.1: Line-frequency transformer.

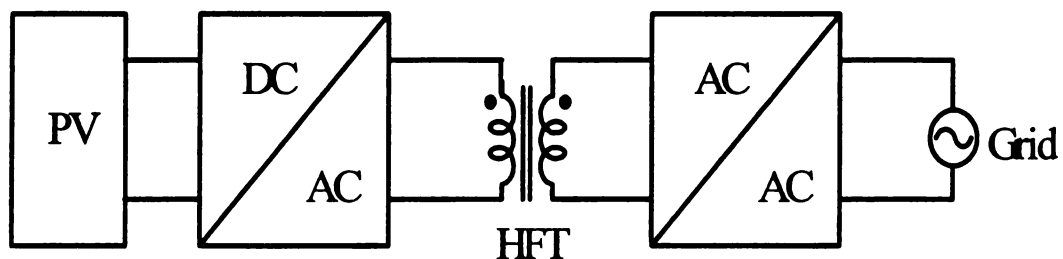


Figure 3.2: High-frequency transformer 1.

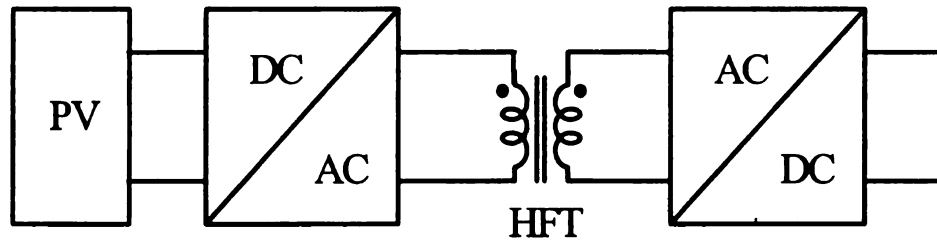


Figure 3.3: High-frequency transformer 2.

For PV inverters, there also can be classified to the centralized inverter and decentralized inverter. Figure 3.4 shows the centralized and decentralized inverter topologies in [21]. Centralized inverter only needs only one inverter for the power conditioner, but decentralized inverter needs more than one inverter to connect PV modules to a common bus (dc, low voltage ac, or the grid). Compared those two topologies, the one central inverter has the advantages of higher efficiency, lower cost, and without the considerations of shading effects. The low voltage ac bus is best selection as the common bus employed in the decentralized inverter.

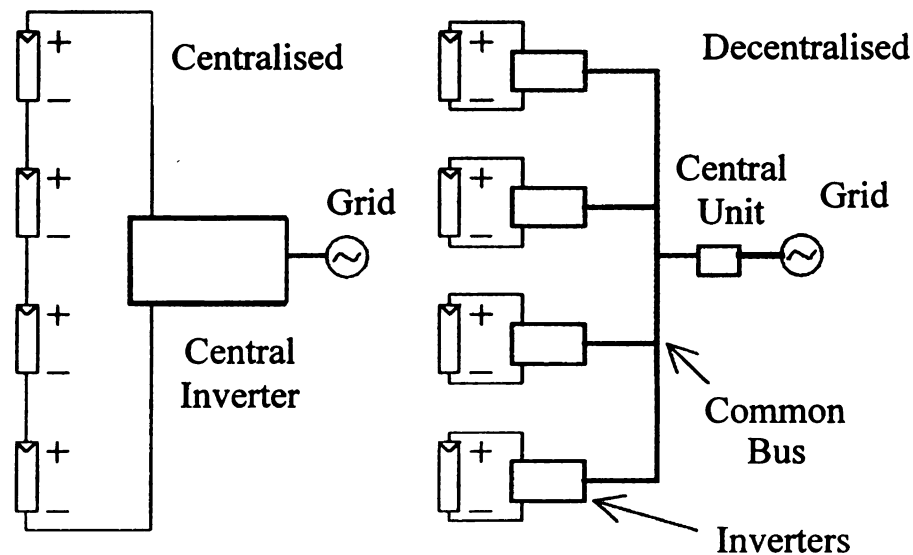


Figure 3.4: Centralized and decentralized inverter topologies [21].

For different power stages, inverter systems can also be classified as single-stage inverter and multi-stage inverter. Both of these two will be described in detail in the following.

### 3.3.2 Single-stage Inverters

Single stage inverters only need one power stage to process power conversion from dc to ac and boost the dc input voltage to required output voltage level as shown in Figure 3.5. Single-stage inverters can be classified to four switch topologies and six switch topologies. Single-stage inverters usually have a relative simple topology, and employ the fewer components, thus cause a higher efficiency. The past literatures have listed a lot of inverters for this type.

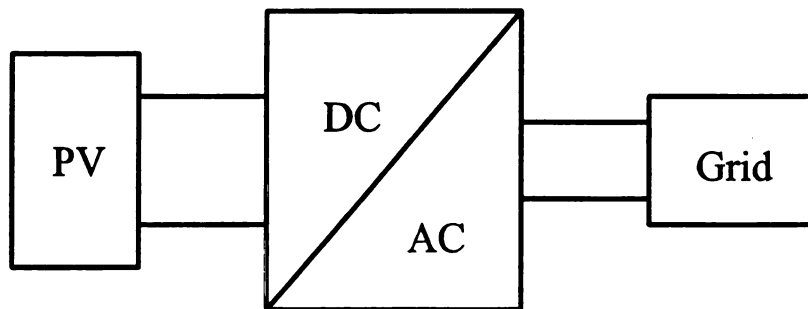


Figure 3.5: A single stage inverter.

#### 3.3.2.1. Four switch topologies

Figure 3.6 shows a nonisolated boost inverter proposed by Cáceres and Barbi [22]. The circuit employs two dc-dc converters, and the load is between the two outputs. Each converter provides a unipolar dc-biased sinusoidal output with a 180 degree phase difference. Therefore, the output waveform is pure sinusoidal. Figure 3.7 shows a buck-

boost inverter proposed by Vazquez et al [23]. In this circuit, similarly to inverter in Fig. 3.6, two buck-boost dc-dc converters instead of boost converters are used in the system. This system can generate output voltage lower or higher than the input voltage due to buck-boost converter. Figure 3.8 shows a four switch buck boost inverter by Kasa et al [24]. The input PV voltage can have a wide operation range, but requires split dc voltage source. A Four switch isolated bidirectional buck boost inverter is shown in Figure 3.9 by Kjær and Blaabjerg [25]. The advantage of this system is the galvanic isolation provided by the two high frequency transformers due to the transformers. But the transformer also will increase the system cost and lower the efficiency. Figure 3.10 shows a zero-current switching buck-boost inverter proposed by Wang [26]. The advantage of this circuit is that the switching power loss can be reduced.

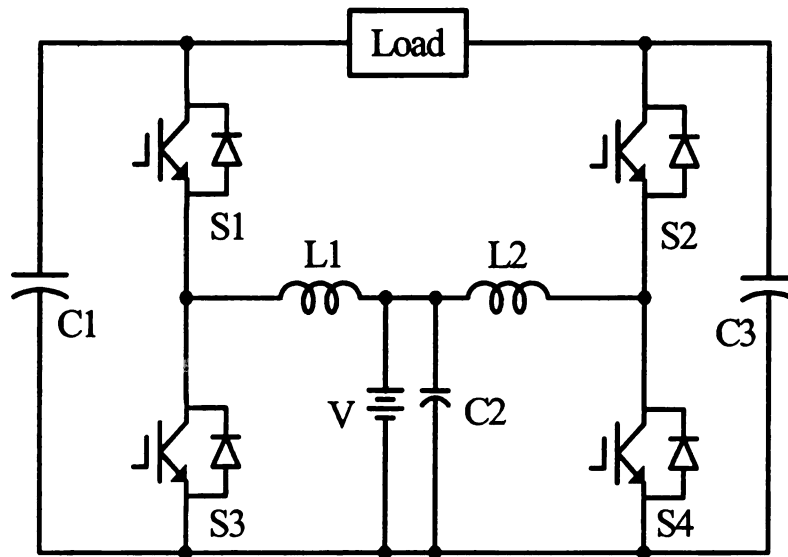


Figure 3.6: Four-switch boost inverter by Cáceres and Barbi [22].

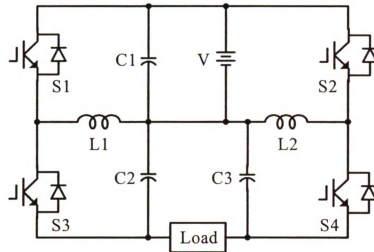


Figure 3.7: Four switch buck boost inverter by Vazquez et al [23].

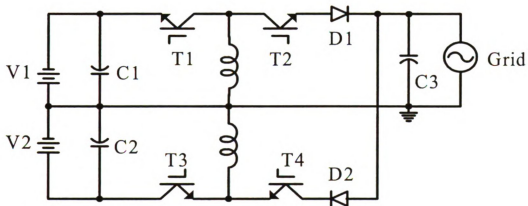


Figure 3.8: Four switch buck boost inverter by Kasa et al [24].

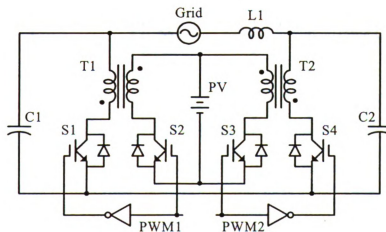


Figure 3.9: Four switch isolated bidirectional buck boost inverter by Kjær and Blaabjerg [25].

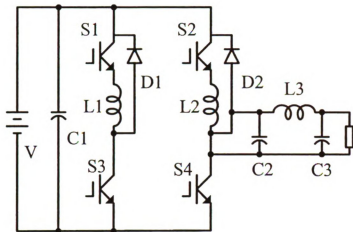


Figure 3.10: Four switch resonant buck boost inverter by Wang [26].

### 3.3.2.2. Six switch topologies

Figure 3.11 shows a six switch isolated buck-boost inverter proposed by Nagao and Harada [28]. In this system, the energy storage inductor is charged from different directions in each half cycle, thus provide an alternative output [28].

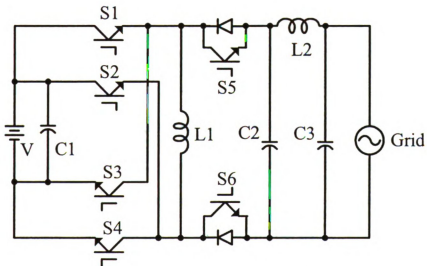


Figure 3.11: Six switch buck boost inverter by Kusakawa et al [28].

Single-stage inverters usually have higher efficiency and lower cost, but the power capacity is limited, and dc source range is also limited.

### 3.3.3 Multi-stage Inverters

Multi-stage inverters have more than one stage to process power conversion as shown in Figure 3.12. Dc-dc converters will perform usually voltage buck or boost or electrical isolation, and then dc-ac can be performed to get the required output amplitudes and waveforms. Multi-stage inverters can solve the problems when single-stage inverters meet with high power, high performance requirement.

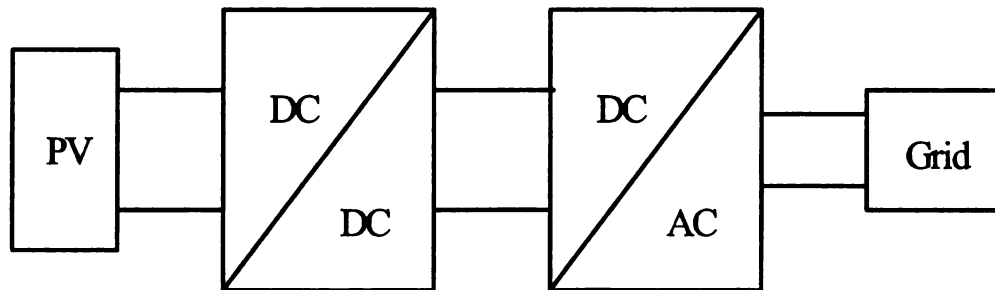


Figure 3.12: Dual power processing inverter.

A two-stage boost inverter is shown in Figure 3.13. In the circuit, a dc-dc boost converter is ahead of the dc-ac inverter. With the first stage, input voltage is boost to suited dc voltage, and output ac voltage can be obtained by a high frequency PWM inverter through the second stage. The whole process flows as the dc-dc-ac process. Figure 3.14 shows a two-stage nonisolated buck boost inverter proposed by Saha and Sundarsingh [30]. This inverter was designed to operate a low dc input voltage as 100 V due to safety reason, thus make the PV operate voltage range very small. The isolated buck-boost inverter with a high frequency transformer shown in Figure 3.15 can draw the power from the PV source even when the distributed generated dc voltage is low. The inverters operate as current source inverter in line frequency in Figure 3.14 and Figure 3.15. The inverter in Figure 3.16 does not have the high-frequency transformer, but

adding a capacitor to the charge loop of energy storage device. This inverter can have a wide range of PV operate voltage. While, Figure 3.17 shows a flyback inverter with enhanced power decoupling by Shimizu [32]. In this kind of inverter, the first stage has the buck boost converter, the second stage has the flyback converter, and the last stage has a transformer. The voltage across intermediate capacitor can have both the dc component and ac component alternating at twice the frequency of the load. This system can have a longer service life of inverter because the large electrolytic capacitor can be replaced by the small intermediate capacitor. In paper [41], similarly topology has been used. The first stage is dc-dc converter to boost voltage, and then the second stage processes the dc-ac conversion. There are only four switches in the inverter operation in line frequency, thus the dead time effects can be disregarded, and the line noise of voltage and current caused by high frequency switching can be reduced. The above several inverters all process as dc-dc-ac topologies.

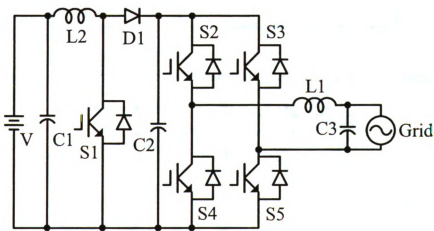


Figure 3.13: Two stage boost inverter [29].

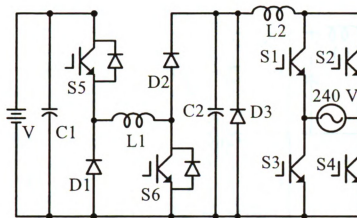


Figure 3.14: Two stage nonisolated buck boost inverter by Saha and Sundarsingh [30].

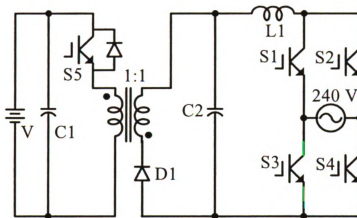


Figure 3.15: Two stage isolated buck boost inverter by Saha and Sundarsingh [30].

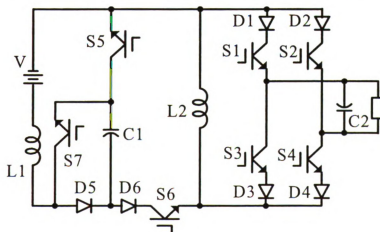


Figure 3.16: Buck-boost inverter by Funabiki et al [31].

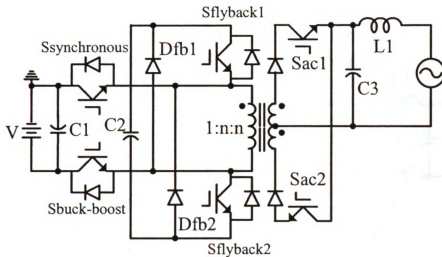


Figure 3.17: A flyback inverter with enhanced power decoupling by Shimizu [32].

Figure 3.18 shows a multi-stage boost inverter with pseudo-dc-link. The circuit has a PWM dc pulse train. Compared to traditional dc-link, the dc filter in the pseudo-dc-link can be eliminated. The inverter operates as line-frequency switching inverter to get the required output voltage from the high-frequency dc pulse train. Therefore, the losses and cost can be reduced because not all stages work at high switching frequency. Figure 3.19 shows a multi-stage boost inverter proposed by GEC [33]. During the last stage, the line-frequency inverter processes the half sine wave to full sine waves and produces ac current to the grid in phase without output filter. This topology has been applied to General Electric Company (GEC) for 10 kW grid-connected PV systems [39]. Those above two are both dc-ac-dc-ac topologies.

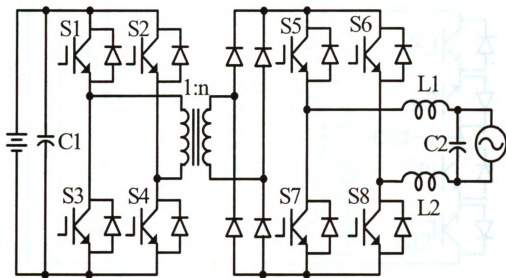


Figure 3.18: Multi-stage boost inverter with pseudo-dc-link.

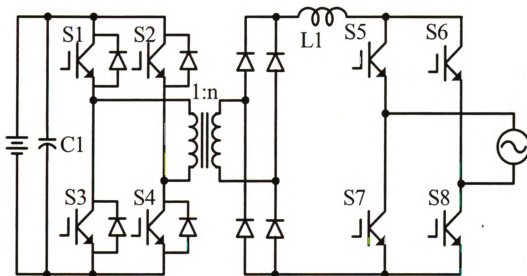


Figure 3.19: Multi-stage boost inverter by GEC [33].

Figure 3.20 shows a bidirectional dc-ac-ac converter proposed by Beristáin et al [40]. In the topology, the second stage is a bidirectional ac-ac converter, and a high-frequency transformer is also employed for voltage variation and electrical isolation.

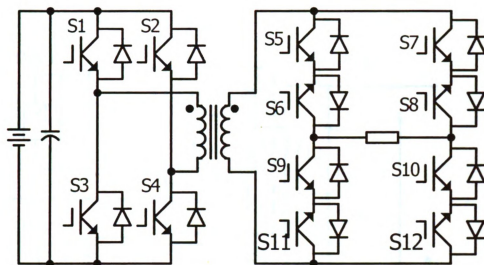


Figure 3.20: Bidirectional dc-ac-ac converter by Beristáin et al [40].

Paper [42] also discussed the cascaded dc-dc converter for PV power system. Buck, boost, buck-boost and Cúk converters are checked as possible cascaded converters. The results show that the boost converter is the best if a specific boost is needed. While flexible in voltage ranges, buck-boost and Cúk Converters usually have the less efficient and the higher cost. Figure 3.21 shows a cascaded inverter PV system [54]. More than one single-phase H-bridge inverters are in series. The cascaded inverter used ready-made ICs for class D audio amplifier was realized. The ready-made integrated circuits (ICs) have the advantages to reduce the parts of the inverter and mass production [54]. Usually, the class D audio power amplifier uses the ready-made ICs, but ICs could not provide utility grid level. Similarly, The PV inverter for grid connected by the ICs without LFT meets the same problem. The cascaded inverter can solve the problem and reach high voltage efficiently.



## 3. 4. Industrial PV Inverter [37-53]

### 3.4.1 Introduction

PV system has the numerous markets in the world. More than 1900 MW of PV were installed worldwide. Japan has the highest installed capacity, followed by Germany and the US. Those three countries represent about two thirds of global PV capacity [43].

### 3.4.2 Manufacture PV Inverter

- *Xantrex*

Xantrex's inverter has a single stage employed with high efficiency transformer. Figure 3.22 shows Xantrex PV series topology. A three phase bridge is used between the PV array and a 60 Hz isolation transformer. The transformer steps the utility line-tie voltage for more efficient power transmission. The circuit has the advantages that the single stage makes the system more efficient, and much more utility grid-tie voltage options can be selected due to the isolation transformer. The circuit has the disadvantage that the overall system efficiency is lowered by using the transformer. The Xantrex Technologies PV 10208 system uses this kind of topology inverter, and was tested at Sandia National Laboratories. The efficiency is around 95%.

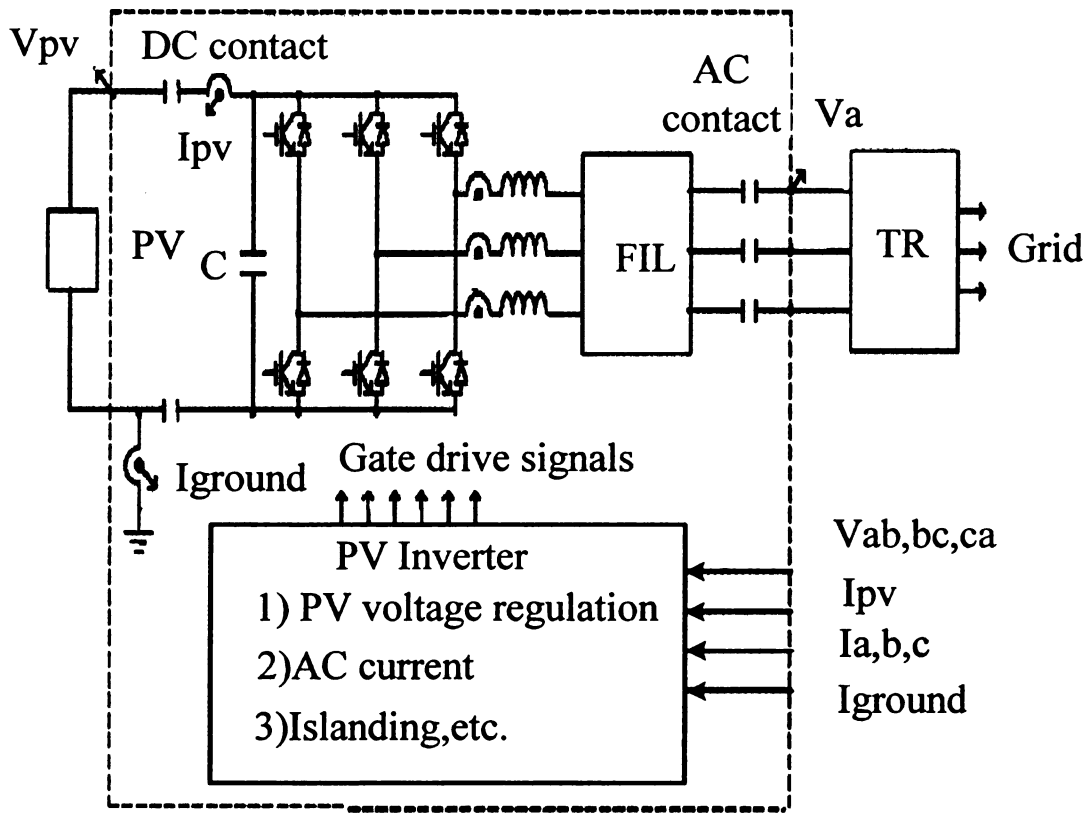


Figure 3.22: Xantrex PV series topology [42].

- Ballard

Figure 3.23 shows the Ecostar Power Converter for PV applications. The topology is similar to Figure 3.22. This inverter is a grid tie utility interactive inverter. The rated voltage is 208 V or 480 V. The output frequency is 60 Hz. The PV array dc voltage range is from 290-595 V. The current harmonic is less than 4%. PV array MPPT ranges from 240 V to 600 Vdc. The peak inverter efficiency is 97% at 75% output. The peak efficiency with transformer is 94.6% at 75% output [44]. This kind of inverter has been installed in Chicago Center for Green Technology, Illinois. The number of kW hours produced from a 76 kW array is around 13,274 kW hours.

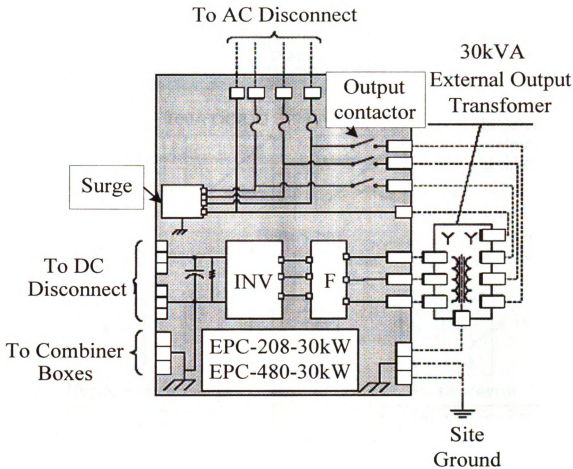


Figure 3.23: Ecostar Power Converter [44].

- Beacon Power

The Smart power M5 inverter is used for grid-connected PV system with battery backup. A 5 kW grid tie PV power system is shown in Figure 3.24. The system employs the dc/dc converter before dc/ac inverter. The PV operating ranges from 48 to 110 Vdc, DC input battery voltage is 44-60 Vdc. AC output voltage is between 106 to 132 Vac (120 Vac nominal). Output frequency is 60 Hz nominal. And the total harmonic distortion is less than 3%. The peak efficiency is 93%.

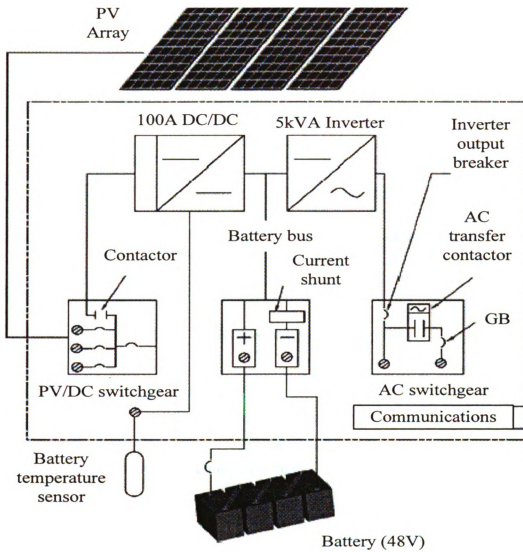


Figure 3.24: Smart power M5 power system [45].

- Phoenixtec Power

Figure 3.25 shows Sunville grid tie inverter. For Sunville 1500, the output power is 1500 W, the nominal dc voltage is 360 Vdc, PV array MPPT operates 150-450 Vdc, operational voltage is 196-253 Vac, the operational frequency is 50/60 Hz, THD is less than 3%, the maximum conversion efficiency is 95%.

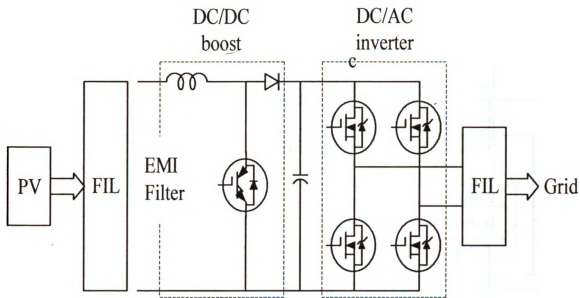


Figure 3.25: Sunville inverter topology [46].

- **Fronius**

FRONIUS IG 2000-LV has the topology shown in Figure 3.26. The nominal output power is 1.8 kW, the nominal output voltage is 240 V, the THD is less than 5%, the maximum efficiency is 94.4%.

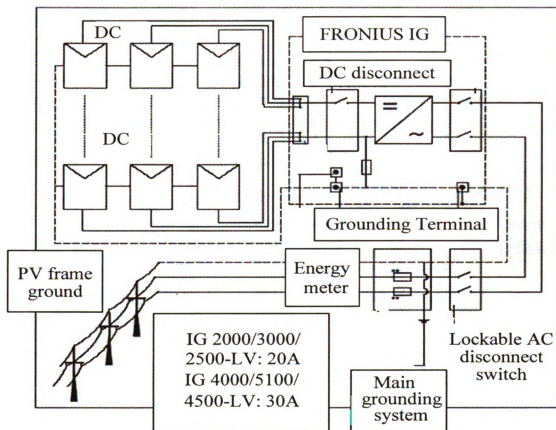
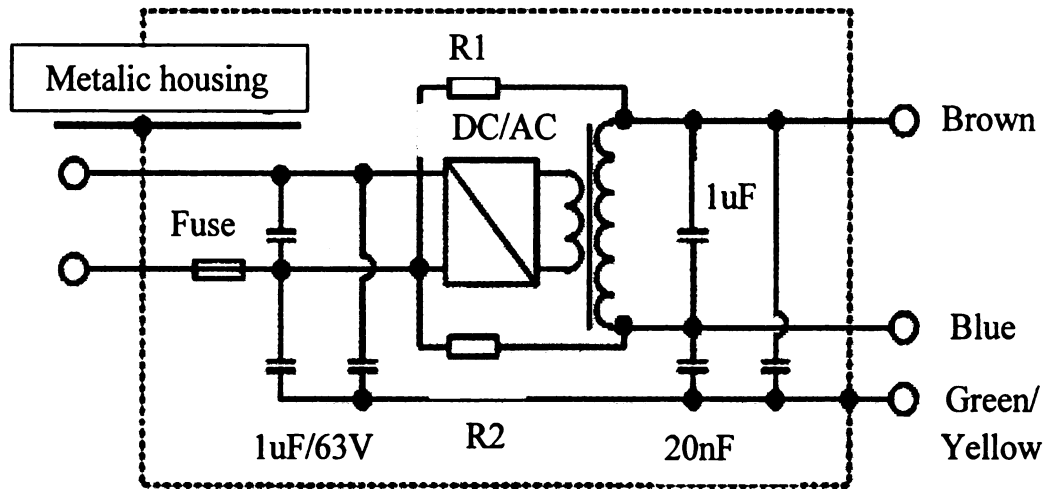


Figure 3.26: FRONIUS IG 2000-LV [47].

- *Studer*

Figure 3.27 shows the AJ series stand by inverters. For AJ 500, the battery voltage is 12 V, the input voltage is 10.5-16 V, the maximum efficiency is 93%, the output voltage is 230 V (115 V).



$R1=R2=2,7M\text{ ohm}$ (not existing in AJ 275-AJ350-AJ400)

Figure 3.27: AJ series inverter [48].

- **SMA**

The SMA Sunny Boy inverter is not only the most popular grid tie PV inverter in Europe, but also in North American. Over 250,000 Sunny Boy inverters have been installed in worldwide. Figure 3.28 shows the Sunny Boy 1100U. The ac input voltage is 213-262 Vac (nominal 240 Vac), ac input frequency is 59.3-60.5 Hz (nominal 60 Hz), dc input voltage is 129-400 Vdc, the maximum ac power output is 1100 W, the power factor is unity, the peak inverter efficiency is 93%, PV start voltage is 180 Vdc. Figure 3.29 shows Sunny Central SC125U. It is a 125 kW grid-tied string inverter for PV system. For SC125U-240, dc input voltage is 275-600 Vdc, the peak power tracking voltage is 275-550 Vdc, ac output voltage is 212-264 Vac (240 Vac nominal), current THD is less than 3%, power factor is unity.

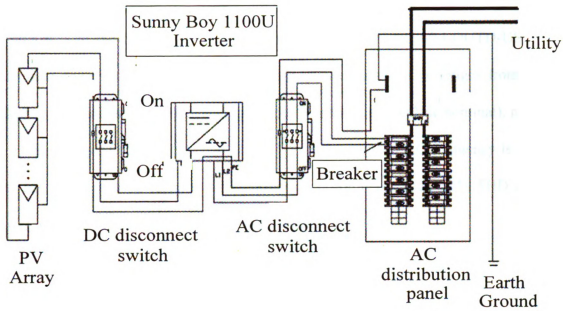


Figure 3.28: Sunny Boy 1100U inverter [49].

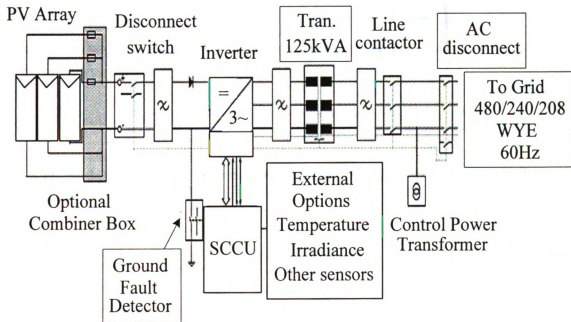


Figure 3.29: Sunny Central [49].

- **Magnetek**

Figure 3.30 shows AURORA isolated outdoor model: PVI 2000-I-OUTD-US. The maximum power rating is 2000 W, the absolute maximum voltage ranges from 0-600 Vdc(360 Vdc nominal), power tracking is from 90-580 Vdc( 360 Vdc nominal), nominal ac voltage ranges from single phase 211-264 Vac, the nominal AC frequency is 59.3 to 60.5 Hz, the line power factor is 1, ac current distortion is less than 2.5% THD at rated power with sinewave voltage, the maximum efficiency is 94%.

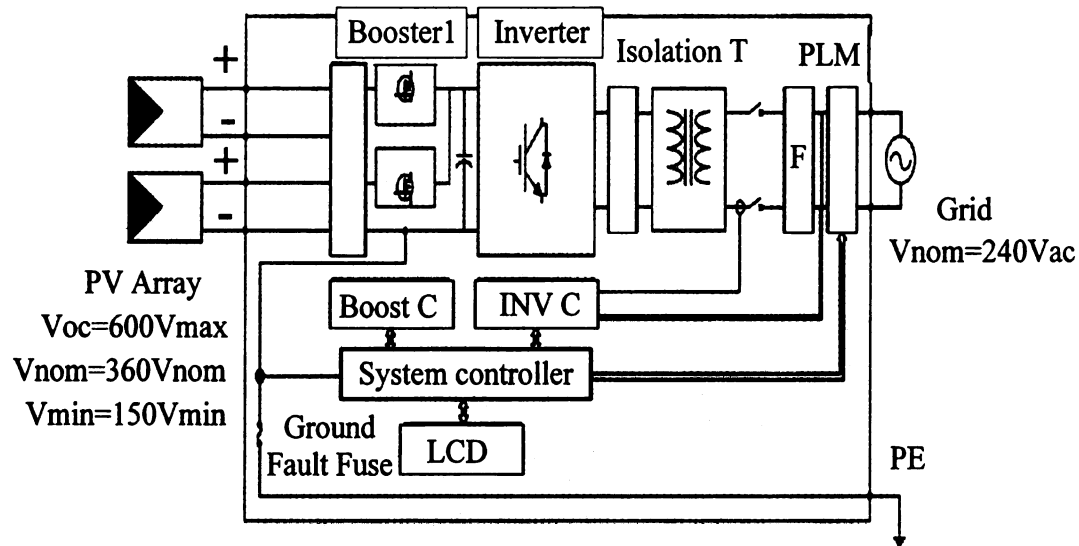


Figure 3.30: AURORA isolated outdoor model: PVI 2000-I-OUTD-US [51].

- **PV Powered**

Figure 3.31 shows PV Powered StarInverter topology. For PVP2000-120, dc input range is 135-450 Vdc, dc operating voltage ranges from 135-320 Vdc, operating ac voltage ranges from 106-132 Vac, operating frequency ranges from 59.3-60.5 Hz, nominal ac output voltage is 120 Vac.

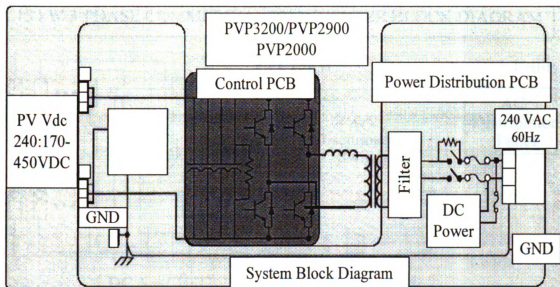


Figure 3.31: Starinverter PCS [52].

- **SOLECTRIA**

Figure 3.32 shows PVI13KW inverter topology. This inverter is used in 5-13 kW, 60 Hz, 208 Vac, 480 Vac, 3 phase, grid tied commercial PV systems. Multiple PVI13KW inverters can be used together for 20-26, 38, 52 kW (ac) or larger PV systems. Fully integrated design includes transformer, filters, ac & dc disconnects, dc combiner-fuses. The maximum continuous power is 13.2 kW, power factor is unity, ac output voltage is 208/480 Vac, THD is less than 5%, ac frequency is  $60 \pm 1$  Hz, the inverter peak efficiency is 94%, the MPPT voltage ranges from 225-385 Vdc.

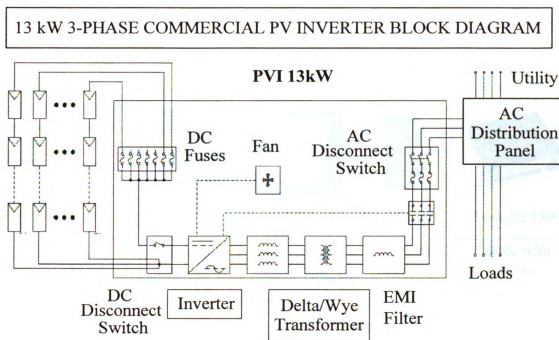


Figure 3.32: PVI13KW inverter system [53].

Also, micro inverter is a type of grid-tie inverter. These inverters are small, usually less than 500 W, and are mounted directly on a solar module or in close to it. This type of inverter reduces the amount of dc wiring and protective equipment used in a PV installation. Xpower Micro inverters-800 has the continuous ac output power 640 W, ac output voltage is 120 Vac nominal, ac output frequency is  $60 \pm 4$  Hz, dc input voltage range is 10.5-15.5 Vdc. This inverter has a wide application for cell phone, camcorder, stereo, etc.

Inverter manufactures are developing new products to compete in the rapidly growing North American grid tie PV markets. There are a lot of PV inverters in the market as summarized in the following table.

Table 3.1: Manufacture PV inverters.

(Xantrex, Ballard, Beacon, Phoenixtex Power [44-46, 53])

PV commercial inverter				
	Xantrex PV Series PV10	Ballard Ecostar	Beacon M5	Sunville 1500
PCS topology	dc/ac with transformer	dc/ac with transformer	dc/dc with dc/ac	dc/dc with dc/ac
Ac output voltage range			106-132 Vac	196-253 Vac
Ac output voltage nominal	208 Vac	208 Vac	120 Vac	
Dc input voltage		290-595 Vdc	48-110 Vdc	360 Vdc nominal
Ac frequency	60+0.5/- .7Hz	60 Hz	60 Hz nominal	50/60 Hz
power factor	>0.99	0.99		>0.99
THD	<5%	<4%	<3%	<3%
MPPT range	330-600 Vdc	240-600 Vdc	50-85 Vdc	150-450 Vdc
Efficiency	>95% (peak)	94.6% (peak)	93% (peak)	93%-95%
Battery			48 V	
Con.power rating	10 kW	30 kW	5 kW	1500 W
Weight	115lb/52kg	430lb,375lb	120lb/54.5kg	8.5 kg
Dimensions(cm)	66*41*30	104*107*41	107*41*26	31.5*26.9*12

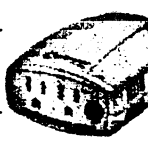
Table 3.2: Manufacture PV inverters.

(FRONIUS, Studer, SMA [47-49])

PV commercial inverter				
	FRONIUS IG 2000	Studer AJ500	Sunny Boy 1100U	SunnyCentral SC125U-240
PCS topology	dc/ac	dc/ac with transformer	dc/ac	dc/ac with transformer
Ac output voltage range	212-264 Vac	219-242/109-121 Vac	213-262 Vac	212-264 Vac
Ac output voltage nominal	240 Vac	230/115 Vac	240 Vac	240 Vac
Dc input voltage	270Vdc nominal	10.5-16 Vdc	129-400 Vdc	275-600 Vdc
Ac frequency	59.3-60.5 Hz	50/60Hz±0.05%	59.3-60.5 Hz	59.3-60.5 Hz
power factor	1		1	1
THD	<5%		<4%	<3%
MPPT range	150-400 Vdc		145-400 Vdc	275-550 Vdc
Efficiency	94.40%	93%	93%	95.70%
Battery		12 V battery		
Con.power rating	1800 W	400 W	1100 W	125 kW
Weight	26lb/11.8kg	4.5kg	56.26lb/21kg	3307lb/1500 kg
Dimensions(cm)	47*41.8*22.3	14.2*8.4*24	32.2*32*18	235*150*60

Table 3.3: Manufacture PV inverters.

(Magnetek, PV Powered, Solectria, Xantrex [50-53])

PV commercial inverter				
	Aurora PVI-2000-I-OUTD	PV Powered PVP2000-120	Solectria PVI13KW	Xpower Micro Inverter800
PCS topology	dc/dc with dc/ac with transformer	dc/ac with transformer	dc/ac with transformer	dc/ac with flyback
Ac output voltage range	single phase 211-264 Vac	106-132 Vac		
Ac output voltage nominal		120 Vac	208/480 Vac	120 Vac
Dc input voltage	0-600Vdc (360nominal)	135-500 Vdc		10.5-15.5Vdc
Ac frequency	59.3-60.5 Hz	59.3-60.5 Hz	60Hz±1Hz	60Hz±4Hz
power factor	1		1	
THD	<2.5%		<5%	
MPPT range	90-580 Vdc	135-360 Vdc	225-385 Vdc	
Efficiency	94.00%	93%	94%	90.00%
Battery				Yes
Con.power rating	1500 W	2000 W	1320 W	640 W
Weight	25kg	76lb	380lb/173kg	11b4oz/852g
Dimensions(cm)	42*32.6*23.2	38.1*19.1*55.3	87.6*66*34.5	19.1*11.4*6.1

# **CHAPTER 4. Z-SOURCE INVERTER BASED POWER CONDITIONING SYSTEM**

## **4. 1. Introduction**

With the development of solar cell technology, the price of solar module has dropped dramatically. Recent worldwide survey shows that in last three years, the retail price of solar module has dropped 16.95%. However, at the same time, the prices for the PCSs almost remain the same. Further more, compared with converters used in drive systems, the prices for the converters used in PV systems are still up to 50% higher. To lower the cost of the PCSs has become a very urgent issue of grid connected PV system [1].

PCS is required to convert the dc output from PV to grid synchronized 50 or 60 Hz ac. Here a Z-Source inverter based PCS, which connects the PV arrays for residential systems that are 60 Hz, 120/240 V split phase power in the US was proposed. By utilizing the Z-Source inverter, the number of switching components and the total volume of the system can be minimized. Moreover, the Z-Source inverter makes it possible to use PV that has a wide range voltage change. Thus the cost of the PCS is minimized.

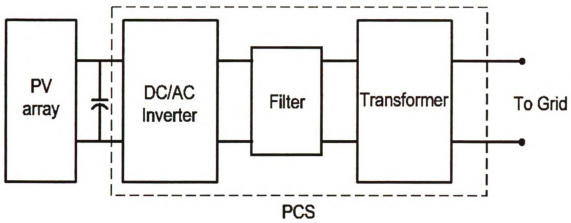
## 4. 2. The Basics Of PCS For Residential Use

In order to feed energy from a PV array into the utility grid, PCS converter system has to fulfill the following three requirements:

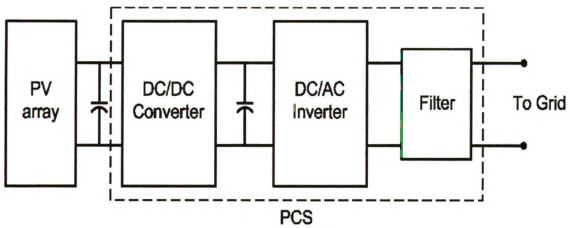
- 1) to convert the dc voltage into ac voltage;
- 2) to boost the voltage, if the PV array voltage is lower than the grid voltage; and
- 3) to insure the maximum power utilization of the PV modular.

Figure 4.1 shows the two most commonly used converter system configurations in practice. In the system shown in Figure 4.1(a), a transformer at line frequency is utilized to boost the voltage after the dc-ac inverter. Usually, a line frequency transformer is associated with huge size, loud acoustic noise, and high cost. In addition, the inverter has to be over-sized to cope with the wide PV array voltage change. The KVA rating of the inverter is doubled if the PV voltage varies at a 1:2 range. So to eliminate the transformer and to minimize the required KVA rating of the inverter, in many applications, a high frequency dc/dc converter is used to boost the voltage to a constant value as shown in Figure 4.1(b). Unfortunately, the switch in the dc-dc converter becomes the cost and efficiency killer of the system [2-3].

Another option is to use a single-stage inverter for direct dc-ac conversion as shown in Figure 4.2. For the split-phase system used in US residential power, two 120 V ac outputs with the same ground and 180 degree phase difference are required. For this purpose, there are two circuit choices for the dc/ac inverters in the PCS: four-switch inverter and six-switch inverter. The circuit structures of these two choices are shown in Figure 4.2.

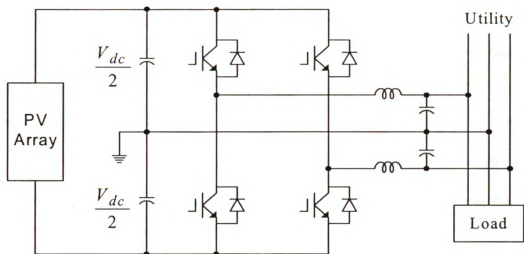


(a). Dc/ac with step-up transformer.

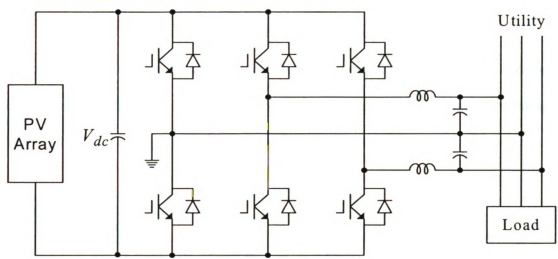


(b). Dc/ac with dc-dc boost.

Figure 4.1: The traditional PV systems.



(a). Four switch inverter.



(b). Six switch inverter.

Figure 4.2: Direct PV inverter systems for  $\pm 120$  V split phase residential power.

For the four-switch inverter as shown in Figure 4.2 (a), the neutral point is tapped from the center of the two dc capacitors, whereas in six-switch inverter shown in Figure 4.2 (b), the neutral point is connected to the third phase leg.

The two phase legs in the four-switch inverter are controlled by SPWM. Two sinusoidal control references with a 180 degree phase difference and the same amplitude are utilized to compare with a triangular carrier.

The basic control scheme of the six-switch inverter is shown in Figure 4.3. Two of the phase legs, "b" and "c", have the exact same SPWM control as in four-switch inverter. The third phase leg, "a", is usually controlled to produce a square waveform with 50% duty ratio at the carrier frequency to serve as the neutral phase and at the same time achieve the maximum utilization of the dc bus voltage. The switching frequency of the third leg can be different from the other two phase legs. By proper coordinating the control of the neutral phase leg and the other two phase legs, the equivalent switching frequency can be doubled, thus the output filter can be optimized. It is generally believed that the six-switch inverter has better performance than the 4-switch inverter for the split-phase application [4].

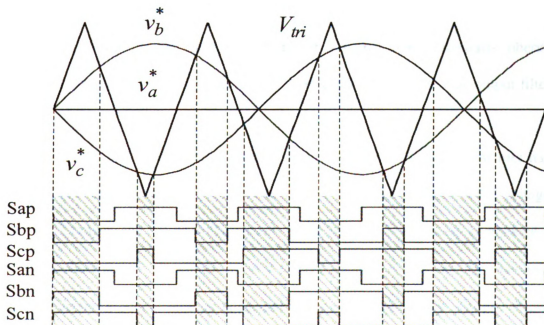


Figure 4.3: The six-switch inverter control scheme.

### 4. 3. The Proposed Z-Source Inverter System

In the proposed PCS, a Z-Source inverter [5] is utilized to realize inversion and boost function in one single stage. Figure 4.4 shows the proposed system. Unlike the traditional voltage source or current source inverters, the Z-Source inverter employs a unique impedance network with split inductor  $L_1$ ,  $L_2$  and capacitor  $C_1$ ,  $C_2$  connected in X shape. With the impedance network, the Z-Source inverter can advantageously use the shoot through states to boost voltage. Further more, with the ability to handle shoot through state, the inverter system becomes more reliable [5-6]. The inductors and capacitors in the Z-Source are both energy storage devices, so their value can be optimally designed to ensure small size and low cost.

Compared with the systems in Figure 4.1, in the proposed system, there is neither bulky transformer nor a dc-dc converter to boost the voltage in the circuit. The size and cost are minimized. Because no dead time is needed, the control accuracy and harmonics can also be improved. Further more, the split-phase Z-Source inverter naturally inherits all the advantages of the split-phase six-switch inverter. Thus, the 120 V ac output filter can be optimized.

Compared with the direct inverter systems in Figure 4.2, the Z-Source inverter has minimum KVA requirement. For the inverter system in Figure 4.2 with a PV voltage change of 1:2 ranges, the PV dc voltage needs to be 340-680 V minimum to produce a  $\pm 120$  V split-phase power. Therefore, 1200 V IGBTs are needed in the system. Given a 10 kW PV system, a 20 kW inverter is needed to cope with the voltage change. Using the proposed system of Figure 4.4, the PV voltage can be designed to be 225-450 V,

which can be inverted to  $\pm 120$  V split-phase power by the Z-Source inverter using 600 V IGBTs. In addition, the required KVA rating of the Z-Source inverter remains the same 10 kW for a 10 kW PV system.

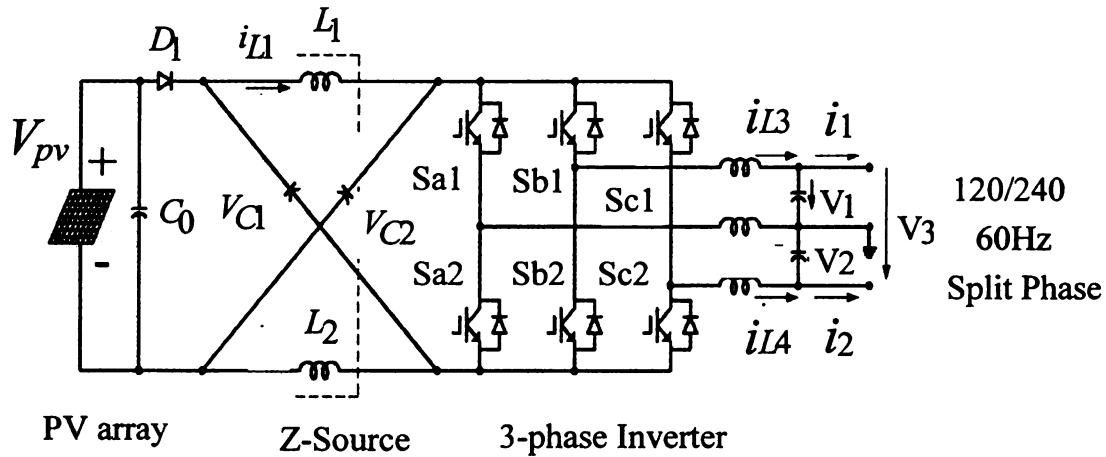


Figure 4.4: The proposed PCS for stand-alone PV system.

Therefore, by utilizing the Z-Source inverter, the volume, the cost as well as the number of active switching devices are minimized. Because of the single stage operation, the efficiency of the system can be greatly improved. The proposed system:

- 1) has only one stage to realize inversion, boost, and maximum power tracking;
- 2) has the minimized number of switching devices;
- 3) needs no dead time;
- 4) can have shoot through state in the inverter; and
- 5) inherits all the advantages of the six switch inverter system.

## 4. 4. Control And Operation Principle

As shown in Figure 4.3, when the triangular waveform is greater than the maximum value or lower than the minimum value of the three reference waveforms, all upper three switches or all bottom three switches are turned on respectively, as indicated in the shadowed area. During these periods of time, the output voltage of the inverter is zero, i.e., zero states. For the Z-source inverter, the basic idea of control is to turn zero states into shoot through states and keep the active switching states unchanged, thus we can maintain the sinusoidal output and at the same time achieve voltage boost from the shoot through of the dc link [5-6].

Figure 4.5 shows the boost control method of the split-phase Z-Source inverter. Phase legs “b” and “c” are controlled by SPWM to synthesize ac output, and the shoot-through command,  $V_{sp}^*$  and  $V_{sn}^*$  is used to boost voltage as desired. The control of these two phase legs is similar to the simple boost control proposed in [5] and [6]. Two straight lines,  $V_{sp}^*$  and  $V_{sn}^*$  are used to control the shoot through duty ratio. When the carrier is greater than the upper straight line, phase leg “b” goes to shoot through state, whereas phase leg “c” goes to shoot through state when the lower straight line is greater than the carrier. Phase “a” in the inverter is switching at 50 percent duty cycle without shoot through. The switching frequency of phase “a” is the frequency of the carrier. By doing this, each phase leg only shoots through once during one carrier cycle, the equivalent switching frequency can be doubled for the output filter.

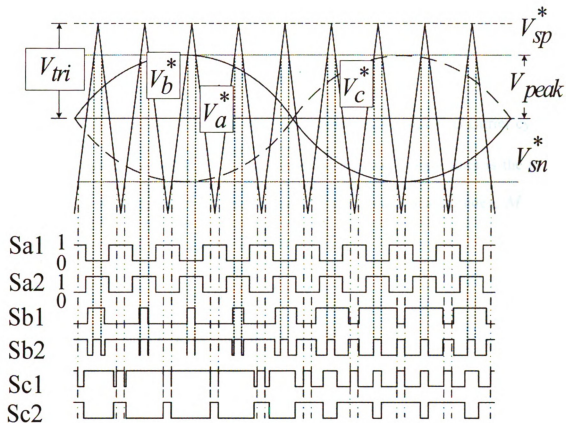


Figure 4.5: Sketch map of the simple boost control.

As described in [5] and [6], the inductors  $L_1$  and  $L_2$ , which can be wound around the same core, have the same inductance, and the capacitors  $C_1$  and  $C_2$  have the same capacitance, the relationship between the output ac voltage and input dc voltage is found as

$$\hat{v}_O = MB \cdot V_{pv} / 2, \quad (4.1)$$

where  $\hat{v}_O$  is the output peak voltage,  $V_{pv}$  is the PV output voltage,  $M$  is the modulation index, which is defined by

$$M = V_{peak} / V_{tri}, \quad (4.2)$$

and  $B$  is the boost factor, which is determined by

$$B = \frac{1}{1 - 2 \cdot T_0 / T}, \quad (4.3)$$

where  $T_0$  is the total shoot-through period per carrier cycle, and  $T$  is carrier cycle. In the simple control method [5,6], the amplitude of the two straight lines is the peak of modulation waveform, therefore the relationship between modulation index,  $M$  and the shoot through ratio,  $T_0 / T$  can be found as

$$T_0 / T = 1 - M. \quad (4.4)$$

Substituting (4.4) into (4.3), the boost factor becomes:

$$B = \frac{1}{2M - 1}. \quad (4.5)$$

From (4.1), and (4.5), the peak amplitude of the output can be expressed as

$$\hat{v}_o = \frac{M}{2(2M - 1)} V_{pv}. \quad (4.6)$$

While the capacitor voltage is:

$$V_{C1} = V_{C2} = \frac{1 - \frac{T_0}{T}}{1 - 2 \frac{T_0}{T}} V_{pv} = \frac{B + 1}{2} V_{pv}. \quad (4.7)$$

When the PV output voltage value is high enough to produce the required ac voltage, the shoot through state is no longer needed, i.e.,  $T_0 = 0$  and  $B = 1$ . Under this condition, the relationship between the inverter peak output voltage and the PV output voltage can be calculated by

$$\hat{v}_o = MV_{pv}/2. \quad (4.8)$$

It also should be noted that the shoot-through states can be created by shorting both legs “b” and “c”, or all the three legs simultaneously during any given shoot through states according to the two straight lines. For all these shoot-through cases, the resulted boost effect and output voltage waveforms remain the same.

In the proposed control scheme, only one phase leg is used to create shoot through at any time, thus minimizing the switching frequency. However, at the same time, the current stress on each switch during shoot through is doubled when compared with shooting through two phase legs simultaneously at any time. A trade off in the control must be made, one can

- 1) either reduce the switching frequency by shorting one or two phase legs; or
- 2) reduce the current stress on each device by shorting all phase legs during shoot-through periods.

To make a decision in real applications, the switching and conduction losses at different conditions need to be calculated and investigated for different cases.

## 4. 5. Design Guideline

In the Z-Source based PCS, the maximum voltage over phase legs  $V_{pn}$  is controlled to maintain the split phase output at different input voltages. For 120 V split phase output, PV cell with maximum output voltage of 450 V can be used. Assume the minimum output voltage is half of the maximum voltage, to achieve the same output ac

voltage of 120 V, the device voltage stress can be calculated by manipulating (4.5) and (4.6), which results

$$V_{pn} = BV_{pv} = 455. \quad (4.9)$$

Thus, 600 V device can be used.

The maximum current stress on the device can be simply calculated based on the following equation

$$I_{\max} = \frac{P_{\max}/2}{V} + 2I_L = \frac{P_{\max}/2}{V} + 2\frac{P_{avg}}{V_{pv}}. \quad (4.10)$$

Where  $I_L$  is the Z-source inductor current,  $P_{\max}$  is the maximum transient output power, and  $P_{avg}$  is the average output power. The current stress can be reduced by turning on two or all phase legs during shoot through to distribute the  $2I_L$  into different phase legs.

To determine the inductance and capacitance of the Z-Source network, the input power is assumed to be constant dc. The ripple power is absorbed by the capacitors of the Z-Source network. The power ripple absorbed by the capacitors is calculated

$$\Delta P = P \int_{-\frac{1}{480}}^{\frac{1}{480}} \cos(120 * 2 * \pi) t dt = \frac{1}{2} C (V + \Delta V)^2 - \frac{1}{2} C V^2, \quad (4.11)$$

where  $V$  is the average voltage across the capacitor,  $C$  is the total capacitance of two capacitors in the Z-source. To limit the voltage ripple to be less than  $x\%$ , the capacitor value can be calculated.

Based on the voltage ripple across the capacitors, the ripple voltage across the inductor is the voltage difference between the capacitor and the voltage across the PN. The capacitor voltage is already known with  $x\%$  ripple. The PN voltage is zero during shoot through and  $2V_C - V_{pv}$  for others. Assume the input voltage is a constant dc value, the PN voltage ripple is  $2V_C D_0$ , therefore, the voltage ripple across the inductor is

$$V_{ripple} = (1 - \frac{2T_0}{T}) * x\% * V . \quad (4.12)$$

To limit the ripple to a special percent, the inductance can be determined.

#### 4. 6. Simulation And Experiment Results

Photovoltaic solar cells have nonlinear V-I characteristics. Its output voltage and power change according to temperature and irradiation. Figure 4.6 shows the typical V-I characteristics for a PV module. For a specified temperature and irradiation, the intersection of the load line with the photovoltaic voltage-current characteristic, is the operation point. In real practice, PV modules are first cascaded then paralleled to form PV array, thus to meet the voltage and power requirement.

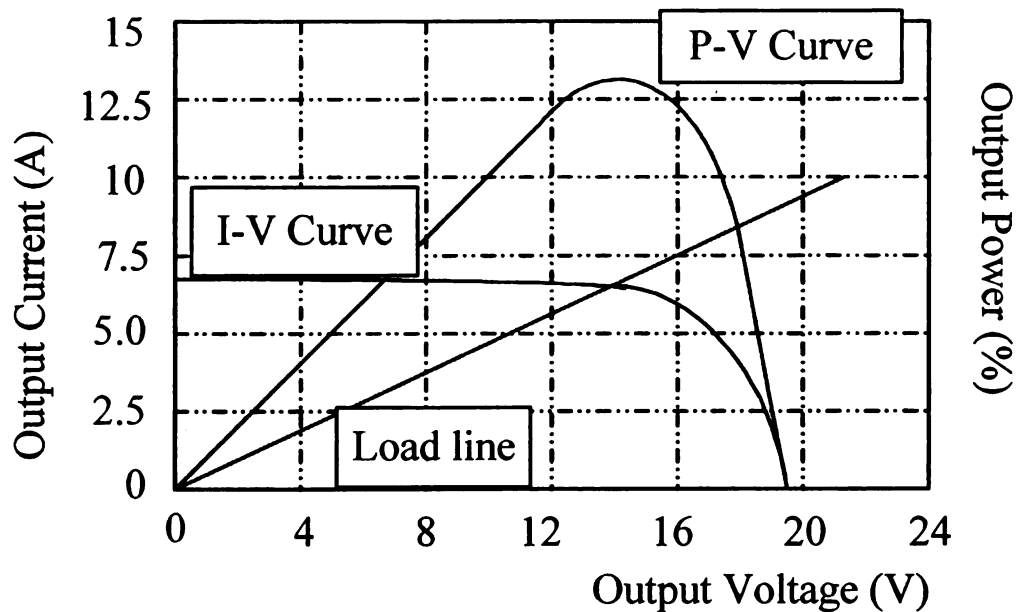


Figure 4.6: Typical V-I and P-V characteristics.

Figure 4.7 shows the V-I curves of PV array at different temperatures and irradiancies. Usually the photovoltaic output voltage changes mainly with the temperature, while the photovoltaic output current changes mainly with the irradiation. With constant irradiation specified, the PV output power decreases when the temperature rises. With constant temperature specified, the PV output power increases when the irradiation increases. One of the functions of the PCS is to extract the maximum power out of the photovoltaic at any given temperature and irradiation. Based on the curves shown in Figure 4.7, simulations and experiments are performed to prove the concept proposed in this thesis at the following two conditions:

- 1) at  $1000 \text{ W/m}^2$ , and  $60 \text{ }^\circ\text{C}$ ,  $V_{pv}=230 \text{ V}$ , the maximum PV output power is  $7200 \text{ W}$ ;

2) at  $250 \text{ W/m}^2$  and  $0^\circ\text{C}$ ,  $V_{PV}=450 \text{ V}$ , the maximum PV output power is  $3360 \text{ W}$ .

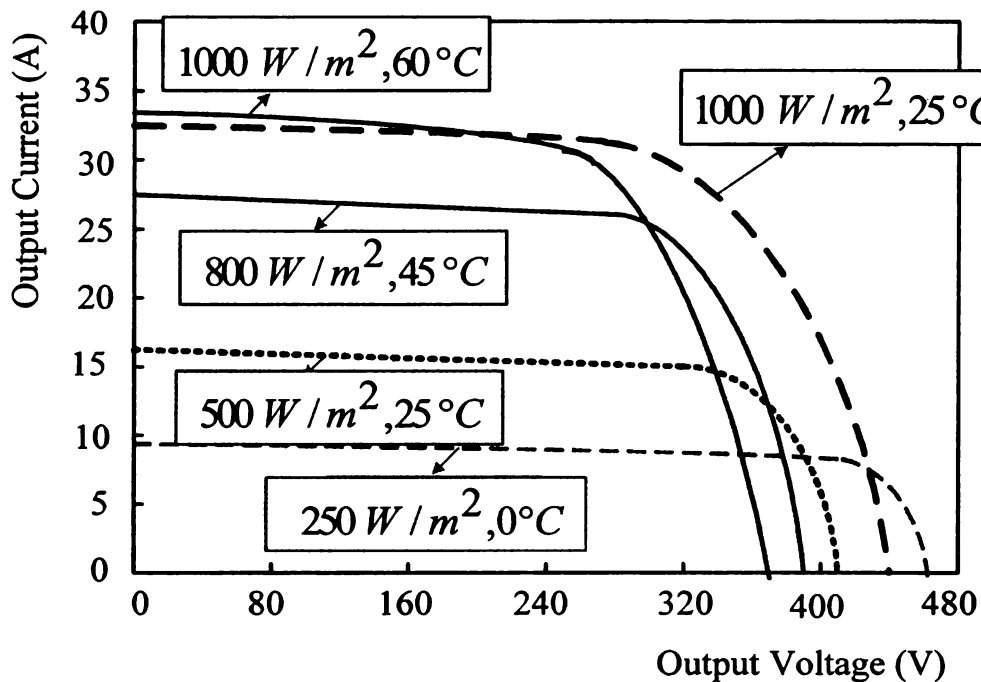


Figure 4.7: V-I characteristics under different conditions.

For both cases, the simulation and experimental systems are setup with the following parameters:  $L_1 = L_2 = 1 \text{ mH}$  at the line frequency and  $C_1 = C_2 = 13,300 \text{ }\mu\text{F}$ . The switching frequency is 10 kHz. Z-source inverter produces PWM voltage waveforms just like the traditional inverter. Thus, a LC filter is added after the inverter to achieve sinusoidal waveform. The filter parameters are  $L = 1 \text{ mH}$  and  $C = 120 \text{ }\mu\text{F}$ . We assume that output voltage range of PV arrays is 1:2. So 600 V IGBTs, which has maximum dc voltage as 450 V, was used to operate in 225-450 V in experiments. Resistive load is used for the simulations and experiments. For case one,  $4 \text{ }\Omega$  is used for

each phase, whereas  $8.57 \Omega$  is used for case 2. A 10 kW Z-Source inverter prototype used in the experiment is shown in Figure 4.8.

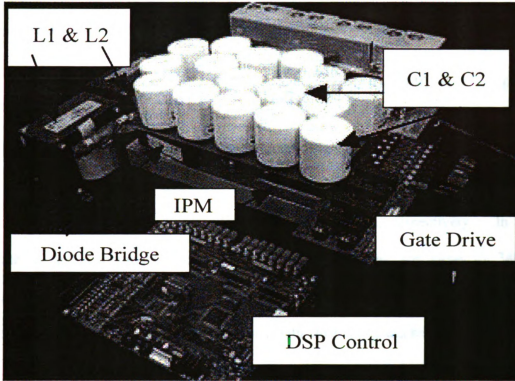


Figure 4.8: A 10 kW Z-Source inverter prototype.

*Case 1:*  $1000 \text{ W/m}^2$  and  $60^\circ \text{C}$ ,  $V_{pv} = 230 \text{ V}$

For the first case, the input voltage,  $V_{pv}$ , is 230 V, to achieve 120 V split phase output, the modulation index can be calculated by the following equation, which is the inverse of (4.6):

$$M = \frac{2\hat{v}_o}{4\hat{v}_o - V_{pv}} = \frac{2 \times \sqrt{2} \times 120}{4 \times \sqrt{2} \times 120 - 230} = 0.755 \quad (4.13)$$

The boost factor is

$$B = \frac{1}{2M - 1} = 1.961. \quad (4.14)$$

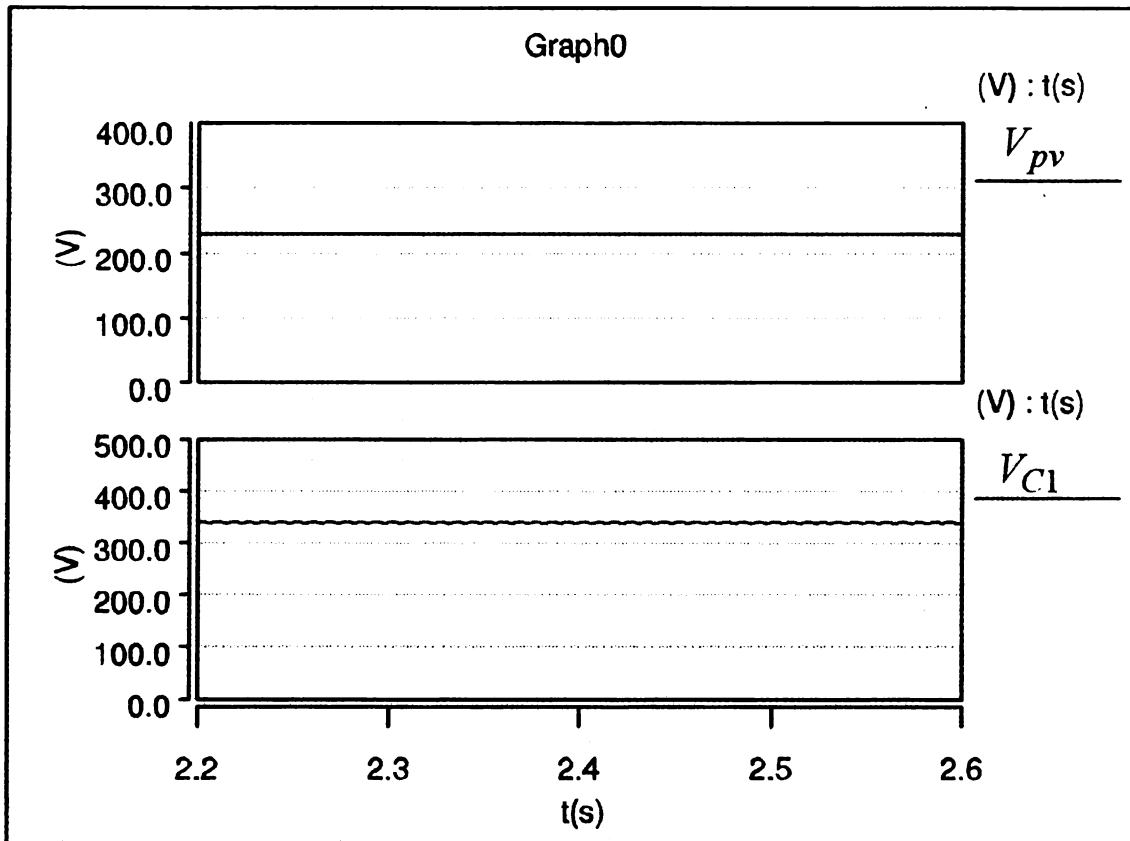
Thus the shoot through duty cycle  $T_0/T$  can be calculated from (4.3), which will result a  $T_0/T$  equals to 0.245. The Z-Source capacitor voltage would be

$$V_{C1} = V_{C2} = \frac{1 - T_0/T}{1 - 2T_0/T} V_{pv} = \frac{1 - 0.245}{1 - 2 \times 0.245} 230 = 340 \text{ V}. \quad (4.15)$$

Figure 4.9 and Figure 4.10 show the simulation and experimental results of case 1. Figure 4.9(a) and Figure 4.10(a) show the simulation and experimental waveform of the input voltage and Z-Source capacitor voltage waveforms, respectively. In both simulation and experimental results, the capacitor voltages are close to 340 V. Meanwhile as shown in Figure 4.9(b) and Figure 4.10(b), the simulation and experimental results of the output voltages are both close to the desired split phase 120 V rms. The output power can be calculated based on the output voltage and the load current waveforms, which are also shown in Figure 4.9(b) and Figure 4.10(b). As the load current is 30 A, the total output power of the inverter is around 7200 W. Thus the maximum power output from the PV at this condition is realized. Figure 4.9(c) and Figure 4.10(c) show the output filter inductor and Z-Source inductor current. The Z-source inductor average current is around 31 A, which on the other hand, proofs again that the PV outputs its maximum power. Both the simulation and experimental results are consistent with the theoretical calculations.

Figure 4.9: Simulation results of case 1 under the conditions of

$1000 \text{ W/m}^2$ ,  $60 \text{ }^\circ\text{C}$ , and  $V_{pv}=230 \text{ V}$ .

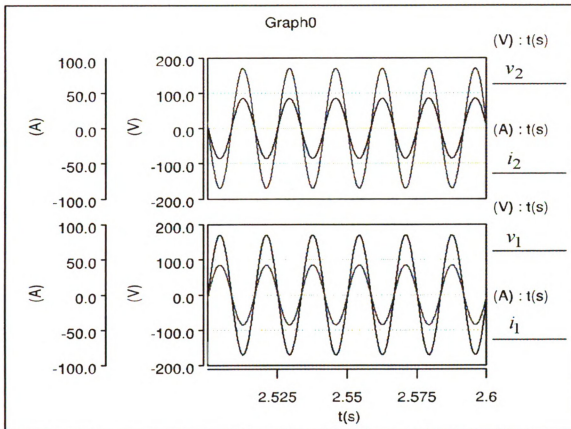


(a). Input Voltage and Z-Source capacitor voltage.

(A)

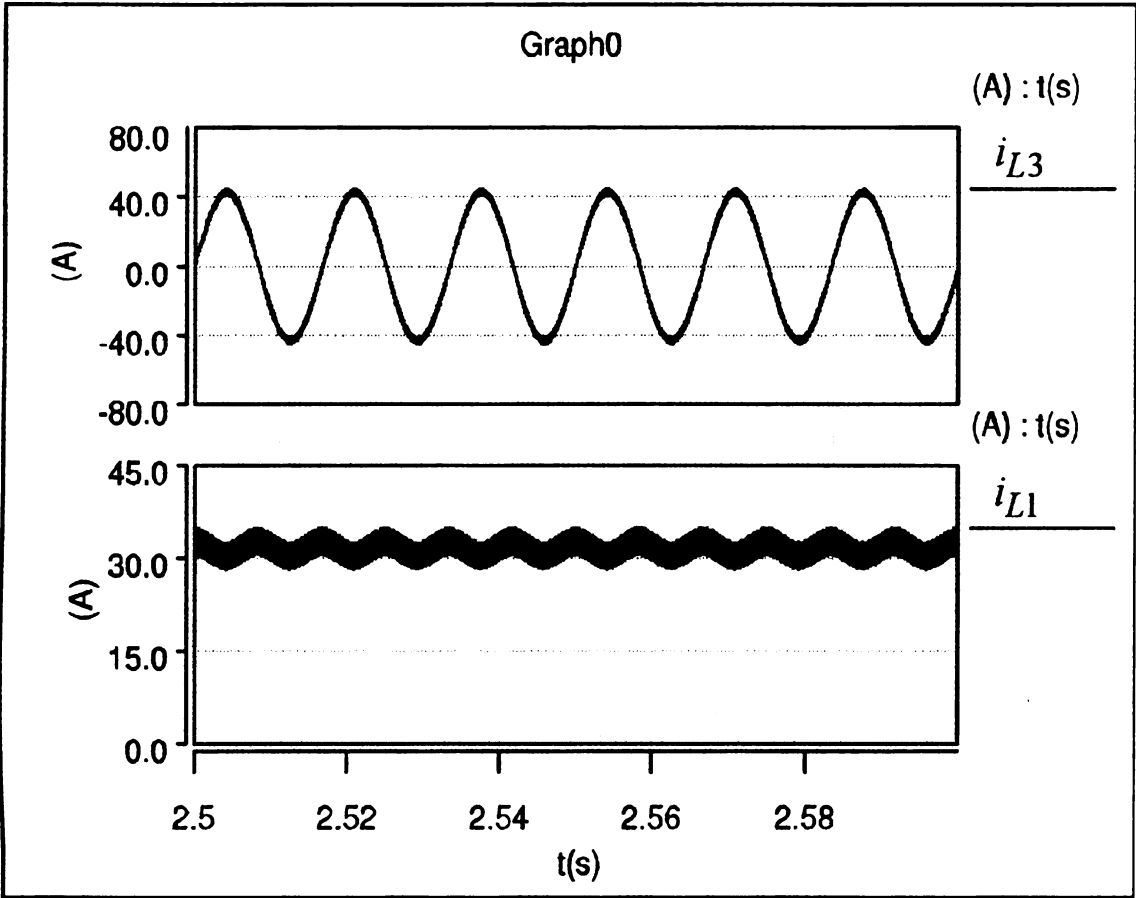
(A)

Figure 4.9 Continues:



(b). Load voltages and currents.

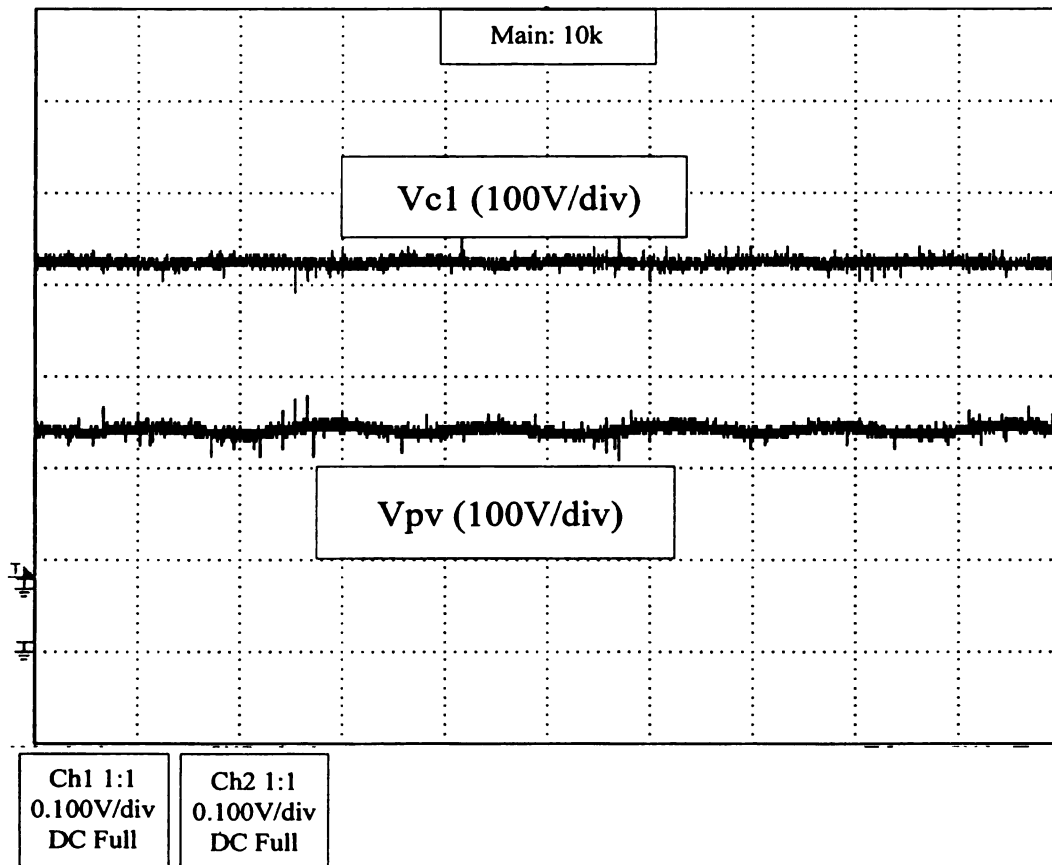
Figure 4.9 Continues:



(c). Filter inductor current and Z-Source inductor current.

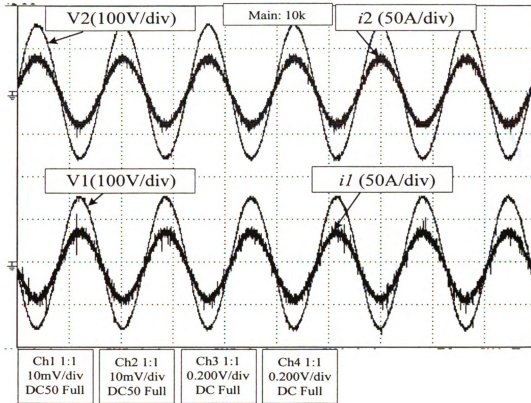
Figure 4.10: Experimental results of case 1 under the conditions of

$$1000 \text{ W/m}^2, 60^\circ \text{C}, \text{ and } V_{pv} = 230 \text{ V}.$$



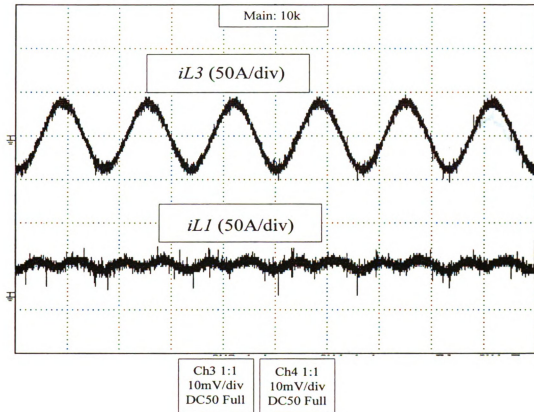
(a). Z-Source capacitor voltage and Input Voltage.

Figure 4.10 continues:



(b). Load voltages and currents.

Figure 4.10 continues:



(c). Filter inductor current and Z-Source inductor current.



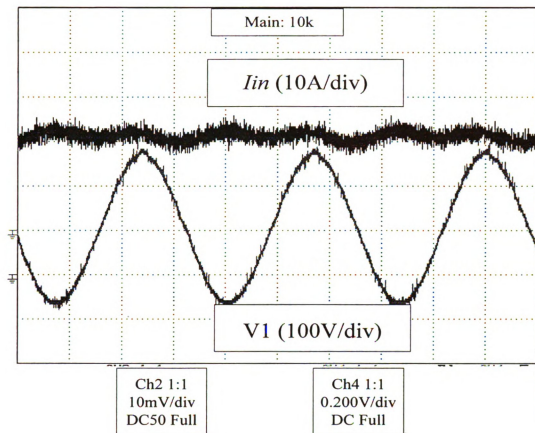
Case

For

strateg

Th

Figure 4.10 continues:



(d). Input current  $I_{in}$  and load voltage.

Case 2:  $250 \text{ W/m}^2$  and  $0^\circ \text{C}$ ,  $V_{pv} = 450 \text{ V}$

For the second case, as the input voltage is much higher,  $V_{pv} = 450 \text{ V}$ , the control strategy is different with the first case. Shoot through is not used for this case.

The modulation index can be calculated as following

$$M = \frac{2\hat{v}_O}{V_{pv}} = \frac{2 \times \sqrt{2} \times 120}{450} = 0.755. \quad (4.16)$$

As n  
capacitor

conditio

Figur

Similar

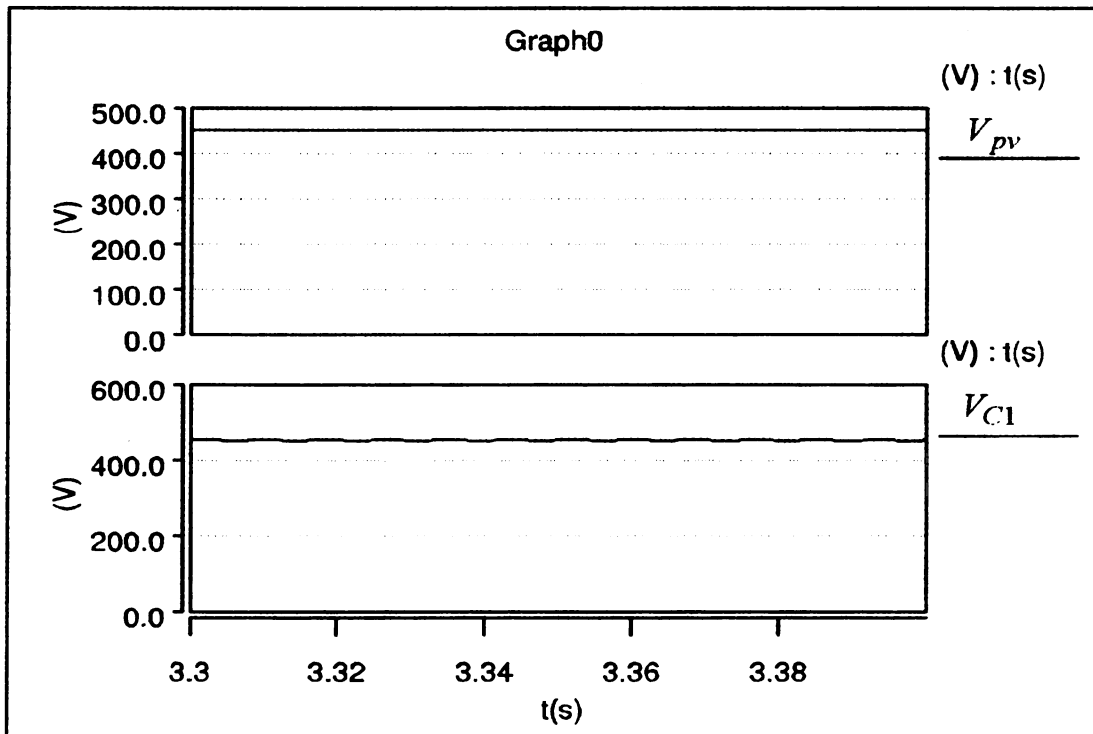
well.



As no boost is needed for this case, the boost factor  $B$  is 1. Thus, the Z-Source capacitor voltage would be the same as the PV voltage, which is 450 V. Under this condition, the theoretical maximum output power from PV is around 3360 W.

Figure 4.11 and Figure 4.12 show the simulation and experimental results of case 2. Similar as in Case 1, the simulation and experimental results also verify the analysis as well.

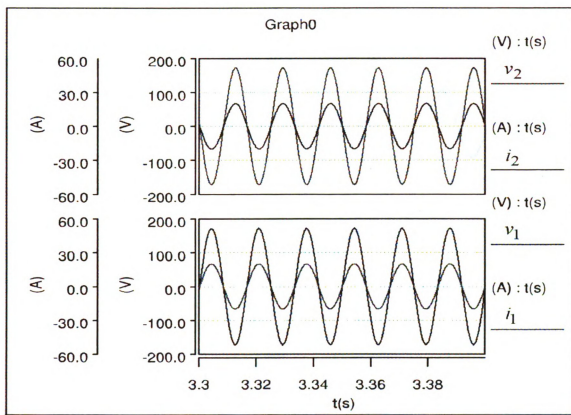
Figure 4.11: Simulation results of case 2 under the conditions of  $250 \text{ W/m}^2$ ,  $0^\circ \text{C}$ , and  $V_{pv} = 450 \text{ V}$ .



(a). Input Voltage and Z-Source capacitor voltage.

6
3
(A)
-3
-6
6
3
(A)
-2
-6

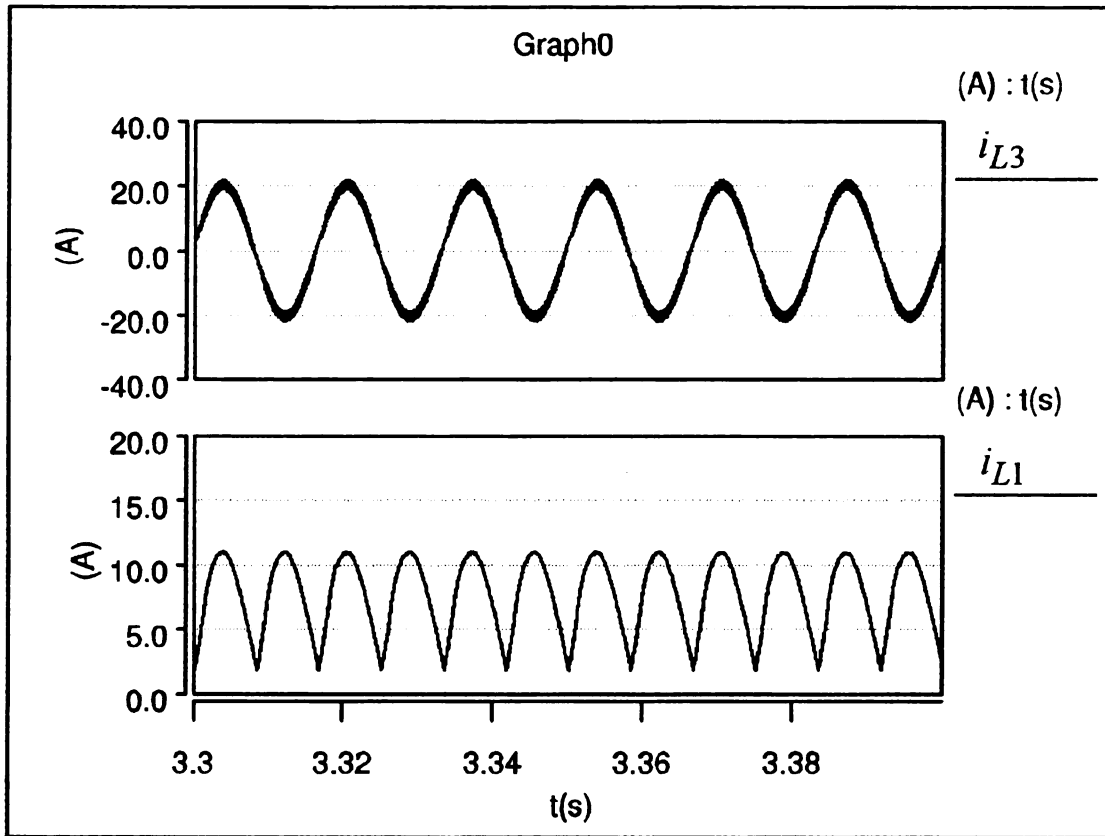
Figure 4.11 continues:



(b). Load voltages and currents.

(A) 4  
2  
-2  
-4  
-6  
(A)

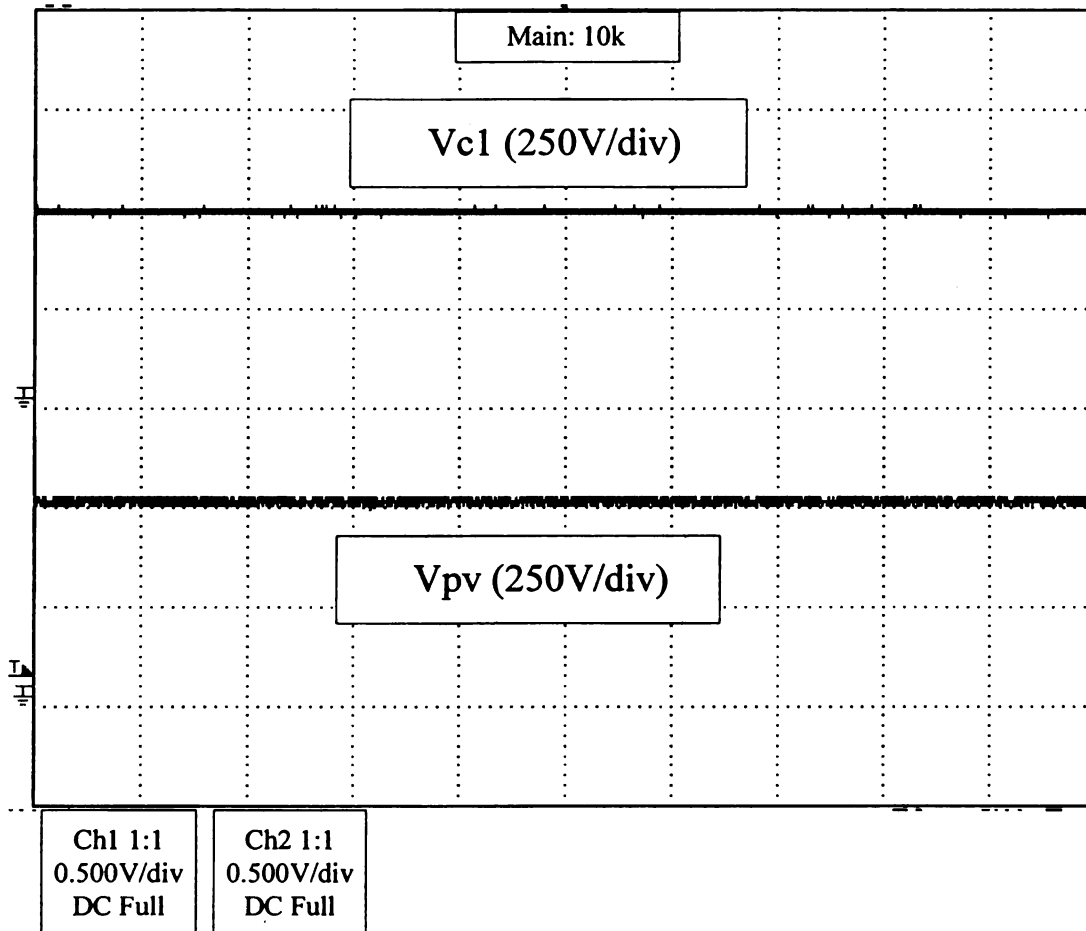
Figure 4.11 continues:



(c). Filter inductor current and Z-Source inductor current.

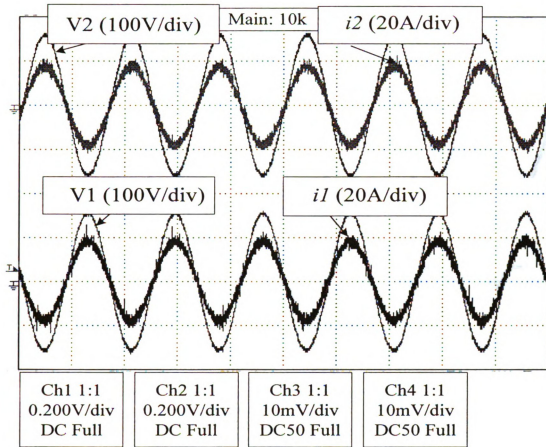
Figure 4.12: Experimental results of case 2 under the conditions of

$250 \text{ W/m}^2$ ,  $0^\circ \text{C}$ , and  $V_{pv} = 450 \text{ V}$ .



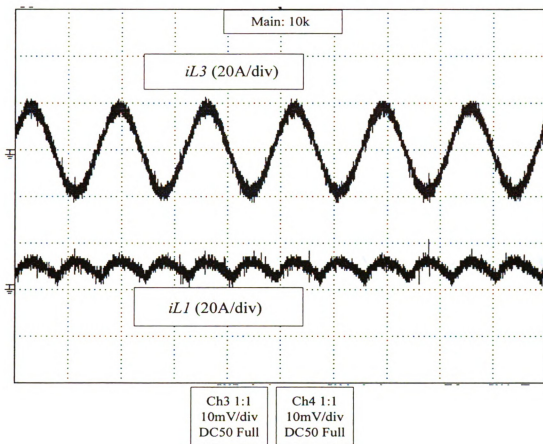
(a). Z-Source capacitor voltage and Input Voltage.

Figure 4.12 continue:



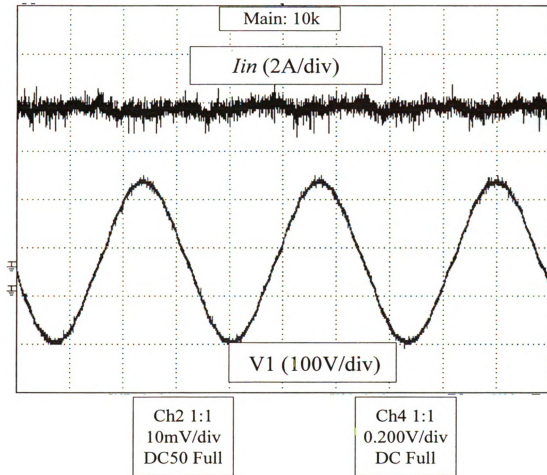
(b). Load voltages and currents.

Figure 4.12 continues:



(c). Filter inductor current and Z-Source inductor current.

Figure 4.12 continues:



(d). Input current  $I_{in}$  and load voltage.

From the above two cases, it can be concluded that the simulation and experimental results show that at different input voltage, the proposed PV system's output voltage maintained at  $\pm 120$  V rms, whereas the output power tracked the maximum PV output power at different temperatures and irradiancies. The basic principle of the proposed system was verified.

4.7. Su

A ne  
propose  
single p  
of Z-S  
togeth  
the ad  
for P

## 4.7. Summary

A new PV power conditioning system based on Z-Source inverter is proposed. The proposed system realizes the boost and inversion with maximum power tracking in one single power stage, thus minimizing the number of switching devices. All the advantages of Z-Source inverter and six-switch split-phase inverter are inherited and integrated together to create a highly reliable PCS system with minimized volume and cost. With the advanced features summarized in section III, the proposed system is very promising for PV power conditioning applications.

O

## 5. 1. In

The  
also on r  
inverter

To e  
range, a  
appropri  
recorde  
unexpe  
simulat  
conditi

# CHAPTER 5. PV SIMULATOR SYSTEM

## 5. 1. Introduction

The PV system performance depends not only on temperatures and irradiations, but also on maximum power tracking function of PV inverter. So it is important to verify the inverter system also.

To evaluate PV inverter system, ideally the inverter need be tested through the entire range, as shown in the Figure 5.1. One method is that inverter is connected to the appropriate size of PV panels in a sunny day, and PV panels' output characteristics are recorded. This method has the disadvantages that the limitations of sized PV panels, the unexpected weather conditions, and the long running time. Another way is to use a PV simulator, which is able to produce repeatable conditions respect of environment conditions.

0.  
0.  
0.  
0.  
0.  
0.  
0.  
0.  
0.  
0.

Module Current (A)

5.2. E

The

but not

low po

core te

charact

techni

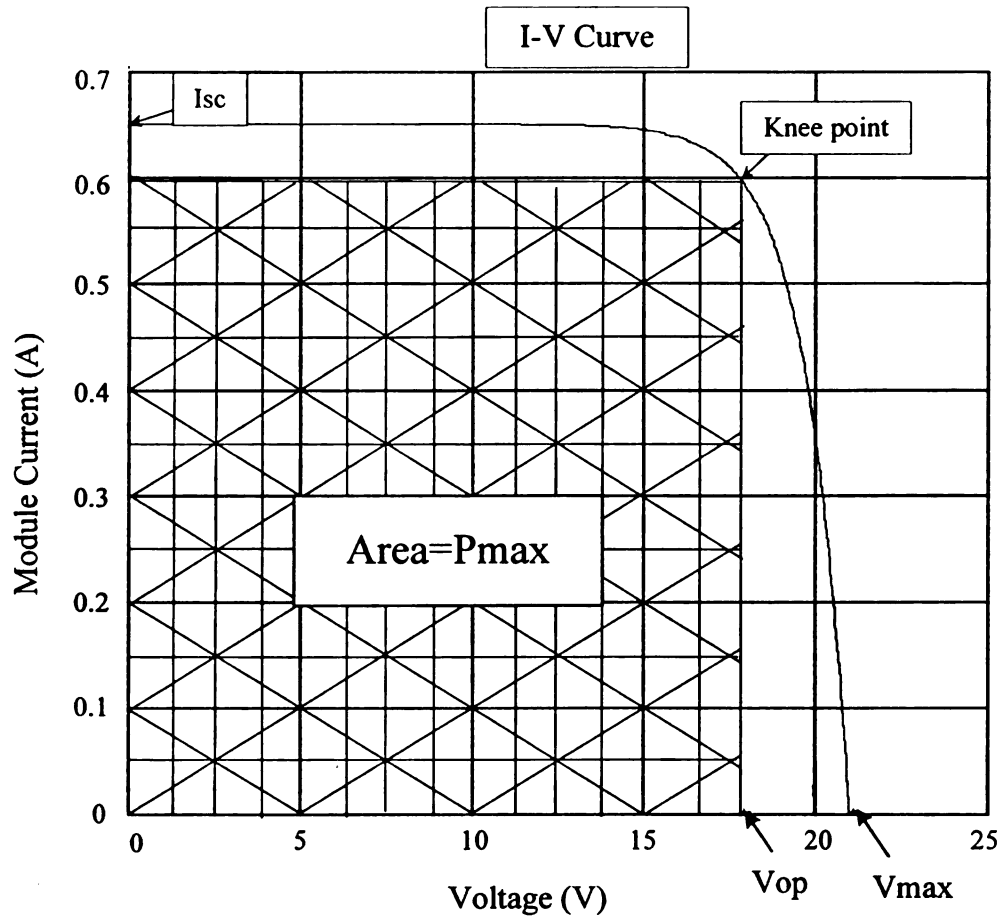


Figure 5.1: Typical PV module curves.

## 5. 2. Previous PV Simulator

There already exist some methods to build up a PV simulator model for simulation, but not too many literatures for hardware implementation. Most of them are capable for low power rating application; some are capable for medium and high power rating. The core technology of the simulator circuits is a control circuit that simulates PV I-V characteristics curves. People can approach it use microcomputers or some other analog techniques.

Figure 5.2 shows a PV simulator concept in [62]. In this paper, a Si and polycrystalline panels with a simulated light source were used. The output current and voltage were recorded as a function time. With the use of class A regulator and switched operation, the fast dynamic response can be achieved. The internal current control which allows additional units to be connected in parallel in order to get higher output currents.

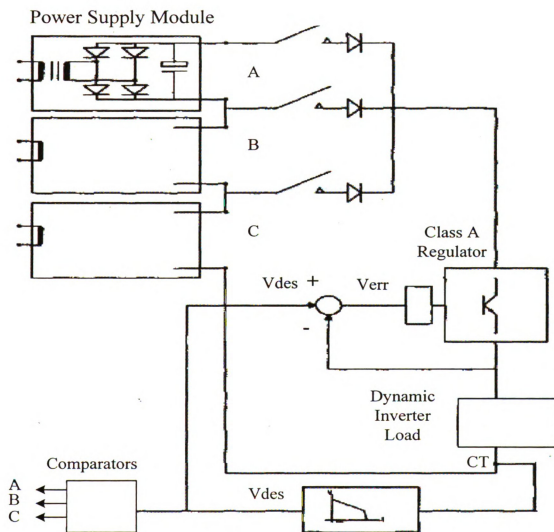


Figure 5.2: PV simulator concept [5].

Figure 5.3 shows a block diagram of the PV generator simulator circuit in [63]. In the circuit, the output of a pn photo sensor, just like a small solar cell, was magnified through a dc power amplifier. The maximum power is around 30 W. But this method is not suitable for high power cases.

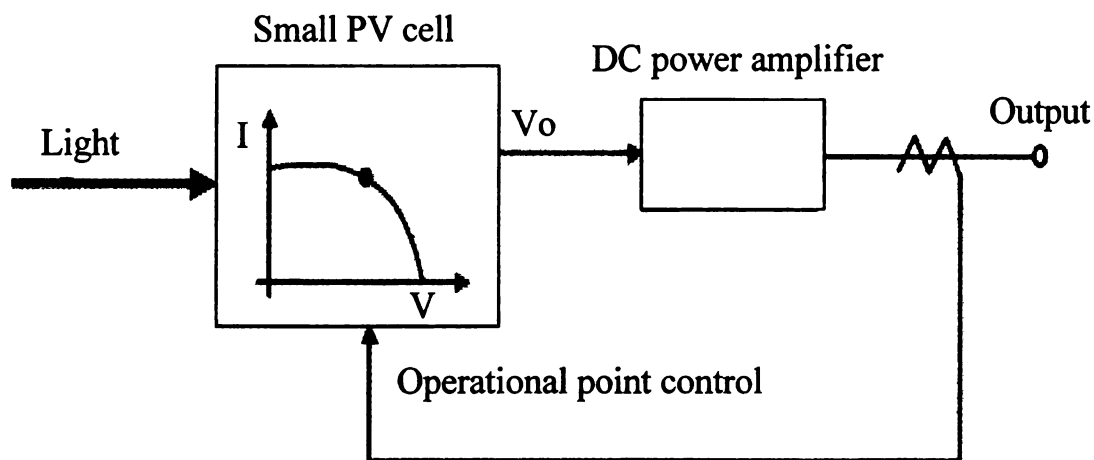


Figure 5.3: Block diagram of the PV generator simulator circuit [63].

Also, some test equipments used lamp to simulate the solar irradiation with its consequent need of huge power for bigger power rating larger than 1 kW, thus to eliminate atmospheric dependency [64]. Others tried to use a current source and a diode chain, which can represent a PV panel through its electrical scheme. But it is still have thermal stability problems and was limited by its diode chain's fill factor. Due to the reasons above, the PV simulator which are applicable for high power was designed in this thesis.

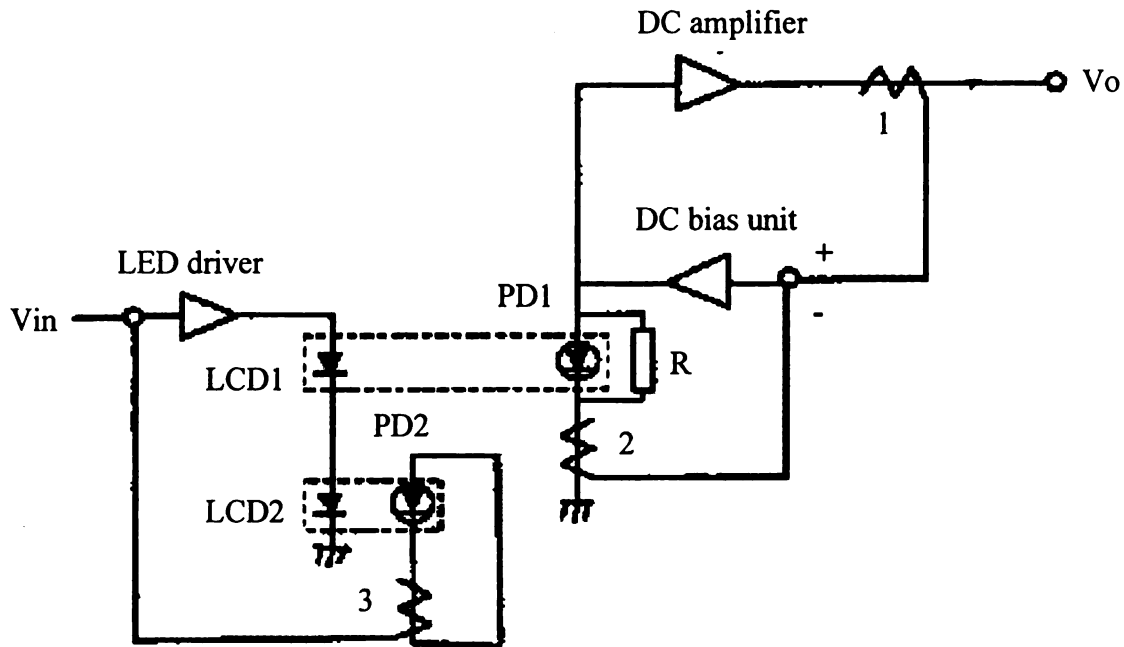


Figure 5.4: The circuit of the simulator with a light emission unit [65].

There already exist some commercial PV simulators in the market, for example Ainelec. This simulator is based on a simplified curve which has the short-circuit current, the open-circuit voltage and the maximum power point. The curve is composed of two parts. The first part is decided by the short-circuit point and the maximum power point, while the maximum point and the open-circuit point works for the other one [92]. This simulator makes the curve simple, but not accurate.

For simulator from Elgar solar, it is has a wider power range and better controllability. The simulator can output more array strings through building blocks [93]. This one is much more complex than the Ainelec.

## 5. 3. Proposed PV Simulator

### 5.3.1 Mathematical Modeling Of PV Cell

In this thesis, a dc-dc converter which can output I-V curves was designed and implemented. To have the I-V curves from the manufacture PV panel, we first need to get the mathematical model in order for it to be useful in a computer controller simulator.

Figure 5.5 shows an equivalent circuit of a PV cell. The short circuit current  $I_{SC}$  is ideally equal to the generated light current  $I_{ph}$ .

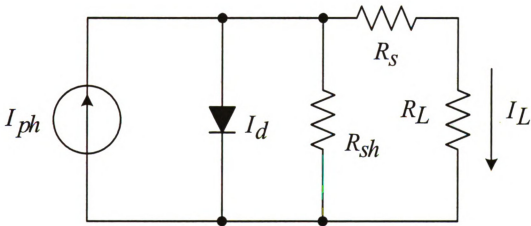


Figure 5.5: An equivalent circuit of a PV cell.

The open circuit voltage  $V_{OC}$  is expressed as the following:

$$V_{OC} = \frac{kT}{q} \ln\left(\frac{I_{ph}}{I_0} + 1\right) \quad (5.1)$$

Where,  $I_{ph}$  is generated light current,  $I_0$  is saturation current of diode,  $k$  is Boltzman constant,  $q$  is electric charge, and  $T$  is operating temperature.

The output current is dependent on temperature since the current increases slightly as the temperature increases. However, as the temperature increases the open circuit voltage tends to decrease. Relationship of the open circuit voltage  $V_{OC}$  and short circuit current  $I_{SC}$  according to the operating temperature variation is as follows,

$$I_{SC} = I_0 \cdot e^{qV_{oc} / kT} \quad (5.2)$$

The diode saturation current can be represented as,

$$I_{rs} = I_{rr} \cdot \left(\frac{T_c}{T_r}\right)^3 \cdot \exp\left[\frac{qE_g}{kA} \cdot \left(\frac{1}{T_r} - \frac{1}{T_c}\right)\right] \quad (5.3)$$

The generated light current can be represented as,

$$I_{ph} = [I_{scr} + k_t \cdot (T_c - T_r)] \cdot \frac{S}{100} \quad (5.4)$$

The operating temperature for output characteristics of PV array can be represented:

$$T = (0.3 \times S) + (0.9 \times T_c) + 273 \quad (5.5)$$

So the output current-voltage characteristics of PV array can be represented as equation (5.6) and it generates nonlinear output.

$$I = N_p \cdot I_{ph} - N_p \cdot I_{rs} \cdot \left[\exp\left(\frac{q}{KTA} \cdot \frac{V}{N_s}\right) - 1\right] \quad (5.6)$$

For a given module, SM 60 module shown in Fig. 5.6, the PV array parameters can be listed as the following:

Table 5.1: The PV array parameters (SM-60 Module).

$A$ : P-N junction ideal factor	2.25	$S$ : Solar radiation	100
$k$ : Boltzman constant	$1.3e-23$	$N_p$ : Parallel circuit	1
$q$ : Electric charge	$1.6022e-19$	$N_s$ : Series circuit	36
$E_g$ : Energy band gap	1.11	$T$ : Temperature	45
$T_r$ : Cell reference temperature	300	$I_{scr}$ : Short circuit current	3.75
$I_{rr}$ : Reverse saturation current	$2.1e-5$	$k_t$ : Constant of $I_{scr}$	$2.3e-4$

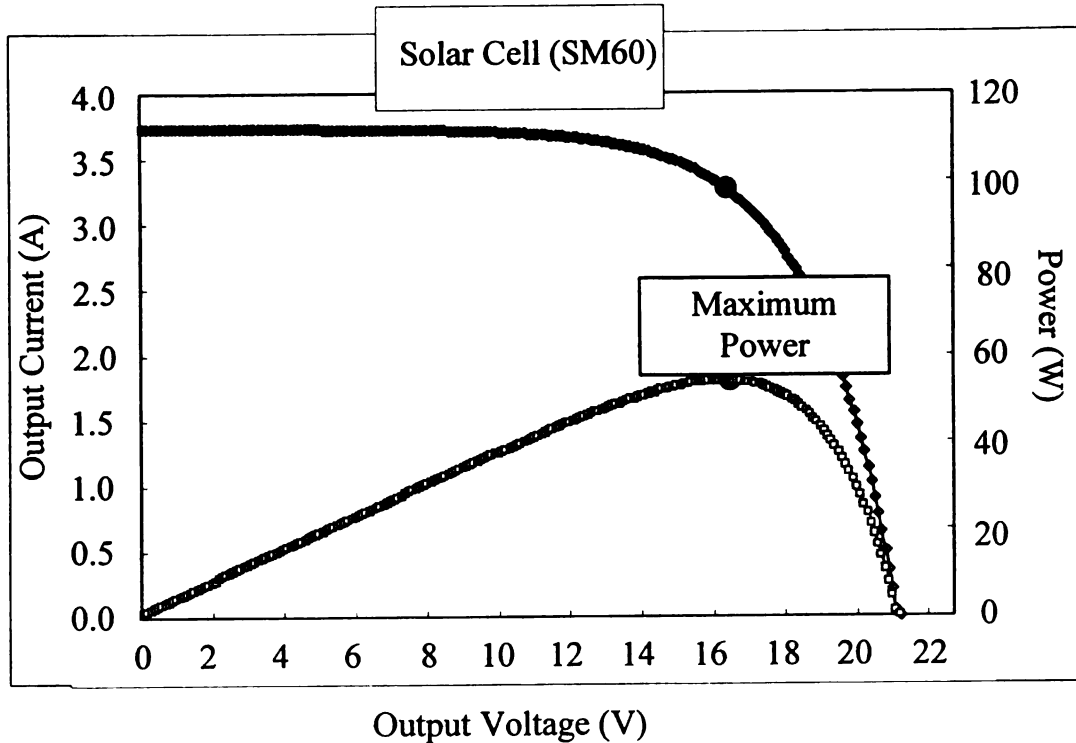


Figure 5.6: The output characteristic of the SM-60 module.

To parallel nine PV cells and series twenty one PV cells, we can get the desired output PV simulator output characteristics shown in Figure 5.7. It is noticed that the parameter values must be changed, depending on the manufacturing process and type of PV cells. The parameter values given here are only for this particular PV array. To change the temperature and irradiation parameters, we can get different curves for PV array. Regardless of values chosen, the DSP controlled PV array will function properly.

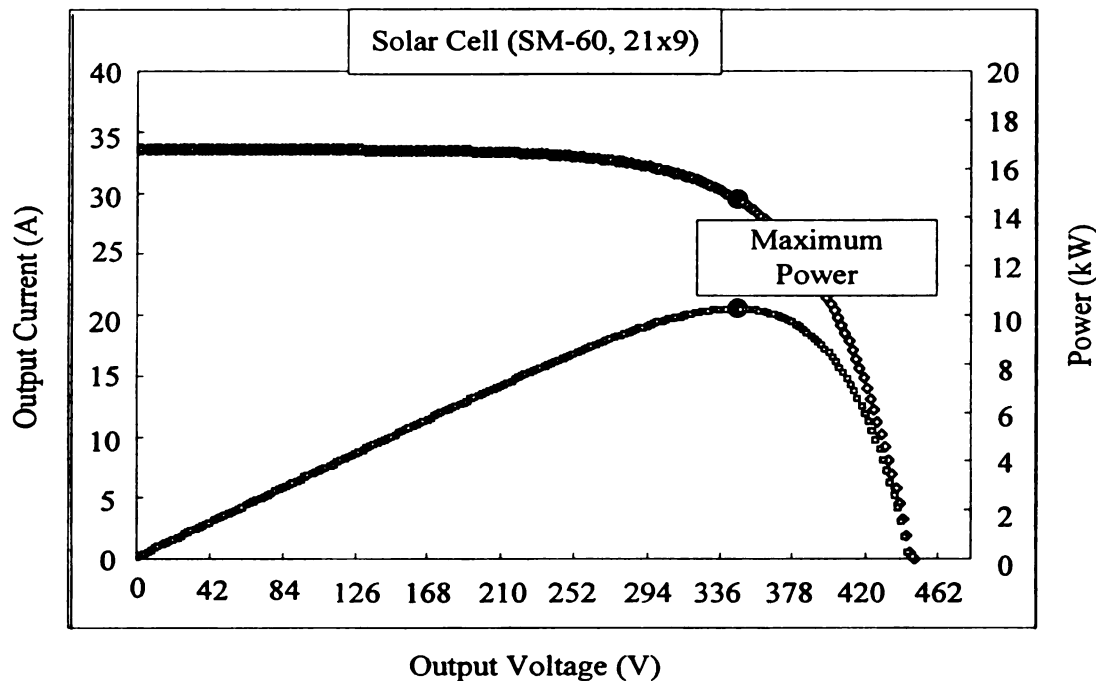


Figure 5.7: The PV simulator output characteristics.

### 5.3.2 Control Strategies

There are voltage control and current control for simulator. As voltage control, the output current is measured and used as index to look up the reference voltage for simulator. While as current control, the output voltage is measured and used to look up the reference current. However, PV characteristics are nonlinear, which is a current

source when resistive load is small and is a voltage source when resistive load is great enough. At current source segment, the change rate of voltage is large while the change rate of current is small, which as a result is infeasible for measured current to look up voltage reference practically. Thus, only voltage control and current control can not satisfy the requirement.

For PV array, the V-I curve changes due to the temperature and irradiation nonlinearly. This nonlinear characteristic source can be simulated by a dc chopper. Figure 5.8 shows the proposed PV simulator and its control strategy.

The method is to use a DC/DC converter to simulate the PV output characteristics, by producing voltage and current defined by PV curves for specified temperatures and isolations. For the simulator, as a current regulator, the voltage is measured and input to the memory which gives a desired current value based on a look up table. As a voltage regulator, the current is measured and input to the memory which gives a desired voltage value based on a look up table. A PI controller is used to adjust the switch duty ratio to achieve desired output voltage.

Because PV inverters always start from open circuit condition, and then approach to their MPP and oscillate around it during the real cases. The dynamic response of the PV array simulator is of particular in order to avoid any significant impact on the MPPT and current control of the inverter's input stage.

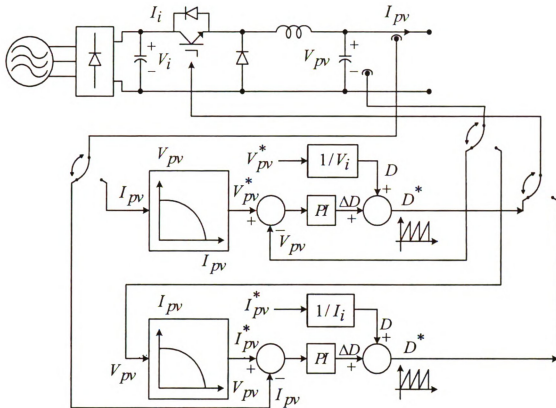


Figure 5.8: Proposed PV simulator and its control strategy.

To see the detail of voltage control as shown in Figure 5.9, we assume PV simulator works at a point A originally. When the equivalent load of simulator changes from  $R_1$  to  $R_2$ , the operation point will change to point B at first since there is a capacitor at output side and the output voltage could not change immediately. According to the voltage control rule, current  $I_{R2} + \Delta I_1$  is measured and the voltage reference  $V_{R2} + \Delta V_2$  (point C) will be given after looking up I-V table, as a result, operation point will move to point D.

The relationship between  $\Delta V_1$  and  $\Delta V_2$ ,  $\Delta I_1$  and  $\Delta I_2$  is:

$$K_R = \frac{\Delta I_1}{\Delta V_1} \quad (5.7)$$

$$K_{PV} = \frac{\Delta I_1}{\Delta V_2} \quad (5.8)$$

$$|\Delta V_2| = |\Delta V_1| \cdot |K_R / K_{PV}| \quad (5.9)$$

Where  $K_R$  is the slope of the load curve,  $K_{PV}$  is the slope of tangential line at supposed operation point on PV curve. It is clear that  $|K_R / K_{PV}|$  plays a key role in the adjustment procedure of operation: if  $|K_R / K_{PV}| < 1$ , and  $\Delta V_2 < \Delta V_1$ , operation point right on the current-voltage curve of PV simulator (point E) will be achieved after several adjustments; if  $|K_R / K_{PV}| > 1$ , and  $\Delta V_2 \geq \Delta V_1$ , then the control procedure would not arrive at stable point.

The equivalent load of PV simulator is resistive load, thus one can get  $K_R$  as

$$K_R = \frac{dI_{R_L}}{dV_{R_L}} = \frac{1}{R_L} \quad (5.10)$$

$$K_{PV} = \frac{dI}{dV} = -K_1 K_2 e^{K_2 V} \quad (5.11)$$

Where  $K_1 = N_p I_{re}$ ,  $K_2 = \frac{q}{KTAN_s}$ .

Thus, one can get the critical point where  $|K_R / K_{PV}|$  equal to one.

$$R_L = \frac{1}{K_1 K_2 e^{K_2 V}} = R_C \quad (5.12)$$

Where  $R_C$  is critical load.

When  $R_L > R_C$ , voltage control will work effectively based on above analysis; on the contrary, when  $R_L < R_C$ , current control will have a better performance.

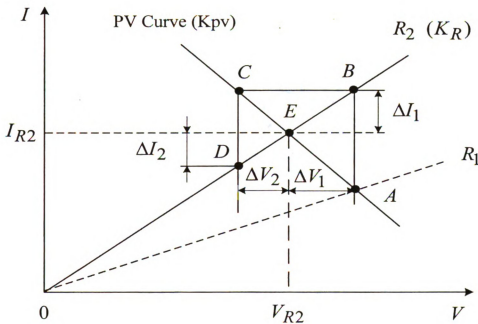


Figure 5.9: Analysis of voltage control.

This thesis applies a hybrid control strategy based on above analysis. The PV curves were divided to three regions shown in Figure 5.10. When  $R_L \geq R_V$ , voltage control is used. Voltage reference is given by measured current through I-V table. While  $R_I < R_L \leq R_V$ , the measured equivalent resistance is used to look up reference voltage. This is because at the maximum power point where  $|K_R / K_{PV}|$  equals to 1, using

either measured current or measured voltage to look up table would suffer an oscillation ( $|\Delta V_1| = |\Delta V_2|$ ), while the value of measured resistance is relatively stable no matter how much measured voltage or current is. When  $R_L \leq R_I$ , current control method is applied. In order to avoid frequently switching between two control method when  $R_L$  is around  $R_V$  or  $R_I$ , an overlap is set at each boundary (i.e.  $R_V \pm \Delta R$ ,  $R_I \pm \Delta R$ ) in practice.

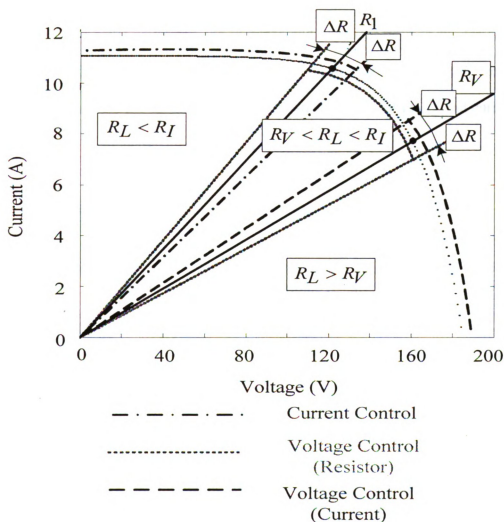


Figure 5.10: Combined voltage and current control divisions.

The simulator act electrically as real solar module for a consumer load, but take the energy from the public grid instead from the sun. The advantage compared to a real solar module is, that the PV simulator makes its power available independent from time and weather situation and additionally the user can change the values of the simulators in wide range. So certain conditions can be produced independently of the weather exactly when they just are required.

### 5.3.3 Hardware Designs

To build up a PV simulator, the inductor and capacitor need to be designed. The requirement of inductor design should follow the way that the converter need operate under the continuous conduction mode. Also, satisfy the power rating and current ripple requirement. The inductor should be calculated:

$$L \geq \frac{V(1-D)}{f\Delta I_{pk}} \quad (5.13)$$

The output capacitor, to satisfy the voltage ripple requirement:

$$C \geq \frac{DI}{f\Delta V_{pk}} \quad (5.14)$$

Where  $D$  is the duty cycle in which converter runs at maximum power,

$f$  is the switching frequency,

$\Delta I_{pk}$  is the peak to peak inductor current ripple,

$V$  is the output voltage under maximum power,

$I$  is the output current under the maximum power,

$\Delta V_{pk}$  is the peak to peak capacitor voltage ripple.

### 5.3.4 Experiment Results

Experiment for the PV simulator is based on the Figure 5.11. The maximum output voltage is happened on 400 V. And the maximum output current is 26 A.

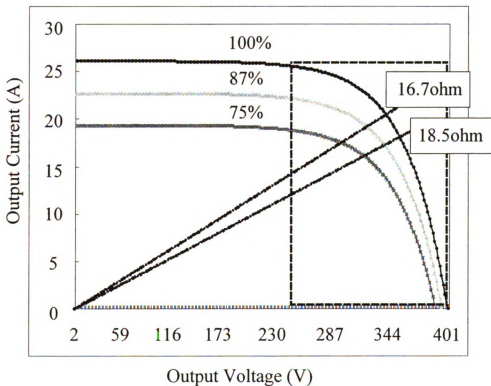
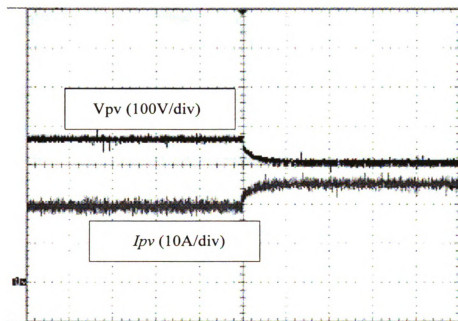


Figure 5.11: PV simulator for resistor load conditions.

To test the PV simulator, we used the resistive load. Figure 5.12 shows the experiment results for load change conditions. During the load change, the output

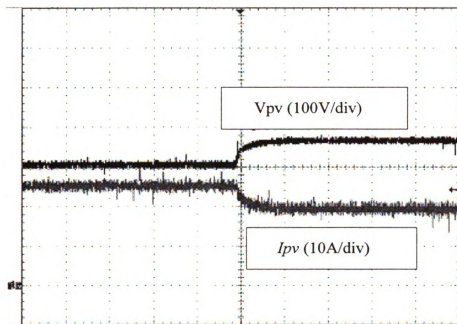
voltage and current still follow the PV characteristic outputs. Figure 5.13 shows the test result during the solar irradiation changed from 100% to 87% and its reverse conditions. Similarly, Figure 5.14 shows the test result during the solar irradiation changed from 100% to 75% and its reverse conditions.

Figure 5.12: Load current change.

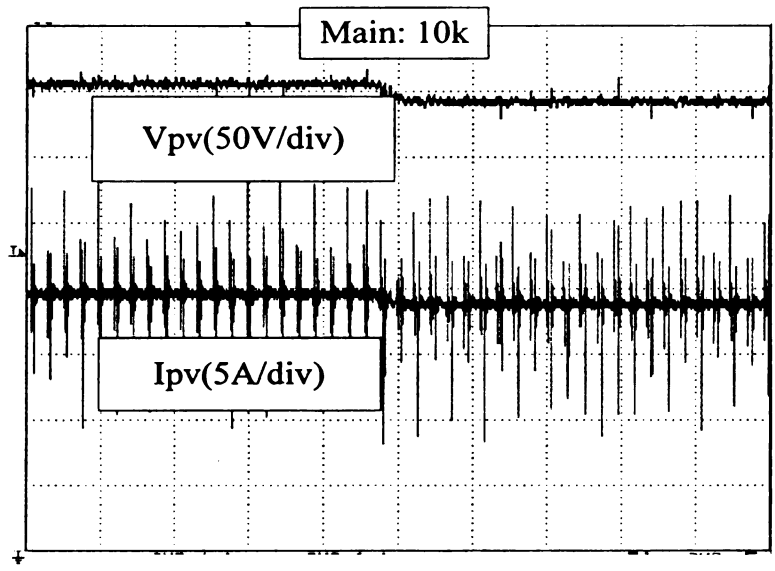


(a). From 20A to 25A.

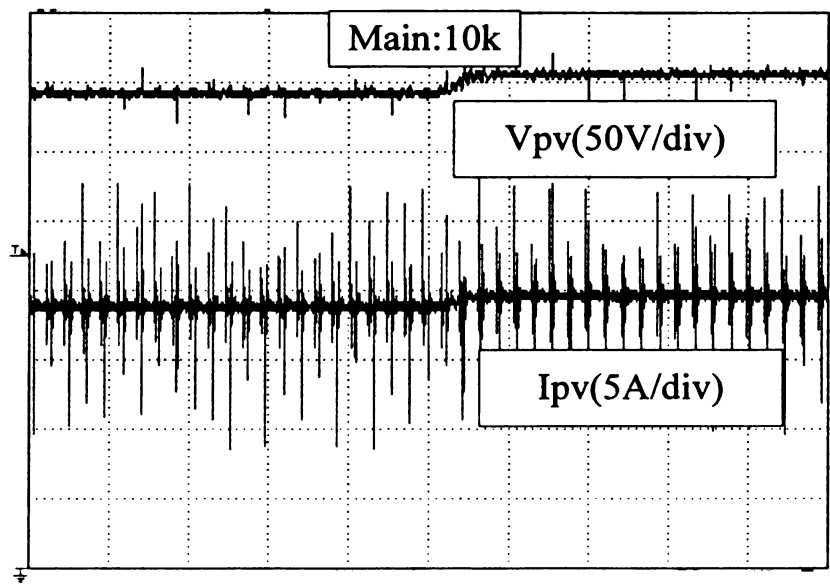
Figure 5.12 continues:



(b) From 25A to 20A.



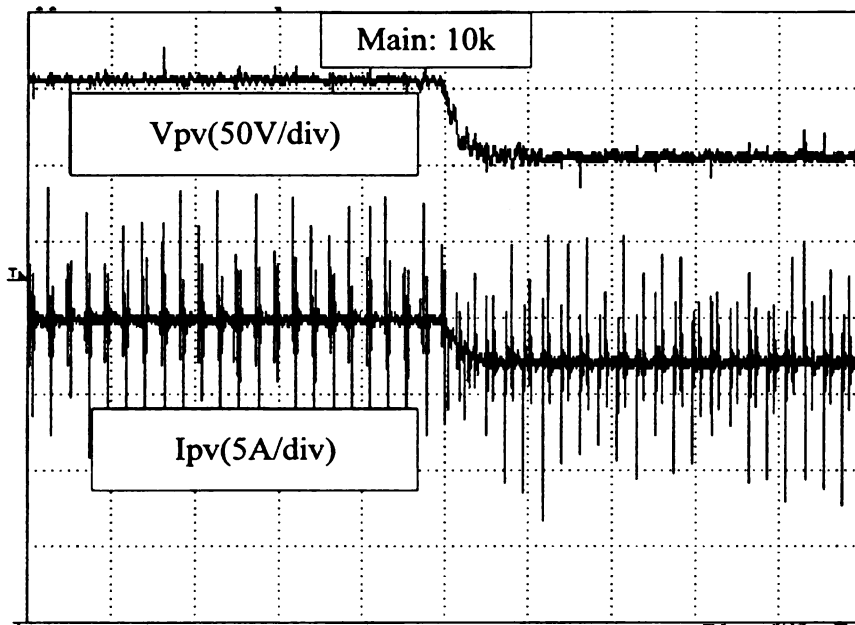
(a). From 100% to 87%.



(b) From 87% to 100%.

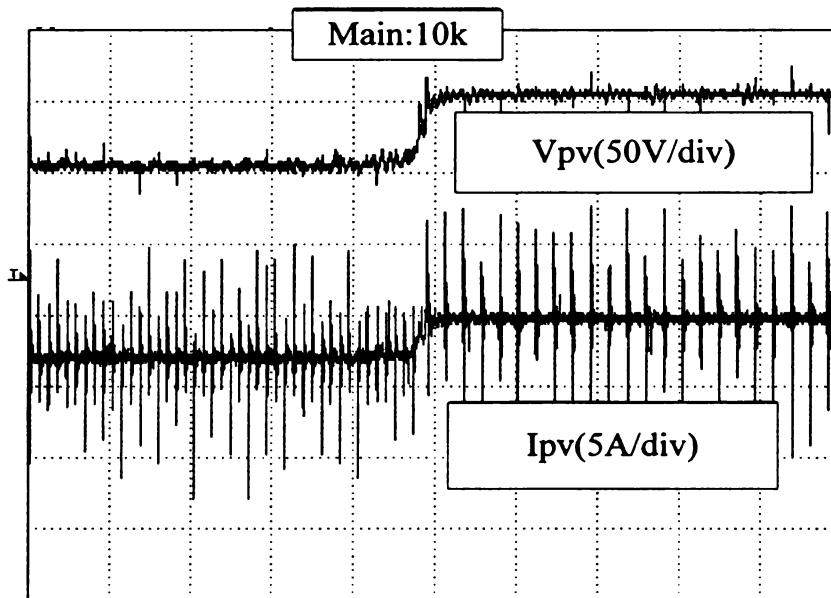
Figure 5.13: Solar irradiation change around load  $R= 18.5$  ohm.

Figure 5.14: Solar irradiation change around load  $R=18.5\ \text{ohm}$ .



(a). From 100% to 75%.

Figure 5.14 continues:



(b) From 75% to 100%.

## 5. 4. Summary

The increasing number of PV inverters is coming to the market stresses the need to carry out a dynamic characteristics under real conditions. In order to repeatable for the laboratory, a PV simulator which is capable to reproduce the current-voltage output characteristics of PV modules was developed. This circuit has the ability to simulate any kind of PV arrays, especially suited for high power applications. The simulator is based on 10 kW design, controlled by a DSP board. It allows testing PV inverters up to 10 kW.

The PV simulator suits research purposes as well as the test of device, that are fed by PV cells, like battery charger controllers, inverters or dc-dc converters. The consumer

load can operate on each point of the I-V curve at the simulator and the characteristic can be modified by the user.

# **CHAPTER 6. GRID-CONNECTED Z-SOURCE INVERTER WITH PV SIMULATOR SYSTEM**

## **6. 1. Introduction**

### **6.1.1 Background**

Because of the rapid development of rural area and increasing demand of clean energy sources, photovoltaic (PV) based electricity production has one major growth sector in distribution system. For most PV systems, grid connected operation are preferred. Grid-connected system has the advantages over stand-alone system:

- Reduced cost
- Extended lifetime
- Higher efficiency

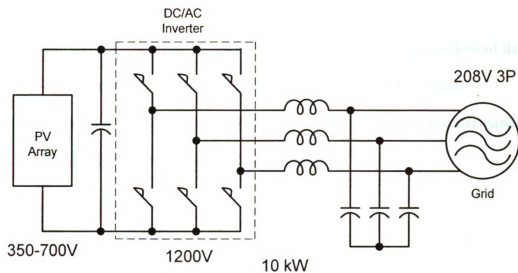
A grid connected PV system can either provide power to loads or feedback power to utility line. But till now, even with great technology improvement of PV cell itself, the cost of grid connected PV system is still high, which is now becoming the major obstacle for the wide application of PV systems. Inverter constitutes almost 20% of the total cost in a typical grid connected system [97]. The balance of system cost is becoming more important since the PV array price drops. To deal with this problem, the most addressed approach is to lower the cost of the inverter. One of the key issues now is to reduce the cost of the power conditioning unit for the PV systems.

In order to connect the PV cells to utility, an inverter/converter based power conditioning unit is required to transfer the dc energy to regulated ac. For the grid-connected inverters, the general requirements are: low line current distortion, high power factor, high efficiency, simple circuitry, high reliability, and most importantly low cost [66, 67].

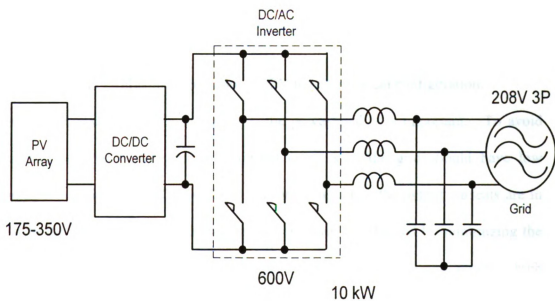
## 6. 2. Proposed Grid-connected Z-Source Inverter System

For PV system, the output power and voltage typically depends on a variety of uncontrollable factors, such as irradiation intensity and temperature. Also, the output voltage of PV cell changes with the loading current. The typical change rate can be as high as 1:2. So to achieve the best performance of a PV system, besides converting DC power to AC, the power conditioning unit will need to be accommodation a wide input voltage range and realize maximum power utilization.

For high power PV system, traditionally, there are two basic circuits shown in Figure 6.1. The first one is PV array plus inverter plus ac grid. The PV array is directly connected to the inverter [68]. For this case, if to feed a 1:2 ratio PV array, generally a higher number of PV cell in series is needed to accommodate the minimum required dc voltage for a traditional inverter to output constant voltage. Since the number of PV cell is increase, the maximum dc input is also increase, which results in higher maximum voltage stress and high cost on the switching devices. So to reduce the overall system cost, the system show in Figure 6.1 (b) is often used in real applications [69, 70, 71, 72].



(a). DC/AC inverter to grid.



(b). DC/DC converter plus DC/AC inverter to grid.

Figure 6.1: Traditional medium power stage grid-connected PV inverter system.

In this case, a boost converter is added in front of the inverter. Thus, the minimum dc voltage from PV cell can be lower. And the maximum voltage stress on the switches

can also be regulated to the minimum level. So the cost of the total system goes down. But the additional dc/dc converter usually increases the cost and power loss of the power conditioning unit, and at the same time lower the reliability of the system.

So to deal with this problem, this thesis proposes a Z-Source inverter based power conditioning unit to utilize grid-connected PV system.

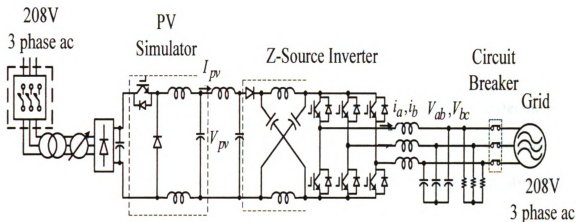


Figure 6.2: Grid-connected Z-Source PV inverter system configuration.

For grid-connected inverter applications, the power quality is important. To avoid the distortion of the utility grid, the injected currents to the grid should have low harmonics and a high power factor [73]. Furthermore, when the output currents are in phase with the grid voltage, the maximum active power is achieved by minimizing the reactive component. The inverters are expected to have high power quality, high efficiency, high reliability, low cost, and simple circuitry. Compared to single-phase inverters, three phase grid-connected inverters have much more advantages.

The grid connected PV energy can be transferred to a grid through one or two power conversions. In PV applications, the proposed one stage power conversion is more efficient and reliable than multi power stage conversions.

## 6. 3. Control Issues

### 6.3.1 General Issues

To enhance development of PV grid-connected system, there are the control issues, such as the input power control, improvement of the strategy of maximum power point tracking, reduction of the voltage and current ripple, improving the total harmonic distortion (THD), and increasing the system efficiency.

The input power of the PV inverter system can be controlled in different ways depending on different control methods. The main task is to transform PV dc voltage to the inverter output ac voltage with the desired amplitude and frequency, also has to perform the maximum power tracking.

If the system is two power conversion stages, which means that a dc-dc boost converter is utilized before dc-ac inverter, the dc-dc output voltage has to be controlled. To achieve this goal, there are two methods usually used. The first one is the dc voltage control, and the second one is dc current control.

For dc voltage control, the reference value is set to be output voltage. On the contrary, for the dc current control, the reference value is set to be output current. Both these two control methods will affect duty cycle of dc-dc converter, thus to get the PWM accordingly.

### 6.3.2 Voltage Control And Current Control

To control the input power of the grid-connected PV system, there are generally two basic control methods. The first is to get a fundamental 60 Hz voltage wave through the control of switching instants. The power flow is realized through the control of amplitude and phase of output PWM which are related to the line voltage, thus produce the necessary voltage across the ripple inductance and get the desired current flow. The second one is to directly control the current flow through instantaneous current feedback. The ac voltages at the switch do not need to be directly controlled.

Voltage control is a simple method of power flow control. However, it has disadvantages that current harmonics and over currents can not be directly controlled, and the transient response is limited. While current control has better transient response, also can reduce harmonics, inherent over current protection, and has soft start capabilities too.

In the grid-connected system, the load is utility grid which has infinite capacity, so the grid connected current can be controlled. Then the outside of inverter can be derived as a current source. So the current control has the advantages than the voltage control.

### 6.3.3 Modulation Methods

In the power electronics converters and inverters, the pulse width modulation methods are utilized to implement the control. The methods of pulse width modulation

method will affect the inverter energy efficiency, waveform quality, and voltage linearity a lot.

There are three main modulation methods: the carrier based PWM methods, the hysteresis current control, and programmed pulse modulation methods. For the programmed pulse modulation methods, the switching patterns are calculated for a specified performance optimization at beginning and stored in a memory which can be accessed through a look-up table. This method has a disadvantage that the huge computer memory resources are needed and the number of pulses per fundamental cycle is limited to a small number.

Compared to the programmed pulse modulation methods, the carrier based PWM methods can operate at the higher switching frequency, at the same time can achieve high quality output waveform. The first carrier based PWM was implemented by Schonung and Stemmler in 1964 [77]. As shown in Figure 6.3, the reference modulation wave is compared to the triangle wave, and the switching times are controlled by the intersections. Based on this fundamental, this thesis proposed a new control which is depicted in detail in the next section.

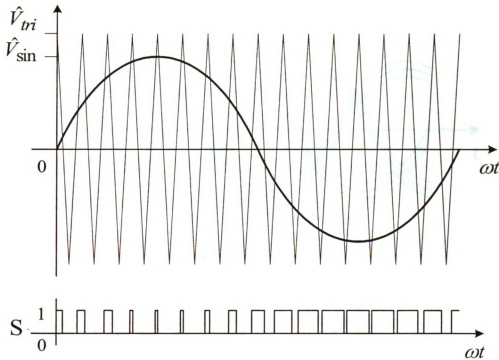


Figure 6.3: SPWM method.

Also, the hysteresis control method is used in some applications. Compared to the hysteresis current control, the proposed control method has some advantages. Considered about hysteresis control shown in Figure 6.4, the error between the desired current value and feedback current value is the input of hysteresis loop comparator. The output of hysteresis loop comparator is the control signal to the power devices. The harmonics components will be different according to the bands width [76]. If the hysteresis bands width is too big, the harmonics components of grid current will be larger. Otherwise, if the hysteresis bands width is too small, the harmonics components of grid current will be smaller, the switching frequency will be higher. The output spectrum of grid current is wide due to the changed switching frequency.

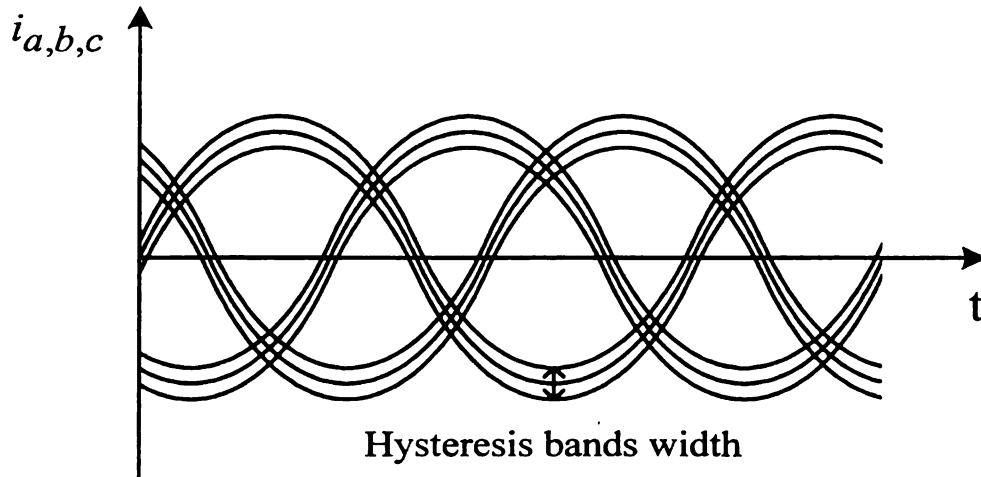


Figure 6.4: Hysteresis current control.

### 6.3.4 MPPT Methods

Because of the PV's nonlinear characteristic, the use of MPPT can make full use of the system and thus reducing the cost of the system. The function of the MPPT is to make the PV array work as close to the maximum power point under any circumstances. There are many methods to realize the MPPT, such as perturbation and observation (P&O) method, incremental conductance method, parasitic capacitance method, constant voltage, and so on [14].

For the perturbation and observation method, the maximum power tracking operates by changing the solar array voltage shown in Figure 6.5. If a perturbation voltage is applied to the PV array, the corresponding perturbation ( $dP/dt$ ) is caused at the same time. Therefore, the maximum power tracking can always seek the maximum power conditions by tracking the perturbation. The perturbation will be updated every single cycle. When approaching the maximum power point, the output voltage of PV array will

oscillate around the operating voltage. Thus a power loss is generated. The perturbation difference has the effect on the resulted power losses. In this method, the worst case is that perturbation in one direction will lead to an operating voltage far away from the actual maximum power point if the system has been oscillating around the maximum power point.

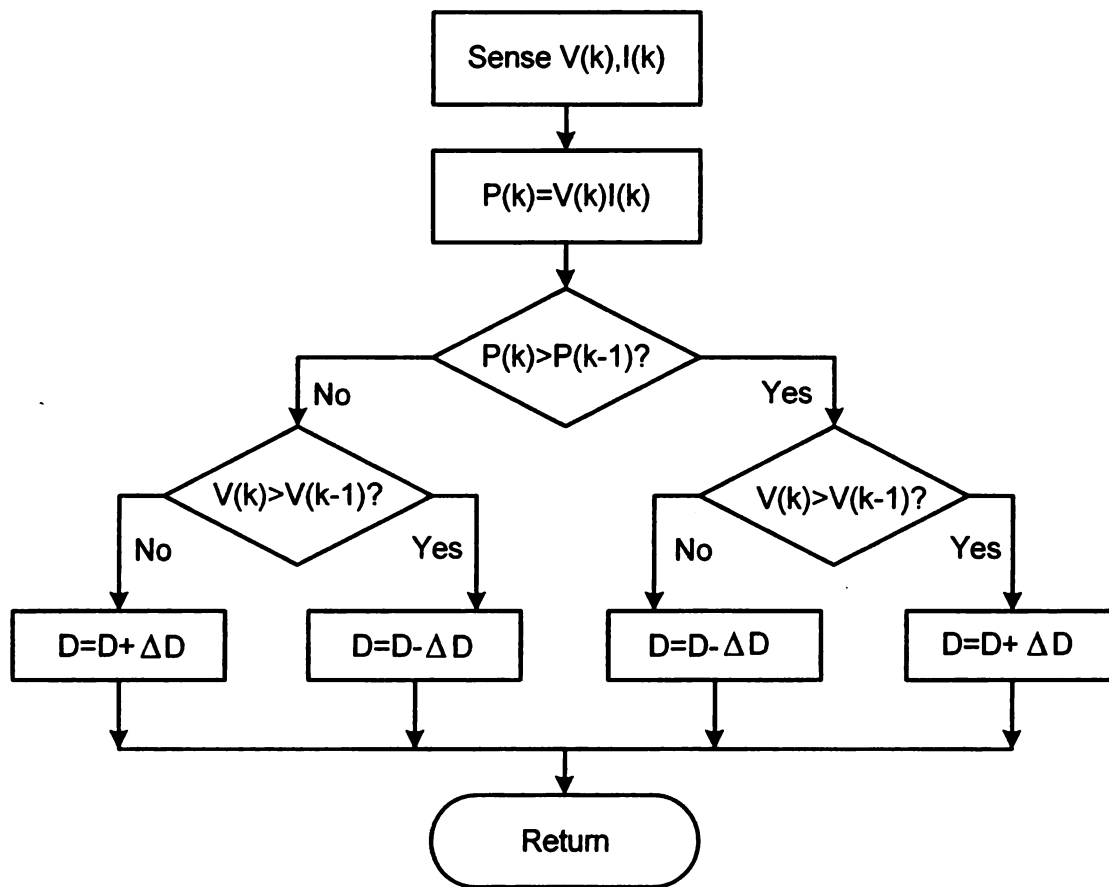


Figure 6.5: P&O MPPT method.

For the incremental conductance method, the PV array voltage varies according to the maximum power point voltage by changing the incremental conductance or instantaneous conductance. This method has advantages over the perturbation and observation method, it can track quickly changing conditions more effectively than the perturbation

and observation method. But this method will be more complex than the perturbation and observation method. The INC flow chart is shown is Figure 6.6.

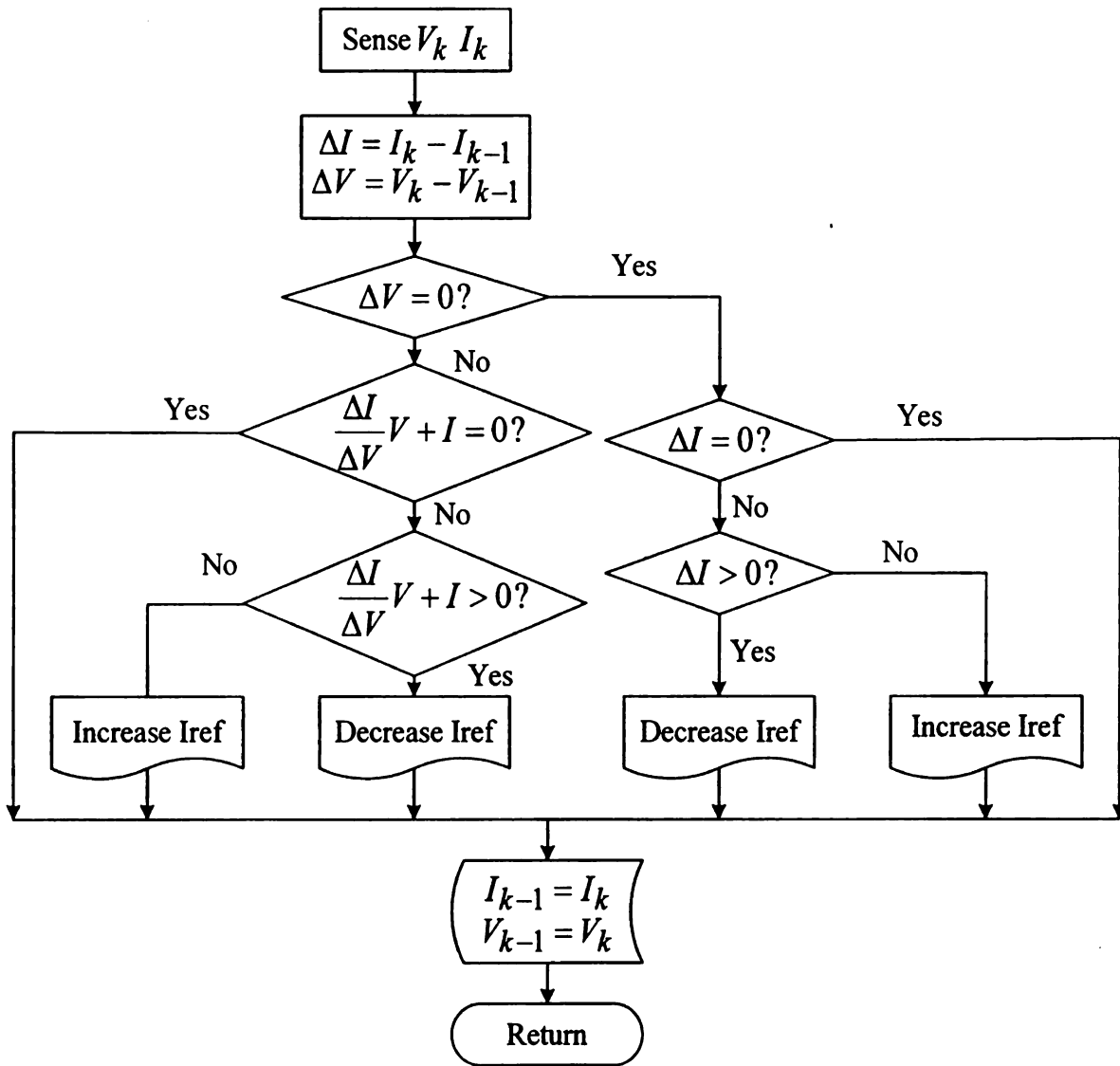


Figure 6.6: INC MPPT method.

The parasitic capacitance method is similar to the incremental conductance method. This method considers the parasitic capacitance in the PV array. The switching ripple of the maximum power point is used to apply a perturbation to the PV array. Then the array conductance can be calculated according to the measured current ripple and voltage

values. Therefore, the incremental conductance method can be used to achieve the MPPT. This method may not be effective when the parasitic capacitance is small. Thus, this method is suited for large PV arrays that have relatively large parasitic capacitance. In addition, the dc/dc inverter usually has an input capacitor to filter out small ripple in the PV array. Thus that capacitor will complicate the parasitic capacitance, thus limiting the use the method.

The constant voltage method assumes that the operating voltage at the maximum power point varies little with irradiation levels. The operating voltage at the maximum power point is usually selected to be 0.76 times of the open circuit voltage of the PV array. In this method, the open circuit voltages of the PV array are updated and set to 76% of the measured open circuit voltage accordingly.

Among these methods, the incremental conductance method has a higher overall MPPT efficiency than others. The constant voltage method has the least MPPT accuracy.

## 6.3.5 Synchronization In Grid-connected Applications

### 6.3.5.1. Synchronization methods

Synchronization is a big issue in grid-connected applications. There are classical two ways to solve the synchronization problem: from hardware or from software approaches. Accurate synchronization is very important in distributed ac power systems and is a key requirement in any real time measurement and control system [74, 75].

The most famous synchronization is the phase-locked loop (PLL) control. The PLL was used in a lot of applications until the development of integrated circuits, thus to make it easier to perform the PLL [76].

A PLL is a device which can track with another signal. With PLL, the output can be synchronized with the desired reference in phase and amplitude.

Figure 6.7 shows one method of a three phase PLL control loop.

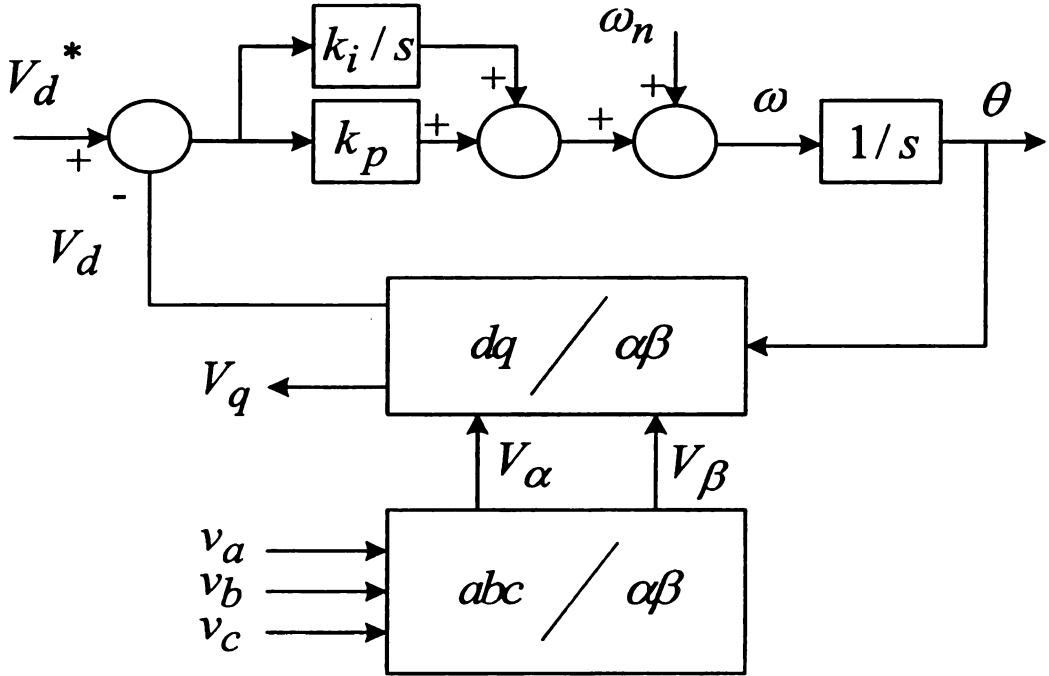


Figure 6.7: PLL control loop.

## 6. 4. Proposed Control Strategies

### 6.4.1 Proposed PLL Synchronization

The proposed system used zero crossing detection method for PLL control. For zero crossing detection PLL, there are hardware loop approach and software loop approach. In this thesis, digital zero crossing detection PLL is implemented to synchronize with the grid. Figure 6.8 shows a zero crossing detection PLL diagram.

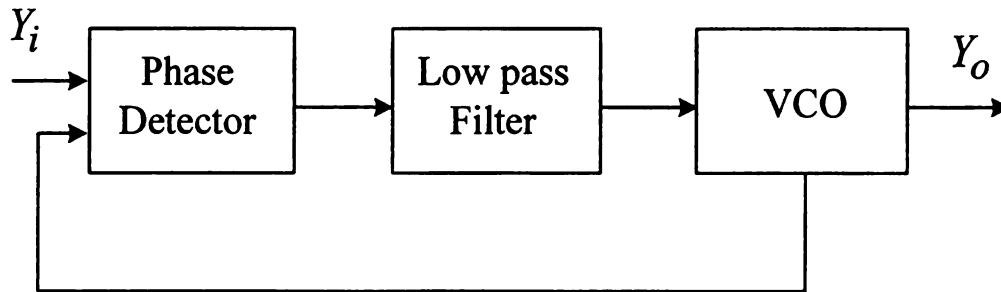


Figure 6.8: Zero crossing PLL.

For phase detector, there can be classified to sinusoidal wave and square wave phase detections shown in Figure 6.9. The former has the detection interval from  $-\frac{\pi}{2}$  to  $\frac{\pi}{2}$ . The latter include triangle phase detection which has the detection interval from  $-\frac{\pi}{2}$  to  $\frac{\pi}{2}$ , the sawtooth phase detection which has the detection interval from  $-\pi$  to  $\pi$  [77, 78, 79]. The sinusoidal phase detection was developed in this thesis.

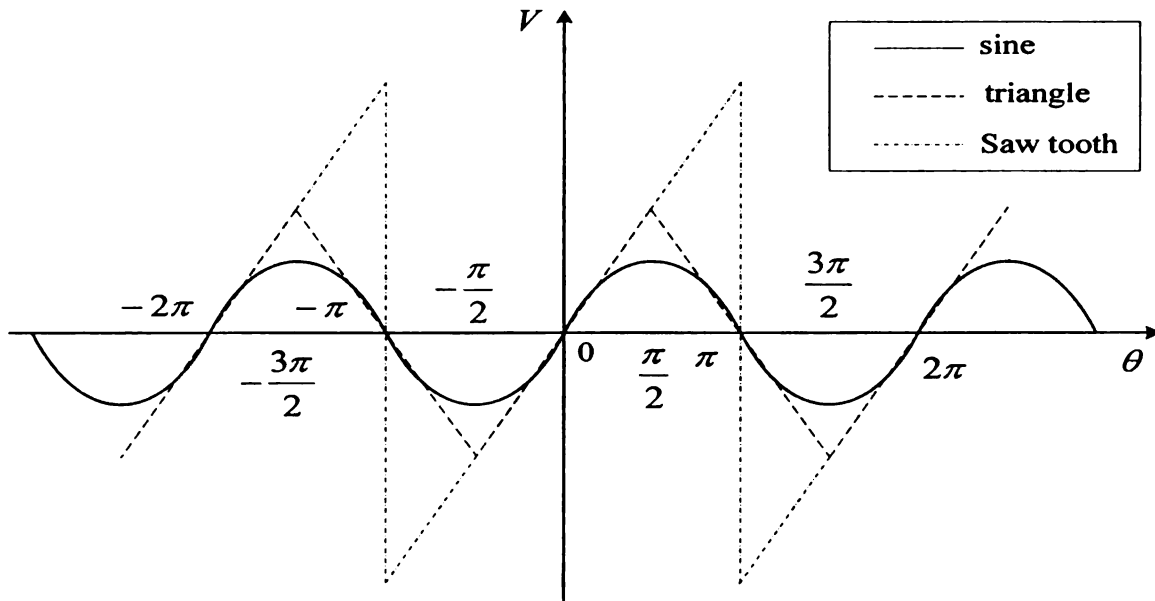


Figure 6.9: Phase detection methods.

The zero crossing detection PLL has the advantages that it has the immunity to harmonics in the input signal. The dynamic response of the zero crossing detection PLL can be improved by adjusting the low pass filter and system parameters.

With the proposed PLL, we can synchronize grid very well.

#### 6.4.2 Proposed Harmonic Injected Feed-forward Control

Grid-connected PV system has two main control requirements: seeking the maximum power tracking and obtain the sinusoidal output current to the utility grid. In the proposed solution, these two goals are realized in a single power conversion stage with two control loops.

The inner loop realizes inverter current output control, which consists of grid voltage and current sampling, phase calculation, and PWM generation. Usually the inverter is

controlled so as to generate the output current in phase with the grid voltage to achieve the maximum active output power by minimizing the reactive output power.

The outer loop is a power control loop, which tracks maximum power point of PV modules by adjusting inverter output power instantaneously. Current MPPT methods are often based on perturb and observe, incremental conductance, parasitic capacitance, voltage based peak power tracking, and current based peak power tracking [80, 81]. The modified P&O MPPT method is implemented and would be shown in detail later. The peak power tracker operates by periodically increasing or decreasing the PV array voltage. If a given perturbation causes an increase in array power, the subsequent perturbation is made in the same direction. Thus, the peak power tracking can be realized [82, 83].

#### 6.4.2.1. Third harmonic injection

Third harmonic injected control method was first utilized by Buja and Indri. In this method, the inverter output voltage can be maximized by adding a triple harmonic which has one-sixth of the fundamental component modulation wave [78] shown in Figure 6.10.

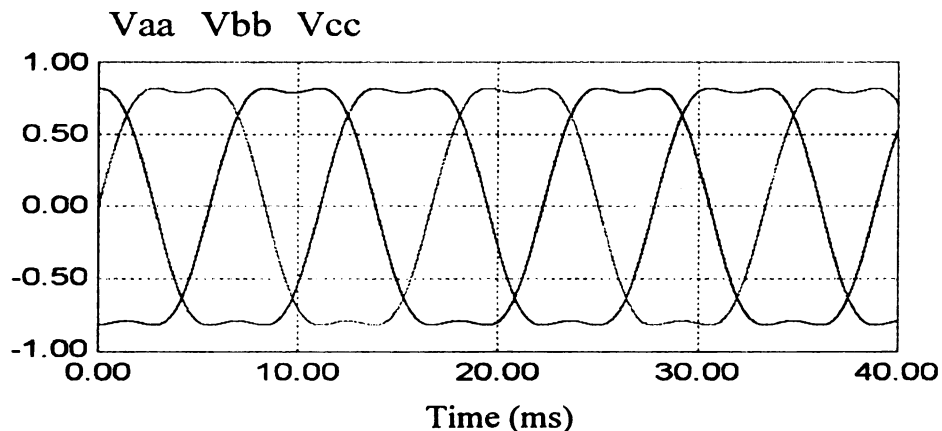


Figure 6.10: One-sixth of the fundamental injected.

If the modulating input signal exceeds the amplitude of the carrier waveform, the output will saturate. For three phase application, the line to line components are immunity to the added third harmonic injection, but the fundamental amplitude can be increased. Also, the switching losses can be reduced.

To connect the PV array with 1:2 voltage change ratio to 208 ac line, when the PV array voltage is low, maximum constant boost control [84] for the Z-source inverter is used in the proposed system. There are three boost control methods listed in table 6.1. The shoot through interval, boost factor and voltage gain are compared in the table. The maximum constant boost strategy configuration is shown in Figure 6.11. With certain amount of third harmonic to the phase voltage waveform, the line amplitude of the fundamental wave will increase without any over modulation [85]. Also, the output line to line voltage wave still remains sinusoidal and undistorted.

Table 6.1 Shoot-through interval, boost factor and voltage gain of three boost control methods.

	$D$	$B$	$G$
Simple boost	$1 - M$ (Max value)	$\frac{1}{2M - 1}$	$\frac{M}{2M - 1}$
Maximum boost	$\frac{2\pi - 3\sqrt{3}M}{2\pi}$	$\frac{\pi}{3\sqrt{3}M - \pi}$	$\frac{M\pi}{3\sqrt{3}M - \pi}$
Maximum boost (with third harmonic injection)	$1 - \frac{\sqrt{3}}{2}M$	$\frac{1}{\sqrt{3}M - 1}$	$\frac{M}{\sqrt{3}M - 1}$

In these three boost control methods, the modulation index must satisfy the following requirements.

For simple boost control, the modulation index must be less than  $1 - D$ , and Z-Source capacitor voltage must be larger than  $2\hat{v}_{ac}$ .

For maximum boost control, the modulation index must be less than  $\frac{2\pi}{3\sqrt{3}}(1-D)$ ,

and Z-Source capacitor voltage must be larger than  $\frac{3\sqrt{3}}{\pi}\hat{v}_{ac}$ .

For maximum constant boost control, the modulation index must be less than

$\frac{2}{\sqrt{3}}(1-D)$ , and Z-Source capacitor voltage must be larger than  $\sqrt{3}\hat{v}_{ac}$ .

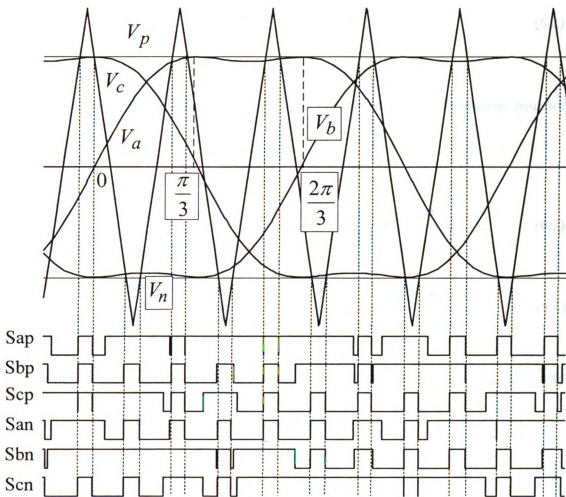


Figure 6.11: Third harmonic injected maximum constant boost.

There are two periods in a switching cycle:

For the first period ( $0 - \frac{\pi}{3}$ ), the upper and bottom curves can be expressed by

following equations respectively.

$$V_{p1} = \sqrt{3}M + \sin(\theta - \frac{2\pi}{3})M \quad 0 < \theta < \frac{\pi}{3} \quad (6.1)$$

$$V_{n1} = \sin(\theta - \frac{2\pi}{3})M \quad 0 < \theta < \frac{\pi}{3} \quad (6.2)$$

For the second period ( $\frac{\pi}{3} - \frac{2\pi}{3}$ ), the curves meet the following equations

respectively.

$$V_{p2} = \sin(\theta)M \quad \frac{\pi}{3} < \theta < \frac{2\pi}{3} \quad (6.3)$$

$$V_{n2} = \sin(\theta)M - \sqrt{3}M \quad \frac{\pi}{3} < \theta < \frac{2\pi}{3} \quad (6.4)$$

Obviously, the distance between these two curves are always constant, that is  $\sqrt{3}M$ .

The Boost factor B and the voltage gain can be calculated:

$$B = \frac{1}{1 - 2\frac{T_0}{T}} = \frac{1}{\sqrt{3}M - 1} \quad (6.5)$$

Figure 6.12 is a plot of equation (6.5) with the modulation index changing from 0 to 1.154. It can be seen that the voltage gain can be close to infinity when modulation index is close to  $\sqrt{3}/3$ .

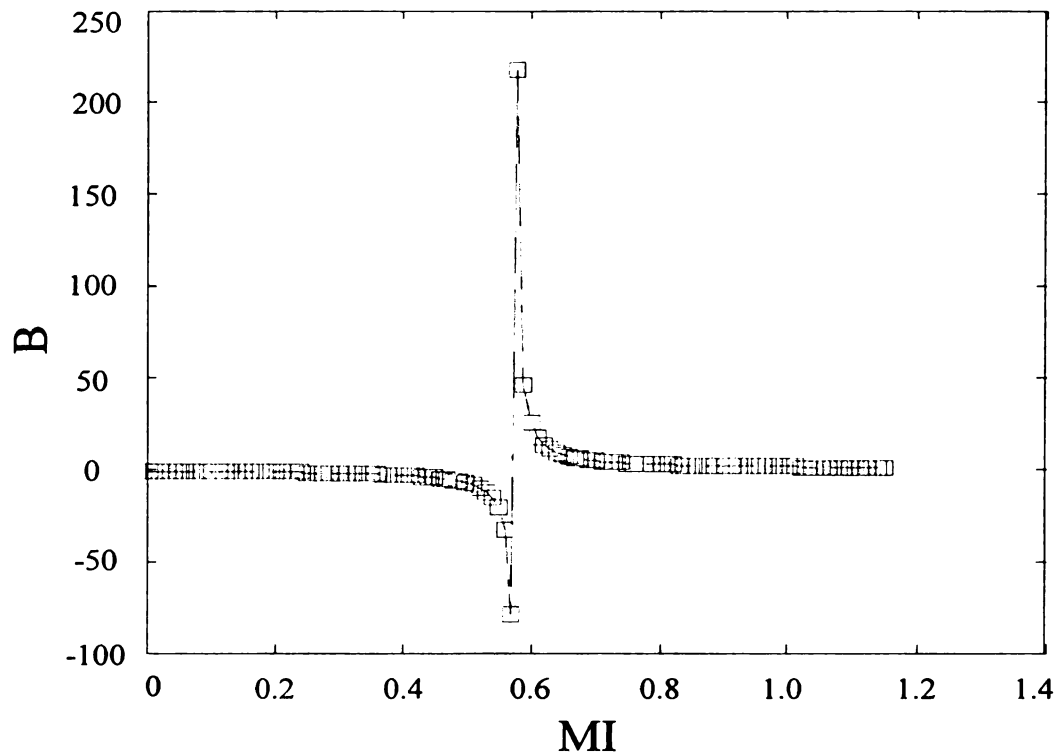
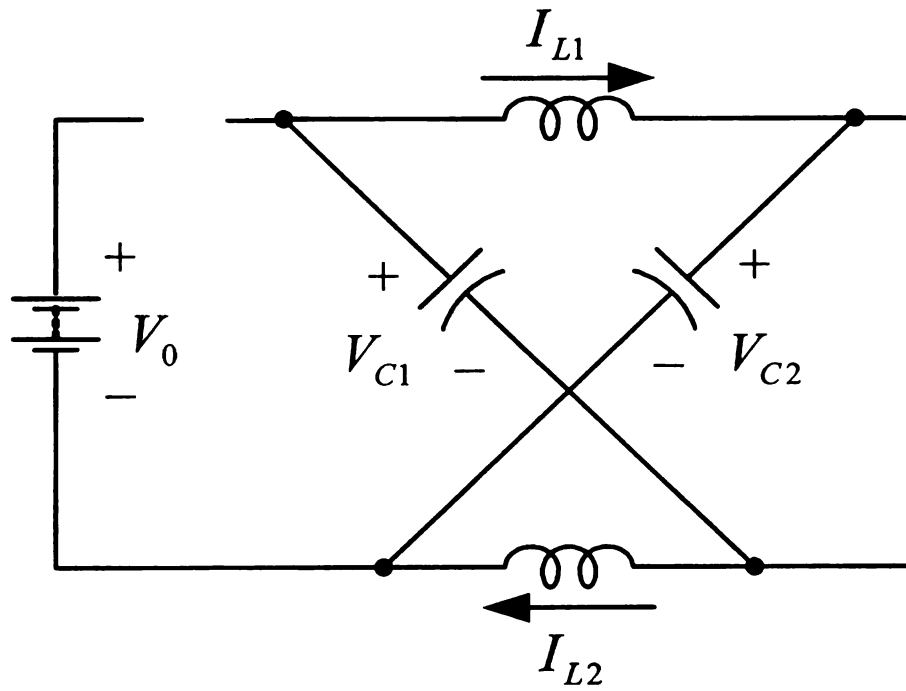
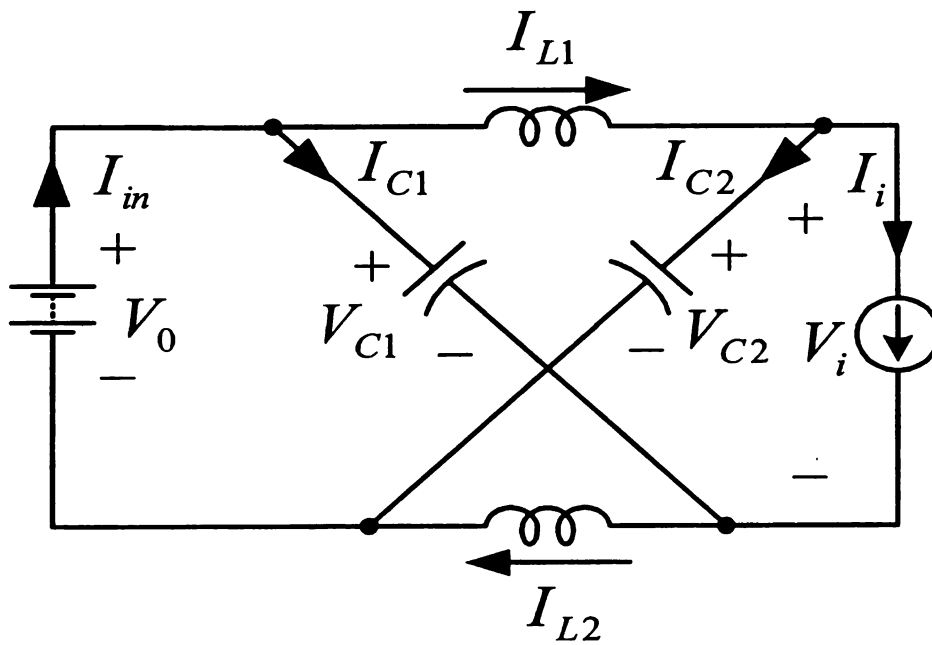


Figure 6.12: The relation between the voltage gain and modulation index.

In this kind of control, the shoot through duty ratio is always constant while the maximum voltage gain can also be achieved. When the carrier triangle wave is greater or lower than the shoot through lines, the inverter is gated to a zero state, working as shoot through mode, just like Figure 6.13 (a). Otherwise, the inverter works as the traditional PWM inverter, which seems to a non shoot through mode, just like Figure 6.13 (b). One advantage of this method is to eliminate the ripple at line frequency.



(a) Shoot through mode.



(b) Non shoot through mode.

Figure 6.13: Z-Source inverter operation modes.

For the traditional three phase PWM, the average squared value of the current ripple can be represented as [A-1]:

$$\Delta i_{ab}^2 = \left(\frac{V_{dc}}{2L}\right)^2 \frac{T^2}{48} \frac{1}{\pi} \int_{-\pi/3}^{\pi/3} \left\{ \begin{array}{l} \cos^2\left(\theta + \frac{\pi}{6}\right) - 3\sqrt{3}M^3 \cos^3\left(\theta + \frac{\pi}{6}\right) \\ -\sqrt{3}M^4 \cos\left(\theta + \frac{\pi}{6}\right)\left(\cos^3\left(\theta - \frac{2\pi}{3}\right)\right) \\ -\cos^3 \theta \end{array} \right\} d\theta \quad (6.6)$$

Then the above equation can be simplified to the following equation:

$$I_{hrms}^2 = \frac{V_{dc}^2 \Delta T^2}{192L^2} \left( \frac{3}{2}M^2 - \frac{4\sqrt{3}}{\pi}M^3 + \frac{9}{8}M^4 \right) \quad (6.7)$$

For the third harmonic injected constant boost PWM,

Similarly, the equation can be derived:

$$I_{hrms}^2 = \frac{V_{dc}^2 \Delta T^2}{192L^2} \left( \frac{3}{2}M^2 - \frac{4\sqrt{3}}{\pi}M^3 + \frac{31}{32}M^4 \right) \quad (6.8)$$

Based on these two equations, the harmonics distortion factor of the two PWM strategies can be defined as:

$$Y(1) = \frac{3}{2}M^2 - \frac{4\sqrt{3}}{\pi}M^3 + \frac{9}{8}M^4 \quad (6.9)$$

$$Y(2) = \frac{3}{2}M^2 - \frac{4\sqrt{3}}{\pi}M^3 + \frac{31}{32}M^4 \quad (6.10)$$

Where  $Y(1)$  is for the traditional PWM and  $Y(2)$  is for the THICB PWM.

Respect of the switching frequency, dc voltage, and inductance, the relation of harmonic current distortion factor and modulation index can be drawn in Figure 6.14. In the figure, the curve  $Y(2)$  represents of third harmonic injected PWM, and the curve  $Y(1)$  represents of traditional three phase PWM. It is clearly that the THICB PWM would start to have significant less harmonics distortion factor when modulation index is bigger than 0.5.

For the specific case that the dc voltage changes from 230 V to 400V, equation 8 and 9 are plotted at the condition that:  $T=100 \mu S$  and  $L_a=1 \text{ mH}$ .

The plotting results in Figure 6.15 clearly show that the current harmonics content in THICB method is much smaller than in the traditional method.

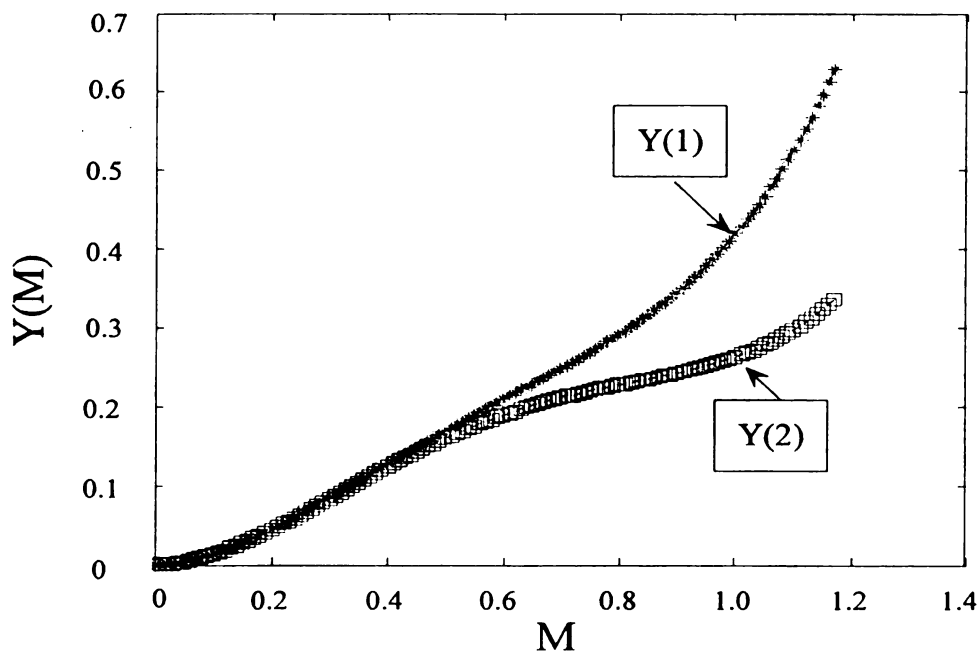
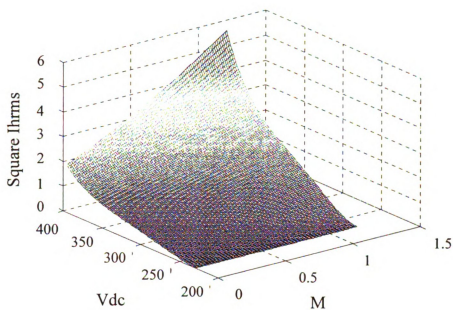
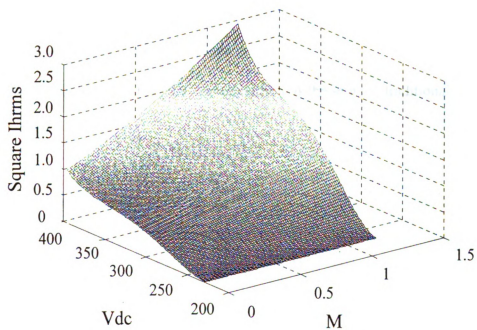


Figure 6.14: Relationship of the harmonic factor and modulation index with different PWM.



a.: Harmonics current component for tradition PWM.



b.: Harmonics current content for THICB PWM.

Figure 6.15: Relationship of the harmonic factor with modulation index and dc bus voltage with and without harmonic injection.

For the Z-Source inverter, the current through the inverter switches is composed of current to the load and the current through the switches during shoot through. The current during shoot through in average is distributed in balanced three phase paths. The current through the inverter during the shoot through is twice of the inductor current.

The average current in shoot through for switch is

$$I_{avs} = \frac{2}{3} I_L \quad (6.11)$$

The average current through the diode is equal to the sum of the average current through inductor and capacitor. During the steady state, the average current through the capacitor is zero, and the average current through the inductor is equal to the current through the diode.

$$I_D = P_m / V_i \quad (6.12)$$

Where  $P_m$  is the PV array maximum power.

Without shoot through state, the average current is the same as traditional inverter,

$$I_{avsn} = \frac{\sqrt{2} P_m}{3 V_0 \cos \psi \pi} \quad (6.13)$$

Thus, the average current in total is

$$I_{avs} = \frac{2}{3} I_L (T_0 / T) + \frac{\sqrt{2} P_m}{3 V_0 \cos \psi \pi} (1 - T_0 / T) \quad (6.14)$$

Under constant maximum boost,

$$T_0 = (1 - M \sqrt{3} / 2) T \quad (6.15)$$

$$V_0 = \frac{M}{\sqrt{3} M - 1} \frac{V_i}{2\sqrt{2}} \quad (6.16)$$

The average switch device power is

$$\begin{aligned}
 (SDP)_{inv} &= 6I_{avs}V_s = 4I_LV_i \frac{T_0}{(\sqrt{3}M-1)T} + 8 \frac{P_m}{\pi M} (1 - T_0/T) \\
 &= \frac{2P_m(2-\sqrt{3}M)}{\sqrt{3}M-1} + \frac{4\sqrt{3}P_m}{\pi}
 \end{aligned} \tag{6.17}$$

#### 6.4.2.2. Current Control Loop

In grid-connected distributed generation systems, three phase pulse width modulation voltage source inverters are usually employed to achieve power conversion, grid interfacing and control optimization. To feed grids with high quality power, the current control of the grid-connected VSI plays an important role since a DG system would not regulate the voltage at the point of common coupling (PCC) [86].

Due to PCC voltage can not be controlled, the power quality is determined by the current quality only. To achieve unit power factor, the output current of the inverter needs to be in phase with the utility voltage. The grid-connected three phase dc/ac Z-Source inverter can be shown in Figure 6.16. And Figure 6.17 shows the unity power factor control of the inverter current to the utility grid. The grid line to line voltages are measured, also the phase lock loop is utilized to ensure system synchronization [87, 88]. Two currents are measured from the outputs of the inverter then fed back into a close loop system. The close loop system is realized with a PI controller.

The PI controller is based on a transform function  $G(s)$  as follows:

$$G(s) = \frac{F(s)}{E(s)} = k_p + \frac{k_i}{s} \tag{6.18}$$

Where  $F(s)$  is the output,  $E(s)$  is the input error,  $k_p$  is the proportional gain, and  $k_i$  is the integral gain.

The above function is an analogue form and need to be transformed to the equivalent digital one before being implemented by the DSP controller.

The final form of the digital PI controller can be represented as:

$$F(n) = Y_p[n] + Y_i[n] \quad (6.19)$$

Where

$$Y_p[n] = k_p E[n] \quad (6.20)$$

$$Y_i[n] = \frac{k_i}{f} E[n] + Y_i[n-1] \quad (6.21)$$

$Y_p$  and  $Y_i$  is the outputs of the proportional and integral loops respectively, and  $f$  is the sampling frequency.

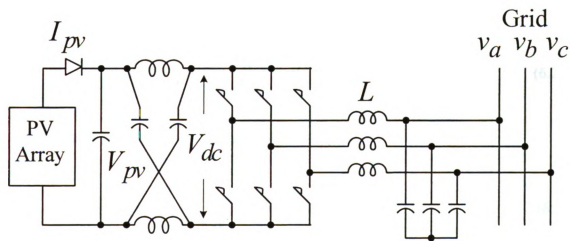


Figure 6.16: Grid-connected three phase Z-Source inverter system.

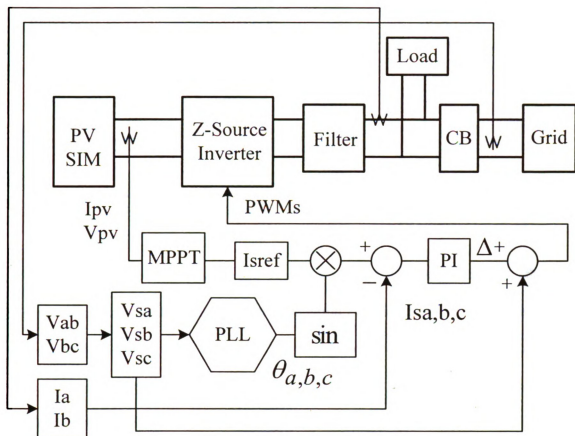


Figure 6.17: Block diagram of control loop.

In Figure 6.16, the output voltage of inverter is:

$$v_i = v_g + L_a \frac{di_a}{dt} + i_a R \quad (6.22)$$

After the transform of Laplace, the output current is:

$$i_a(s) = \frac{1}{sL + R} (v_i(s) - v_g(s)) \quad (6.23)$$

Where  $v_i$  is PWM output waveform of the inverter.  $R$  is equivalent resistance for the inductors and circuit.

Since unity power factor control, the command current is:

$$i_a^* = I_a^* \sin \theta_a \quad (6.24)$$

So the command voltage of inverter becomes:

$$v_i^* = (k_p + \frac{k_i}{s})(I_a^* \sin \theta_a - i_a) + v_g \quad (6.25)$$

If no voltage feed-forward, when the grid voltage suddenly increases, the grid connected current will decrease, thus the deviation occurs. Compared to with/without voltage feed-forward control methods, the grid voltage feed-forward compensation can work more effectively during disturbance. So in the current error compensation part, the feed-forward grid voltage is used to generate voltage references for the PWM, thus the disturbance due to grid harmonics can be suppressed well.

The system open loop transfer function is:

$$G(s) = \frac{V_{in}}{2(RCLs^2 + Ls + R)} \quad (6.26)$$

The PI transfer function is:

$$G_{PI}(s) = k_p + \frac{k_i}{s} \quad (6.27)$$

Based on the following parameters,

Input voltage is 230 V,

Inductor is 1 mF,

Capacitor is 50 uF,

Rresistor is 5 ohm,

$k_p$  is 0.04,  $k_i$  is 60.

With the open loop transfer function, the system bode plot is:

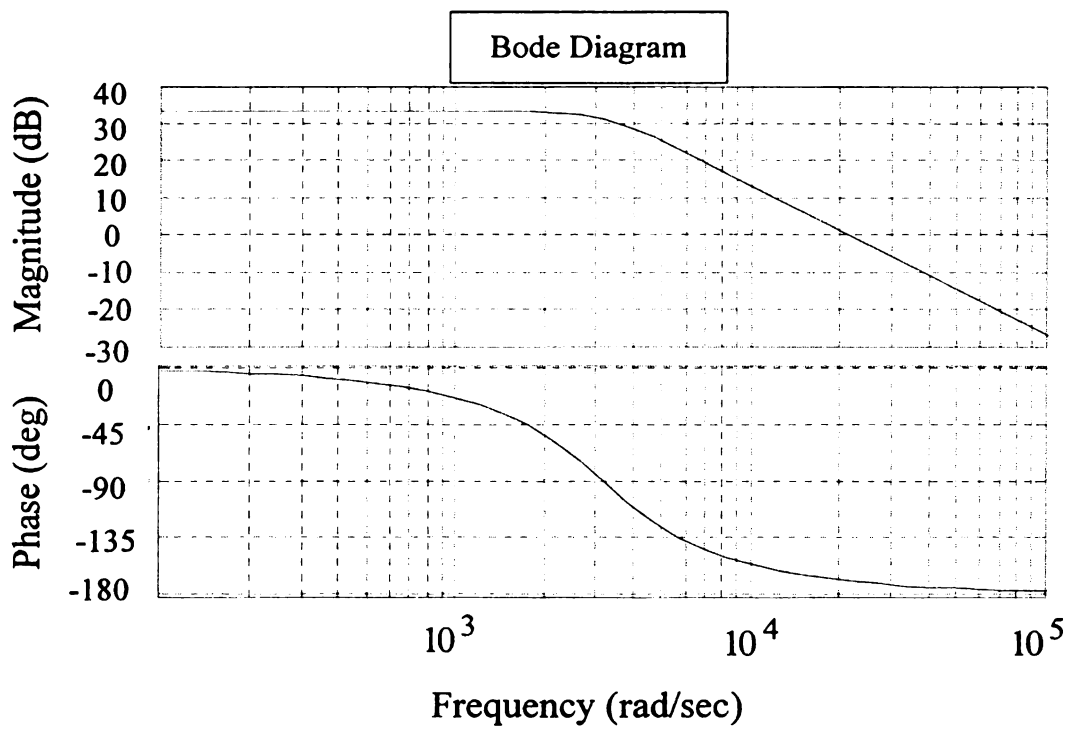


Figure 6.18: Open loop bode plot.

The PI correction bode plot is:

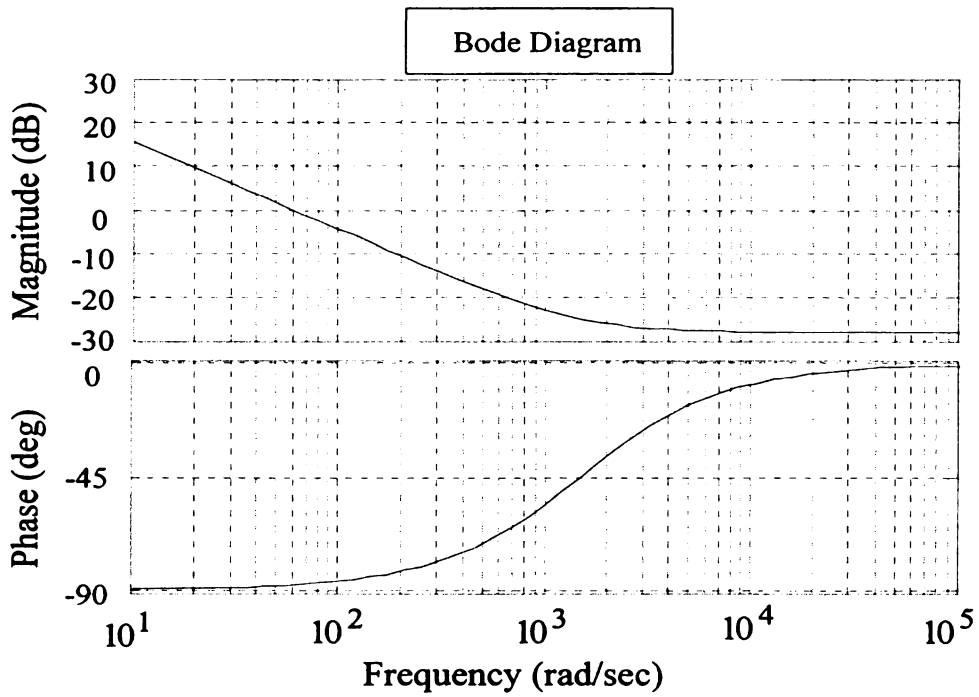


Figure 6.19: PI correction bode plot.

The close loop system bode plot is:

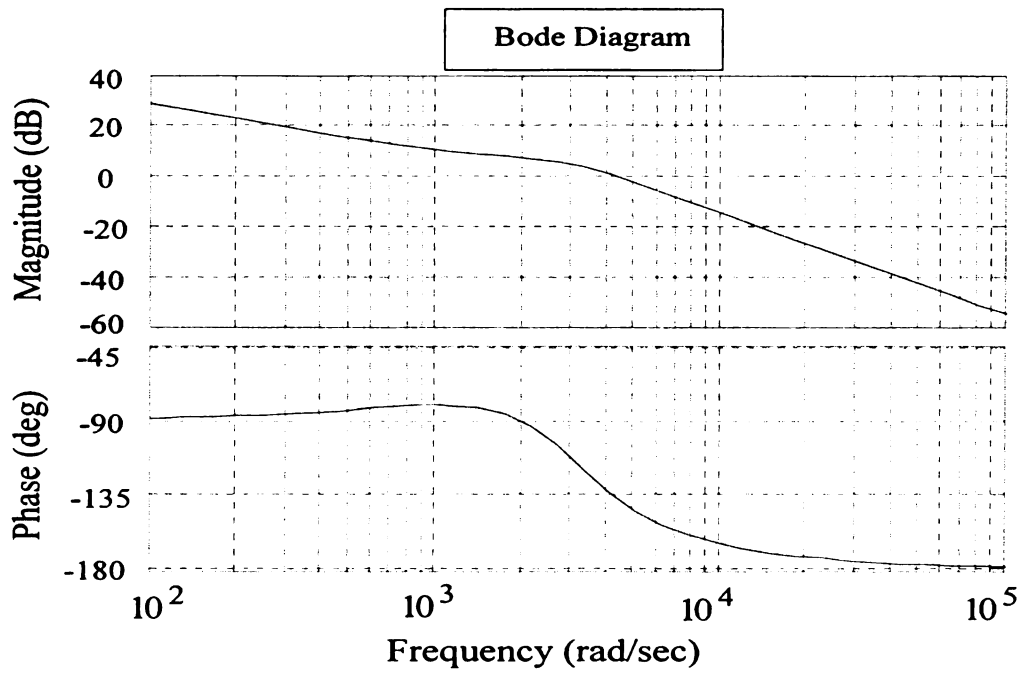


Figure 6.20: Close loop system bode plot.

The inverter feeds the sinusoidal current into the utility grid which its frequency and phase is the same as utility grid. Thus, the unity power factor is realized. By regulating the current loop parameters, tracking speed and tracking error can both be modified [89].

From above, the grid-connected inverter with high power factor is realized and the configuration of the system is very simple. This control configuration has higher efficiency, good performance, and reliability because of its single stage. Also the power can be controlled well for its voltage forward feedback.

For the output filter, there are L filters, LC filters, and LCL filters. Among these three types, the LCL filters is a third order filter which is easily to cause the stability problem. The filter inductance is designed by the consideration of the utility grid voltage, the switching frequency, the amplitude of grid connected current. The output grid connected current may be distorted for the small inductance. Otherwise, the power loss on the filter and damping and time-delay will increase also.

#### 6.4.3 Modified P&O MPPT Control

PV inverter operation status will be affected by operation range on the PV curves. Figure 6.21 shows the constant power curves for different values of power. From this figure, it can be seen that there exist two equilibriums for a given power point. When the constant power curve is tangential to the PV I-V curve, the maximum power point is achieved. If the given  $P$  is higher than  $P_{\max}$ , there is no real solution and the

operating point will approach to the short circuit. So there exists the possible two solutions for a given  $P$ .

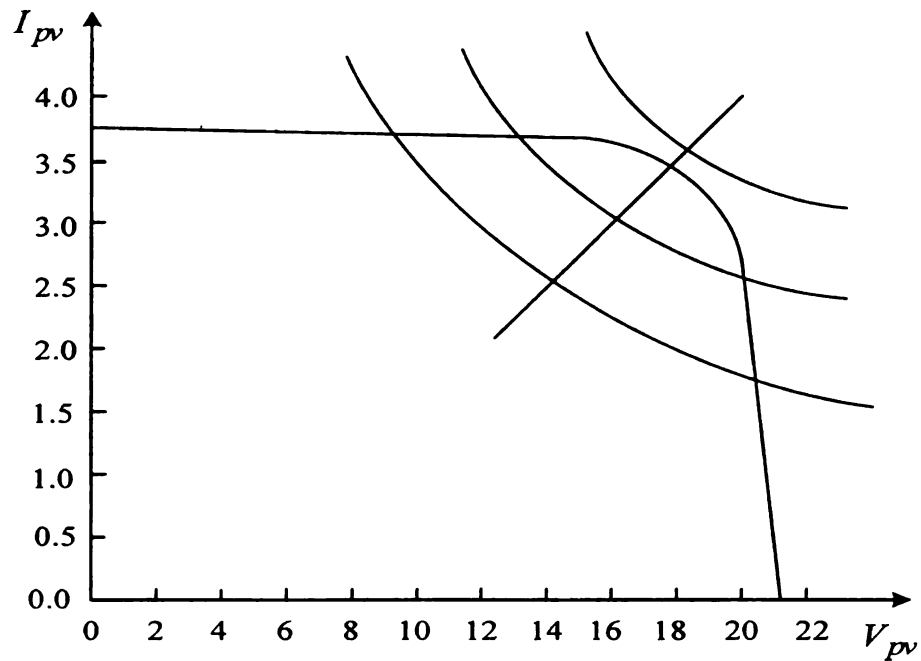


Figure 6.21: PV I-V and constant power curve.

From the Figure 6.22, it can be verified that the solution to the left intersection of constant power curve with I-V curve is unstable; on the contrary, the right side is stable. The voltage would collapse if the operating point is pulled toward to the left side. So the PV inverter should operate on the right side.

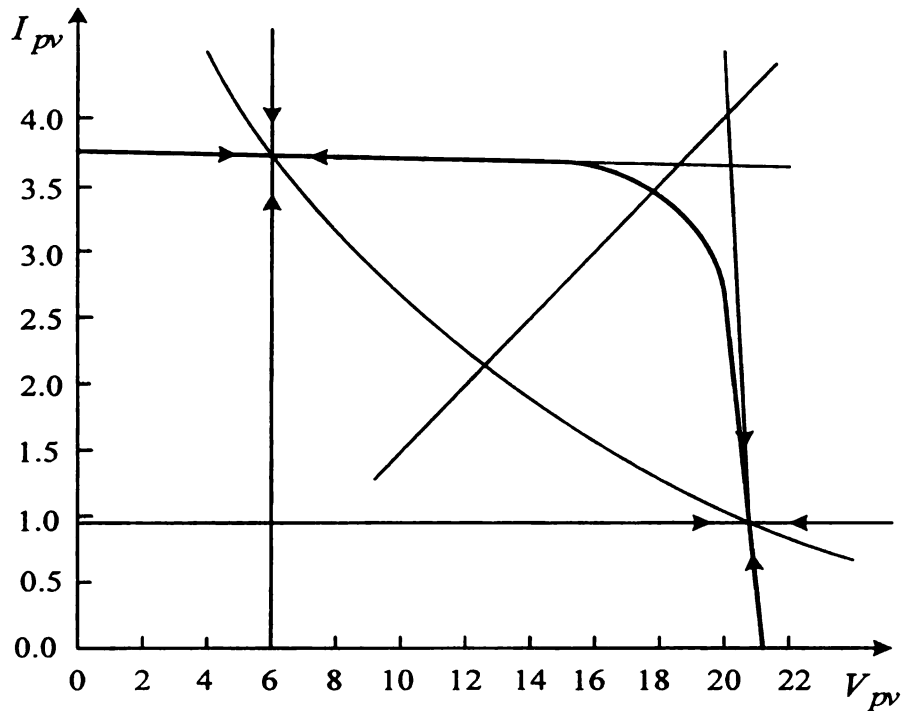


Figure 6.22: PV I-V and constant power curve analysis.

Generally, the PV inverter starts from open circuit condition, then draws the power from the PV panel and at the same time approaches to the maximum power point, finally oscillates around the maximum power point.

Since the proposed Z-Source based PCS is directly connected to the grid, the PCS will be controlled to transfer maximum power from the PV array to the grid all the time. Because of nonlinear characteristic of PV models, the maximum power can not be achieved by directly connecting the PV models. Tracking of the MPP must be used to effectively get the maximum output power. Thereby, many researches of the MPPT have been done [7]-[10]. There have been perturbation and observation method, the incremental conductance method, and the hill climbing method, etc. Here a simple power feedback method can be used for Z-Source based PCS to achieve MPPT as shown

in Figure 6.23. The power can be measured and used as feedback. The PV modules' voltage can be regulated to an optimal point, which presents the maximum power.

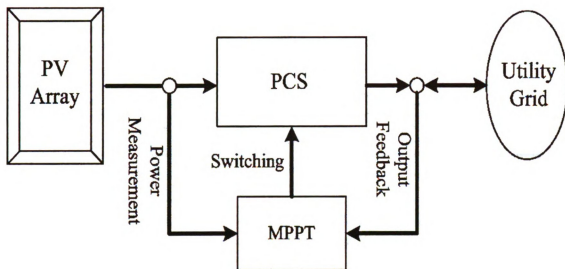


Figure 6.23: The block diagram of the MPPT control.

In this thesis, the modified P&O MPPT method was implemented. Figure 6.24 shows the modified P&O MPPT method.

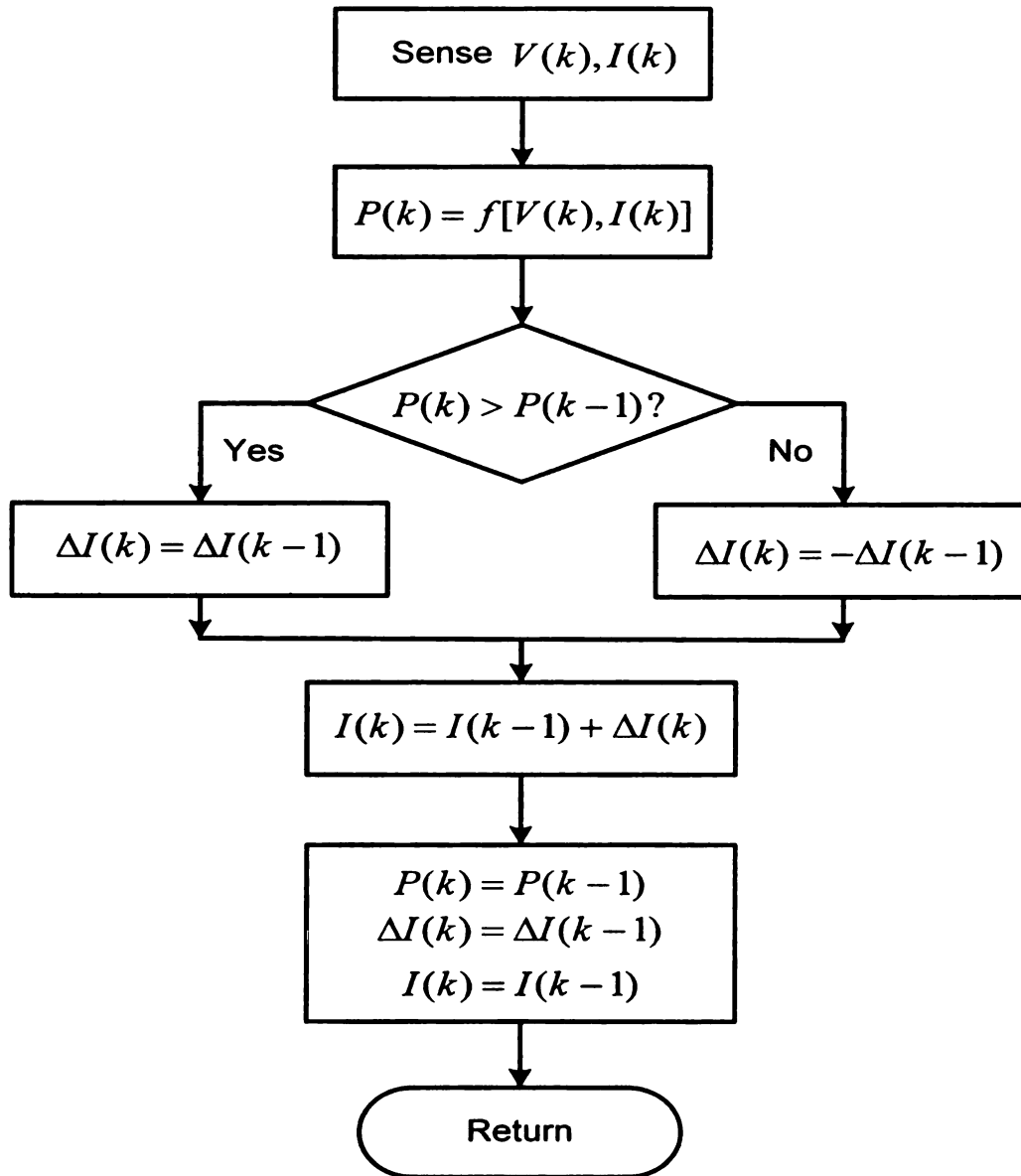


Figure 6.24: The modified P&O MPPT method.

## 6. 5. Hardware And Software Implementation

### 6.5.1 Hardware Implementation Of System Setup

Testing of the 10 kW Z-Source inverter began with low power operation while verifying the stable, safe operation of the inverters. The input power was supplied from

a PV simulator. This allows for the complete control of the input parameters, independent of weather conditions, which is necessary to demonstrate the inverter performance over a wide range of normal and fault conditions.

The following equipments were utilized in the testing of the whole system:

- Rex manufacture Transformer 1, 10 kVA, three-phase, 230 V Delta to 260/460 V Wye.
- Sylvania Transformer 2, 11 kVA, three-phase, 460 V Delta to 460 V WYE.
- Powerstat Variac 1, 10kVA, three-phase, 0-240V.
- Powerstat Variac 2, 10kVA, three-phase, 0-280V.
- Z-Source inverter, 10 kW.
- DC-DC converter, 10kW.
- Rectifier bridge, three-phase, 60A.
- Three-phase grid, AC power source, 208 V.
- Circuit breaker, three-phase, 30 A, 20 HP.
- LEM current sensors, LA 205S.
- LEM voltage sensors, LV 25.
- Inductors, capacitors, and resistor bank.
- Tek TDS 7054 Oscilloscope.
- Tek AM 503B current probe amplifier.
- Tek TDS 2014 Oscilloscope,
- Fluke Voltmeters.

Partial of the equipments are listed in the appendix 2.

## 6.5.2 Hardware Of Control Unit

The control unit of the system consists of DSP boards, three current sensors, four voltage sensors, gate drive boards, and power supplies.

The universal DSP control board shown in Figure 6.25 was developed in MSU Power Electronics and Motor Drives Laboratory. It is based on TMS320LF2407A DSP from Texas Instrument (TI). The board was designed to fit controls for all kinds of inverter and converters. To maximize the control possibility of the board, a Xilinx CPLD is used in series with the DSP chip to expand the logical calculation capability and available I/O numbers. To enable feedback control, the board also includes the analog signal processing circuits for the analog input channels of ADC converter.

The main features of the board are summarized as following:

- LF240F operating at 40 MIPS with 64K words of zero wait state memory for debugging or data stored
- 16 channels Analog to Digital Conversion with signal processing circuits
- Dual event managers multiple PWM and capture channels on chip
- On chip UART with RS232 Drivers, 485 and CAN drivers
- 32K words of on chip Flash ROM
- SPI interface data memory for parameter stored
- On board IEEE 1149.1 JTAG Connection for Optional Emulation
- 15V, -15V, and 5V power input, (onboard 3.3 volt regulators)
- Expansion Connectors (data, address, I/O, control and PWM out signals)
- Xilinx CPLD (XL95288-10TQ208) providing many control or out signals

The ADC module in 2407A chip provides a flexible interface with 16 channels to event managers A and B. The ADC interface is built through a fast, 10 bit ADC module with total conversion time of 500 ns. Since the ADC has a resolution of only 10 bits, while the registers of the timer are 16 bits, scaling has to be done for result registers ADCFIFOs before the values in them involve calculations. This is realized by shifting the ADCFIFO register result to the right.

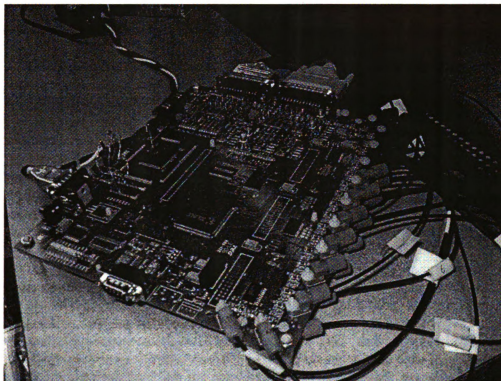


Figure 6.25: Universal DSP 2407A board.

The DSP chip communicated with the program in the computer named Code Composer Studio. Code Composer Studio interfaced to a JTAG emulator pod, which was connected to the DSP. The JTAG emulator allowed for incremental stepping of the control code for eased debugging. The JTAG emulator was also the way to download the program to the DSP chip. The structure of the control system is shown in Figure

6.26. The control system is isolated from the power stage by using plastic optical fiber and isolated sensors.

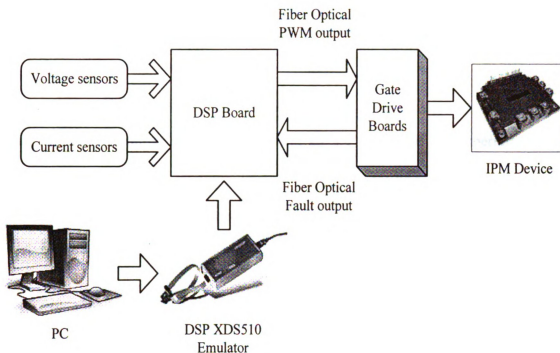


Figure 6.26: Control Unit diagrams.

With the advantage of DSP technologies for power electronics applications, analog feedback and status sensors are fed directly into the DSP and multiple PWM outputs directly provide the drive logic for the converter and inverter power switches.

The PWM controller maintained the output current waveforms within the performance specification requirements for THD and unity power factor.

### 6.5.3 Software Implementation

As mentioned above, the software environment is code composer studio for DSP, and Xilinx for CPLD. For code composer studio, it has the features [90, 91]:

- Integrated editor, debugger, profiler and project manager
- Probe points connected to the file I/O, graphical display
- Fully integrated Code Wright Editor
- Source code debugger common interface for both simulator and emulator targets
- DSP/BIOS Host tooling support

In the code composer studio environment, all the DSP code for experiment were developed and written in assembly language. In the XILINX environment, all the CPLD code was developed and written in ABEL language.

The control of the DSP is composed of an initialization routine followed by periodic interrupts triggered by an internal timer. These interrupts occur once per switching cycle and set the reference. This reference is then sent to the PWM modulator on the DSP so that it can be transmitted over the optical fiber. A flow chart describing the operation of the interrupt is shown in Figure 6.27. The system control flowchart is shown in Figure 6.28.

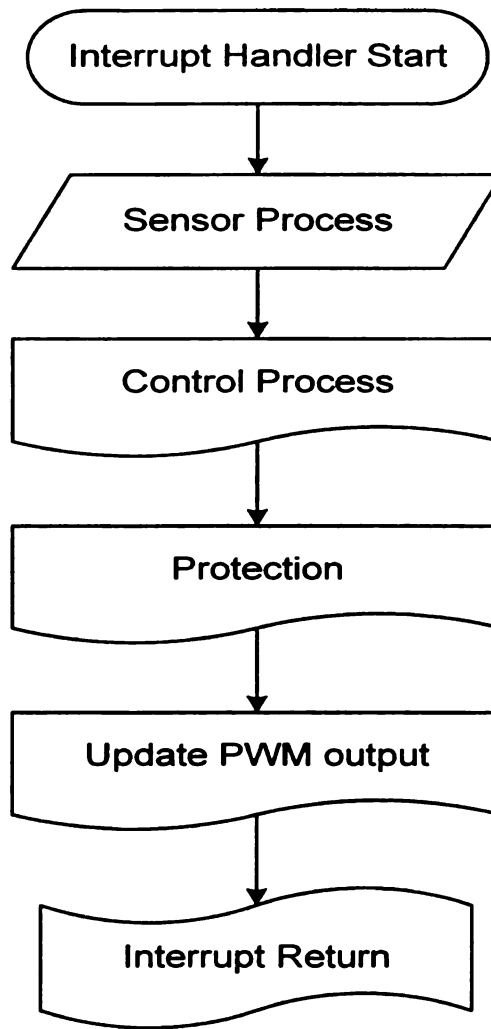


Figure 6.27: Interrupt handler flow chart.

Figure 6.28: Flowchart of DSP code.

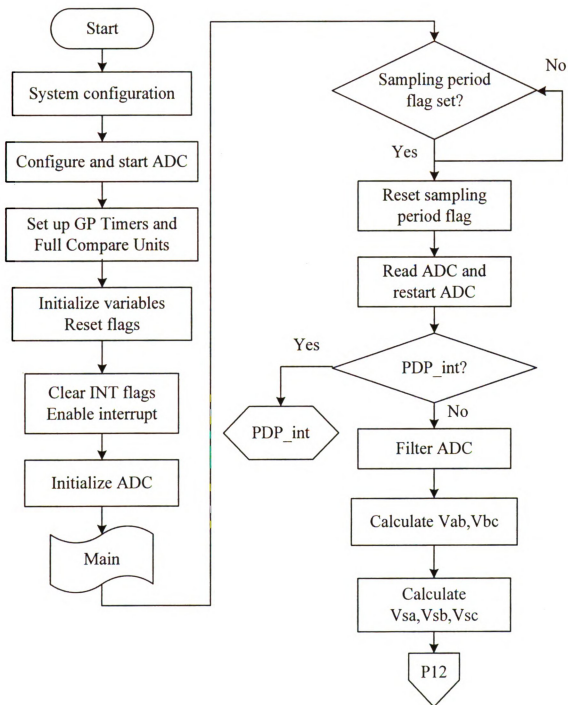
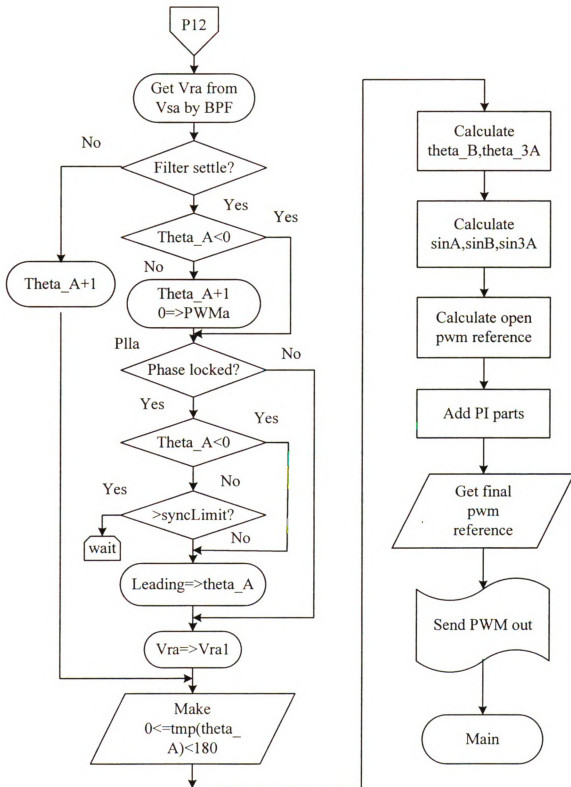


Figure 6.28 continue:



All the PWM generated from DSP need be controlled in logic before sending out to the gate drive board. Figure 6.29 shows the CPLD control block diagram.

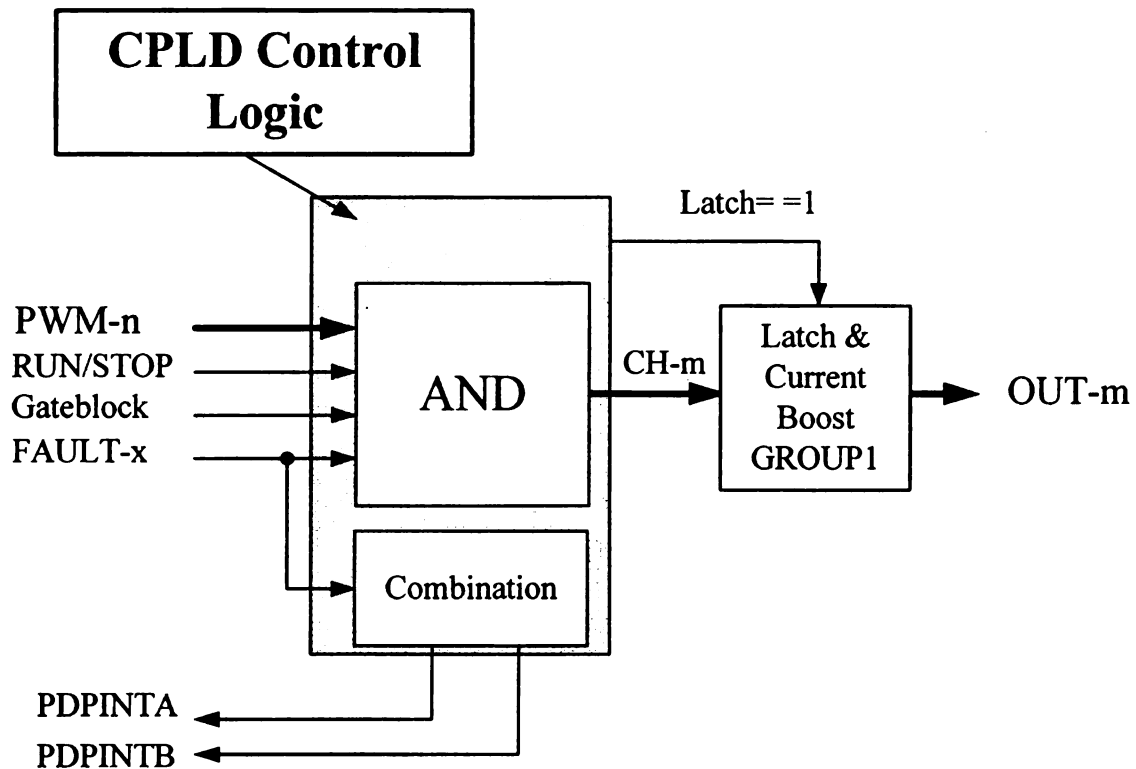


Figure 6.29: CPLD control block.

Also, all the fault protections are implemented and updated in the system.

Inside the IPM module itself, it has:

- Over current protection
- Over temperature protection
- And UVLO protections

Besides these protections, the following protections were implemented through DSP and CPLD:

- Z-Source inverter dc over voltage protection
- Z-Source inverter inductor over current protection

- Z-Source inverter capacitor over voltage protection
- Inverter output current protection

The fault signals will be sent to XILINX CPLD chip, then the output will be shut down, and the protection signal is fed back to the DSP board. At the same time, the LED which indicates the fault condition will light on instantaneously.

## 6. 6. Simulation and Experiment Results

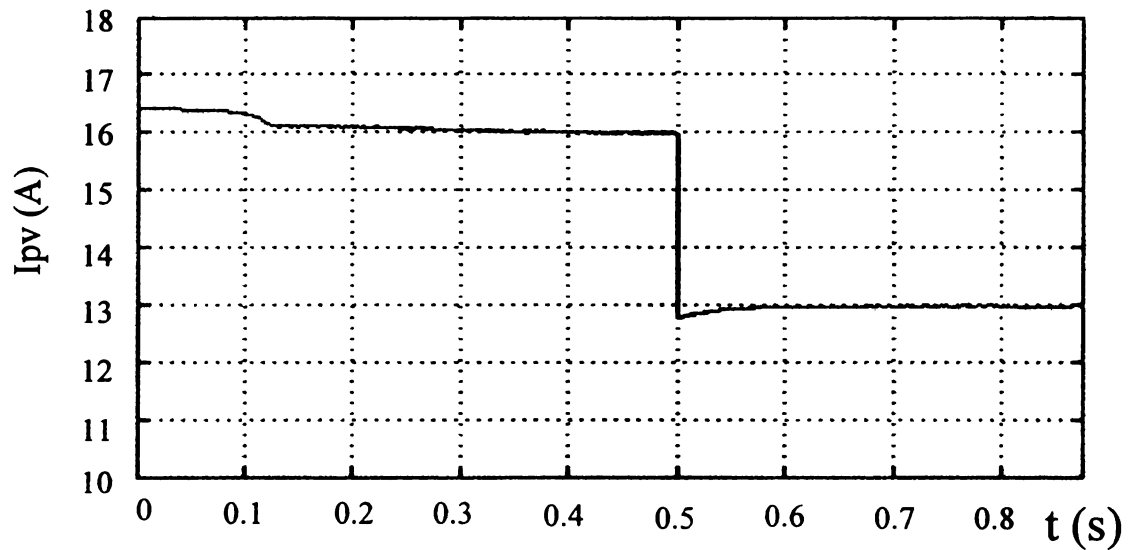
To prove the proposed system, the simulation and experiment are both performed based on the PV curves shown before. The maximum power is achieved when PV array voltage approaches to 330 V. The experiment hardware of the Z-Source inverter and DSP control parts are shown in appendix 2. In the crossed LC network, the inductor is 1  $mH$ , and the capacitor is 1.3  $mF$ . The system switching frequency is 10 kHz. The Z-Source inverter is connected to the grid with 60 Hz frequency, 208 V line to line voltages.

The Z-Source PV inverter can also work as manual mode, which means the inverter can be tested intended for maintenance and debug test function, to provide with manual control of basic inverter function. In this mode, one adjustable meter on the DSP board is available to adjust the inverter power level. The manual mode was utilized during the testing of inverter in order to maintain operating conditions independent of the MPPT circuit, and to create fault conditions. The output current was adjusted from 5% to 100% of rated output current power while the input varied from the specified ranges.

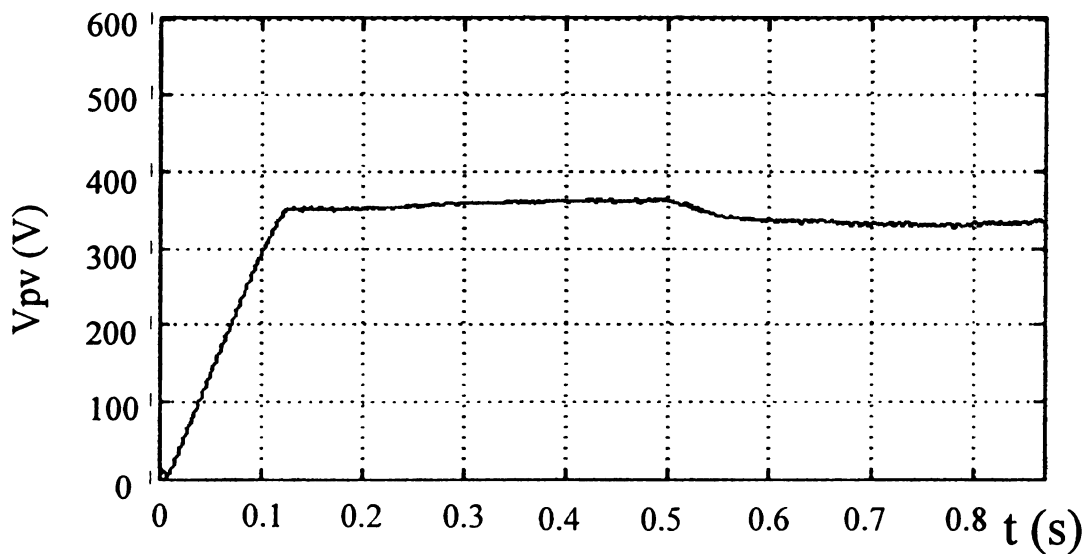
The simulation of the whole system is performed with PSIM and Matlab software. Figure 6.30 shows the PV output current, voltage and power when irradiation changes

from  $1000 \text{ W/m}^2$  to  $800 \text{ W/m}^2$ . Figure 6.31 and Figure 6.32 shows the grid line to line voltage and Z-Source inverter line to line voltage.

Figure 6.30: PV output characteristic during irradiation change.

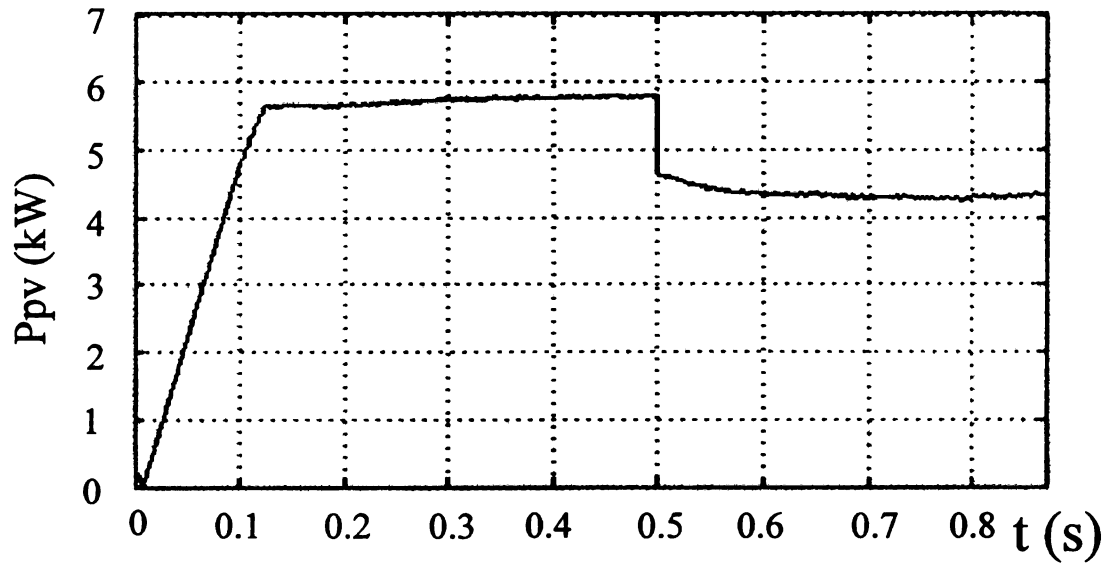


(a). PV array output current.



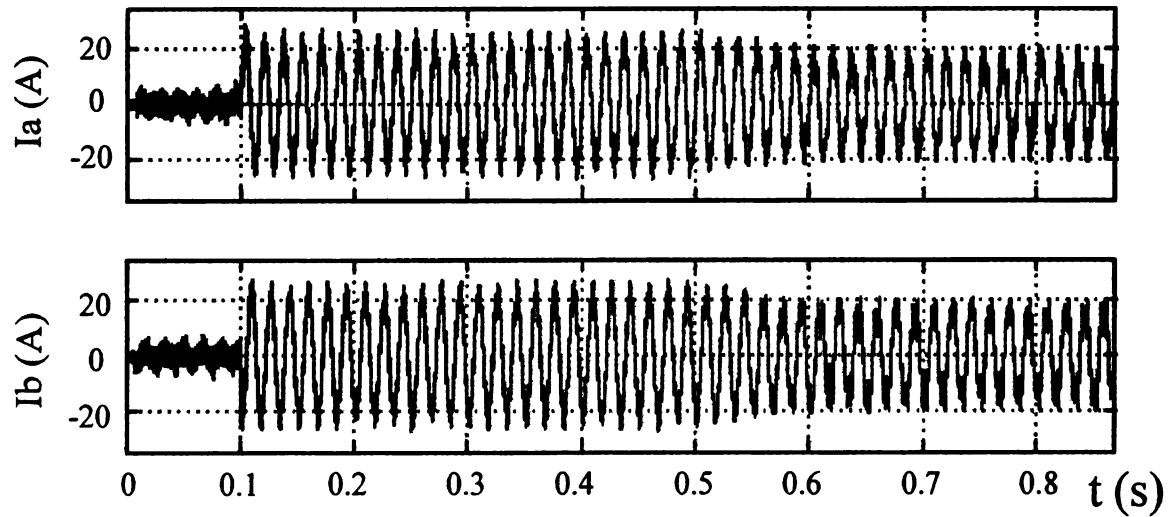
(b). PV array output voltage.

Figure 6.30 continues:



(c). PV array output power.

Figure 6.31: The grid connected Z-Source inverter output current.



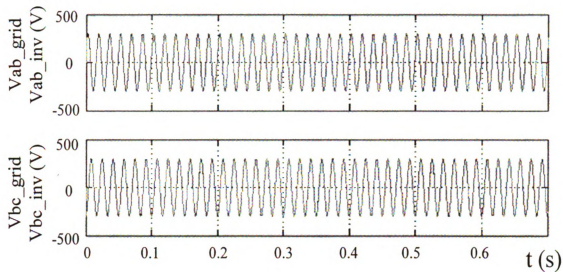


Figure 6.32: The grid line to line voltage and Z-Source inverter line to line voltage.

For PV voltage changes from 230 V to 400 V, the Z-Source inverter can work continuously and automatic change from boost mode to non-boost mode and vice reverse. The experiment results were recorded every 10 volts difference as the following Figure 6.33.

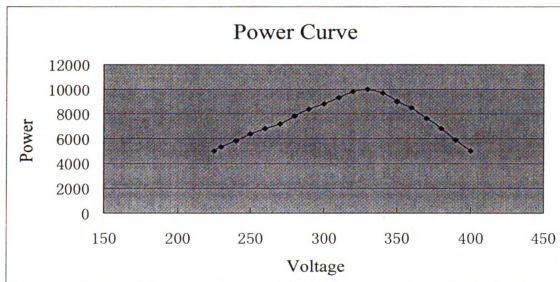
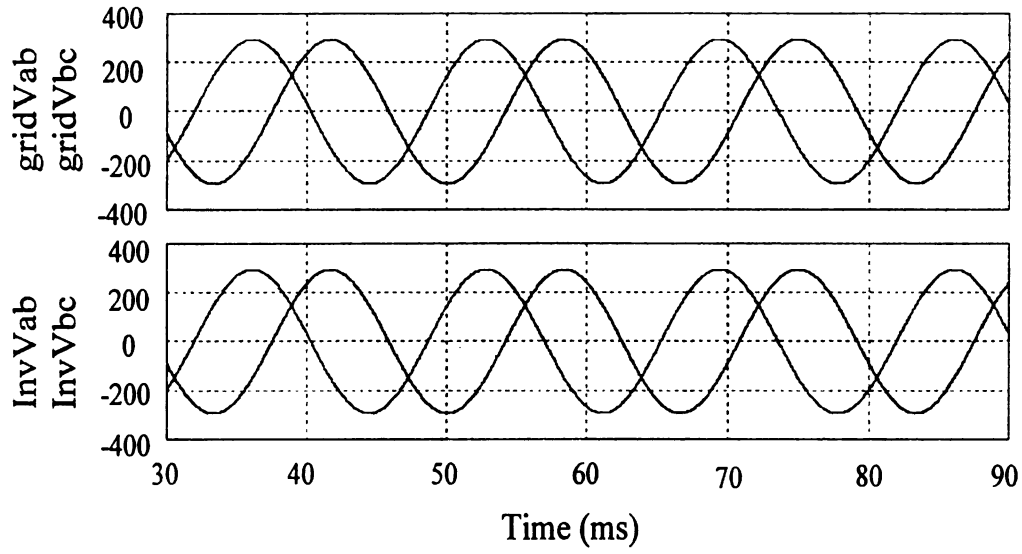


Figure 6.33: The experiment results of power curve changed with voltage.

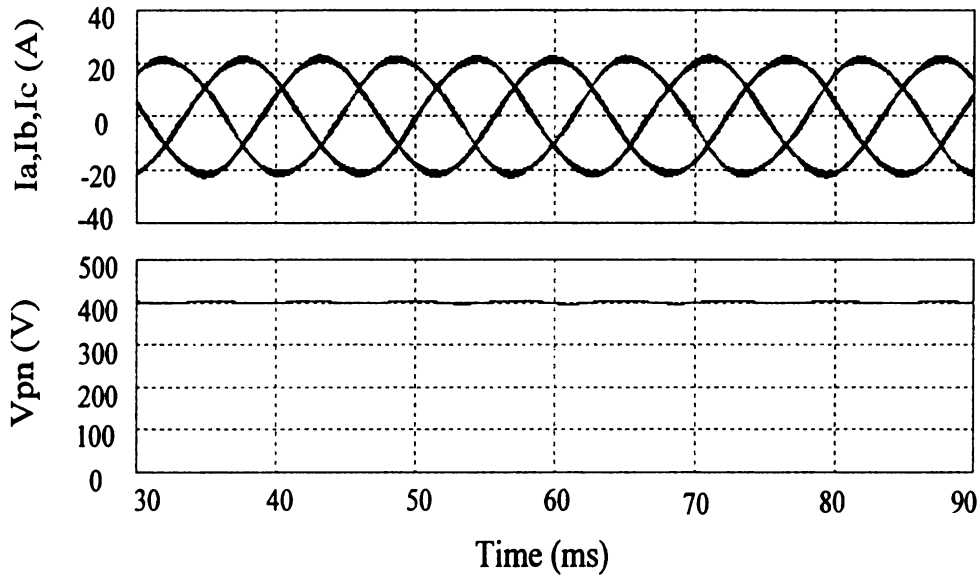
Figure 6.34 shows the results when PV voltage is around 400 V. Figure 6.34 (a) shows the grid line to line voltage and Z-Source inverter line to line voltage after filter. These two waveforms should be the same due to PCC. Figure 6.34 (b) shows the inverter output current and Z-source inverter PN voltage. Because the PV voltage is high enough, the shoot through is not needed. Figure 6.35 shows the experiment result for the same condition of above simulation conditions. From the figure, it can be seen that the inverter line to line voltage after filter is exact as grid line to line voltage sinusoidal. Also, the output current is as desired value and waveform, the unity power factor can be achieved finally. The experiment result consists with the simulation results well.

Figure 6.36 (a) shows the grid line to line voltage and Z-Source inverter line to line voltage after filter. Figure 6.36 (b) shows the inverter output current and Z-source inverter PN voltage. Figure 6.37 shows the experiment result. At this stage, the maximum power is around 10 kW; the current injected to the grid is around 40 A peak value just as shown in Figure 6.36.

When the PV voltage is lower, the shoot through is utilized to ensure the exact output values. Also, Figure 6.38 and Figure 6.39 both confirm the analysis well.



(a). Grid line to line voltage and Z-Source inverter line to line voltage after filter.



(b). Z-source inverter output current and PN voltage.

Figure 6.34: Simulation results of  $V_{pv}$  is around 400 V.

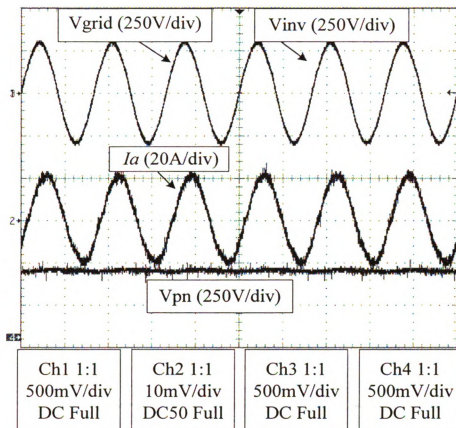
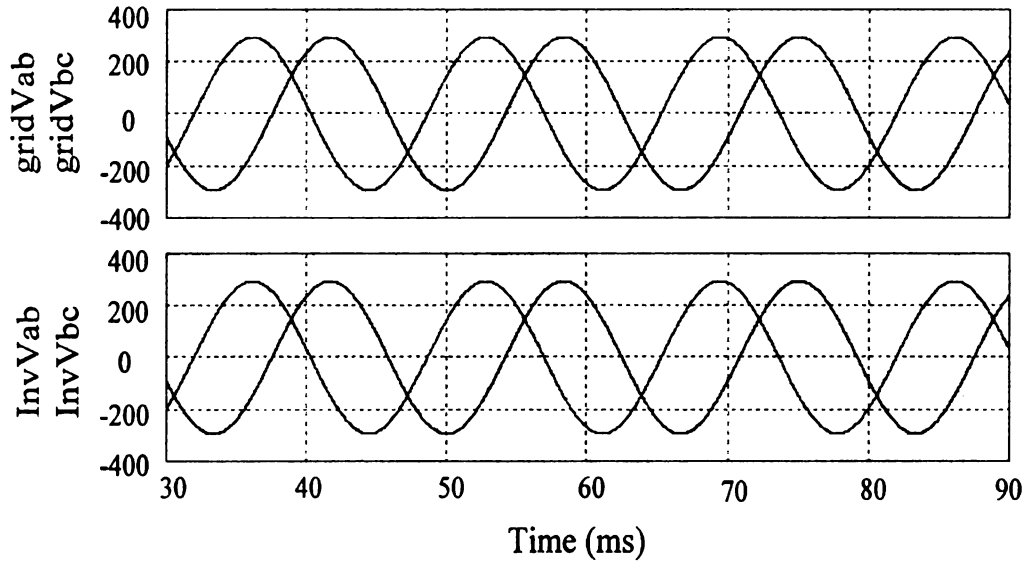
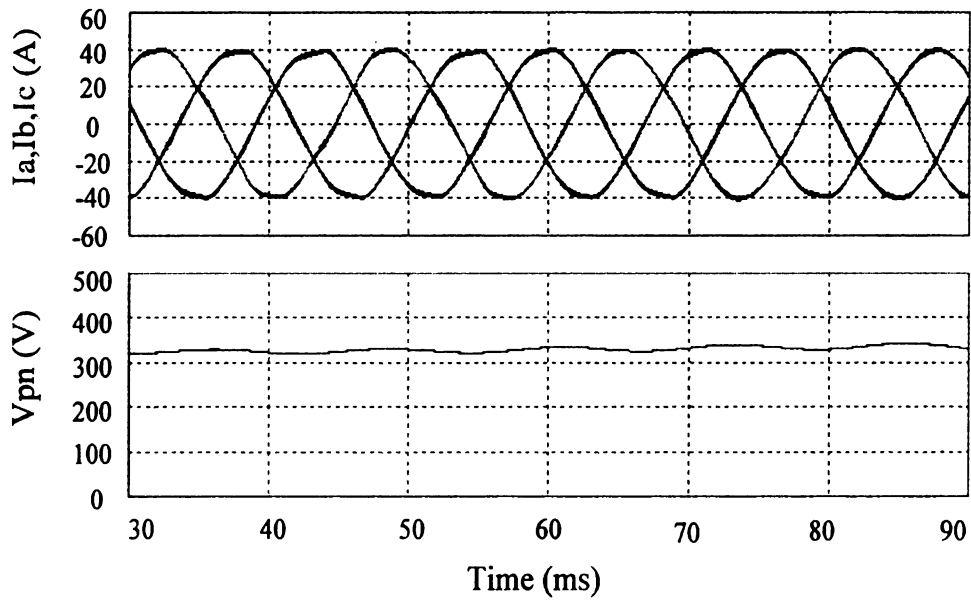


Figure 6.35: Experiment results of  $V_{pv}$  is around 400 V.



(a). Grid line to line voltage and Z-Source inverter line to line voltage after filter.



(b). Z-source inverter output current and PN voltage.

Figure 6.36: Simulation results of  $V_{pv}$  is around 330 V.

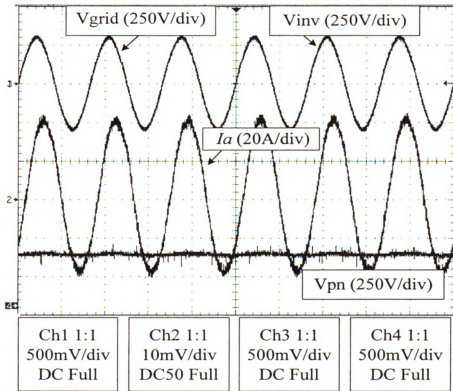
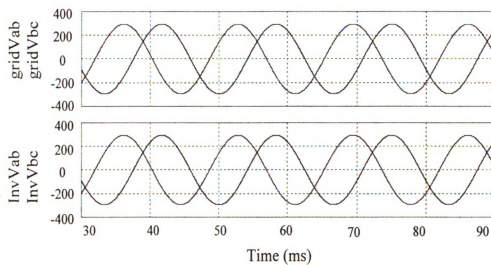
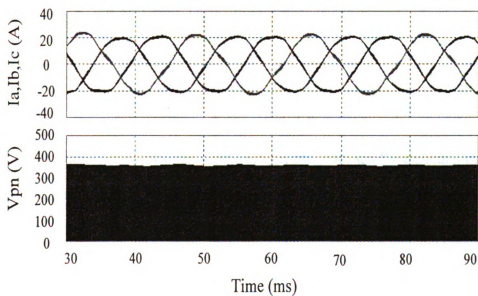


Figure 6.37: Experiment results of  $V_{pv}$  is around 330 V.



(a). Grid line to line voltage and Z-Source inverter line to line voltage after filter.



(b). Z-source inverter output current and PN voltage.

Figure 6.38: Simulation results of  $V_{PV}$  is around 230 V.

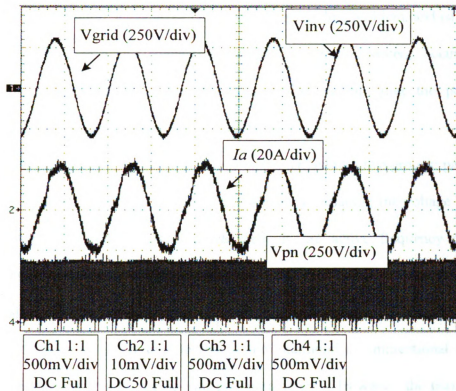


Figure 6.39: Experiment results of  $V_{pv}$  is around 230 V.

From the above results, it can be concluded that the simulation and experimental results both show that at different input voltage, the proposed PV system's output line to line voltage maintained at 208 V RMS, the current injected to the grid is sinusoidal without distortion, also unity power factor is realized. The basic principle of the proposed system was verified very well.

## 6. 7. PCS Requirements And Standards

Grid-connected PV inverter systems should handle the need to perform output control and safety disconnecting or stop of the inverter if any failure mode happens. The major

failure modes of a grid connected PV system include loss of mains protection, over voltage protection, galvanic isolation, system grounding problem, and islanding.

Islanding of a grid connected distributed generation system, occurs when the DG continues to energize a portion of the utility system after the portion has been disconnected from the main utility grid [95].

Islanding detection methods can be characterized into two groups: passive and active. Passive methods include detecting the frequency variation, the voltage phase jump, and the three-phase drop. The active methods are active frequency drift, impedance measurement, and reactive power fluctuation. No matter which islanding method is used, there is a dead range for the islanding operations. It is not difficult to detect islanding, and it is possible to reduce the likelihood of unintentional islanding almost completely by monitoring several grid parameters. However, the maximum allowable time that an inverter may continue to work after the grid has been switched off, together with suitable test methods; need to be established before common international guidelines can be reached [96].

There are many standards for PV PCS systems to comply with, such as IEEE Std. 929-2000 (Recommended Practice for Utility Interface of Photovoltaic Systems), UL1741 (Standard for Static Inverters and Charger Controllers for Use in Photovoltaic Power Systems), IEEE Std. 519 (Recommended Practices and Requirements for Harmonic Control in Electrical Power Systems), 1999 National Electric Code (NFP A 70), IEEE Std. 1374-1998 (Guide for Terrestrial Photovoltaic Power System Safety), and related ANSI and FCC standards.

In addition, all PCS topology should include a blocking diode, thus to prevent reverse currents. The diodes should have a voltage and current ratings at least twice the open-circuit voltage and short-circuit ratings of the source circuits.

## 6. 8. Conclusions

Utility connected PV power systems on residential and commercial buildings are likely to become more important in alternative energy generation for the near future. This chapter presented a new grid-connected PV power conditioning system based on Z-Source inverter. The proposed system realizes the boost and inversion with maximum power tracking in one single power stage, thus minimizing the size and cost.

The main elements in the control structure are the synchronization algorithm based on PLL, inverter current controller with the power feed-forward and PI controller. A PLL structure is used to ensure the current to synchronize with the grid. The control structure has the following advantages:

- High reliability, high immunity
- Lower harmonic distortion
- High efficiency

With the proposed control method, the system has low output distortion and unity power factor. The simplicity and good performance of the proposed system make it a great candidate for grid-connected PV based generation.

## CHAPTER 7. CONCLUSIONS

### 7. 1. Summary Of Circuit Topologies And Their Suited Applications

In PV world market, grid connected PV system has a large portion in the all PV systems. Grid connected system is less expensive if the grid is used as storage instead of batteries. In off-grid PV system, batteries cost up to 20% of the whole system. If backup power is not required, a grid connected system does not need batteries and can get the excess energy from the PV array. For grid connected PV system, there can be summarized to three types: central inverter, string inverter, and module integrated inverter. Table 7.1 shows different specifications of them. Table 7.2 shows summary of different inverter topology.

From previous works, the single stage large central inverter is not a good choice, the input voltage must be high to provide to inverter. For ac modules and cells, the dual stage inverter is much better. It is effective to use HFT in large systems to avoid resonance. Grounding on input and output terminals also helps on the resonance. LFT CSIs are applicable for low power ac module applications; HFT VSIs are applicable for low power and high power systems, the ac module, the string, etc.

Table 7.1: Summary of central, string, and module integrated inverter.

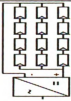
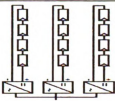
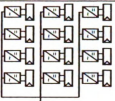
Type	Central Inverter	String Inverter	Module Integrated Inverter
Circuit Topology			
Dc bus	high voltage, high current	high voltage, low current	low voltage, low current
advantages and disadvantages	higher power losses, mismatch losses, nonflexible design, higher current harmonics, lower power quality	separate MPPT for each string, higher overall efficiency than central inverter	higher installation cost, no mismatch losses, individual MPPT, flexible design for extendency, higher efficiency
Applications	large scale PV system(>5kW), three phase	Medium scale PV system(2-3kW), single phase	Small scale PV system(<2kW), single phase

Table 7.2: Summary of the inverter topologies.

Inverter Type		Topology	Characteristic
Inverter with Transformer	dc/ac with LFT		line frequency transformer, low switching frequency, large transformer volume
	dc/ac with dc/dc(HFT)		high frequency transformer, small transformer volume
	flyback inverter		no dc/dc converter, less component, low cost
Transformer-less Inverter	single stage dc/ac		no boost stage, need required PV voltage, has a higher efficiency
	dc/ac with dc/dc		first stage is dc/dc boost converter, the second stage is full bridge dc/ac.
	dc/ac with bi-directional switches		lower output current ripple, lower switching frequency
	Z-Source inverter		can have shoot through, higher inverter reliability, less component, small size, low cost
	single stage half bridge with dc/ac		higher device rating voltage, lower switching frequency
Single phase	Single phase three wire dc/ac		6 switches for split phase, suitable for single phase three wires residential power system
Three phase	three phase three wire dc/ac		suited for three phase three wires power system, applicable to large scale grid connected PV system

## 7. 2. Conclusions

Solar energy is available everywhere. Photovoltaic is a new source of energy where all of the world can participate. So PV power will become an effective contributor for distributed resource applications. Photovoltaic has a lot of benefits for use as a distributed resource including peak demand shaving and improved asset utilization.

As photovoltaic system is one of the most promising alternative energy sources in DG. The power electronics converters based PCS in the PV system now becomes the key point in cost reduction.

This thesis presented a new power conditioning system based on Z-Source inverter for renewable energy sources. The PV system performance depends not only on temperatures and irradiations, but also on maximum power tracking function of PV inverter. So it is important to verify the inverter system also.

This thesis first introduced the basics of PV power system, then summarized all the existing inverter topologies of PCS mainly for PV systems. Then, the Z-Source inverter for split single phase with stand alone application was proposed and implemented. Continually a dc-dc converter based PV simulator was proposed and implemented for test purpose. Finally, a grid-connected Z-Source inverter system with PV simulator system was proposed and implemented.

By utilizing the Z-Source inverter, the volume, the cost, and the switching device count are minimized. Because of the single stage operation, the efficiency of the system can be greatly improved. The reliability can be enhanced greatly due to the shoot through states. With all these advanced features, the Z-Source inverter based

PCS is very promising for renewable energy applications.

### 7.3. Contributions

This thesis has the following contributions which already illustrated in the thesis:

- ◆ Summarized previous PCS topologies for PV power system, helpful for other educations for further research. Also summarized commercial PV inverter features, helpful for applications of industrial engineers.
- ◆ A new split-phase Z-Source inverter based stand-alone residential PV power system has been proposed and implemented. The proposed control strategy suits application well. The simulation and experiment results both consistent with analysis.
- ◆ A new three-phase grid-connected Z-Source inverter system has been proposed and implemented. The proposed harmonic injected, unity power factor current control which also employed modified P&O MPPT method is used for the control strategy. The simulation and experiment results verified the proposed system. The proposed scheme gives a low cost and high quality power conversion for PV power system.
- ◆ A dc-dc converter based PV simulator system is proposed and implemented for test purpose. A new combined control method was applied to realize functions. The experiment results are shown to verify the circuit.
- ◆ The DSP based control unit for Z-source inverter with PV simulator system was realized and tested. All the software parts include DSP code, CPLD code, and lookup tables, are developed and implemented.

- ◆ The proposed topologies and control strategies can not only contribute to PV power system, but also to other renewable energy sources, such as fuel cell, wind power, TEG and so on.

#### 7. 4. Recommended Future Works

Renewable energy is very diverse in resources used and conversion. With the steadily increasing technologies, the PCSs of renewable energy sources are important for DG applications. People are seeking the new topologies to gain much more efficiency. This thesis presented a new power conditioning system based on Z-Source inverter and PV simulator for renewable energy sources. For PV simulator, it is still have margin to improve performance based on hardware and software implementation. For grid interconnected PV Z-Source inverter system, battery can be added as energy storage, also the according control can be studied.

In the future, inverter technology still needs advanced switching components, improved capacitors, and the fewest interconnections, etc. The inverter lifetime has better to be longer than 10 years. The design leads to a high integrated and fewer component trend. Based on advanced technologies, such as DSP, and modular power electronics, more and more new inverter topologies will arise.

# APPENDIX 1. HARMONIC DISTORTION FACTOR OF THE CURRENT RIPPLE

For a single carrier switching period with the load between output phase legs a and b, shown in Fig. A.1.

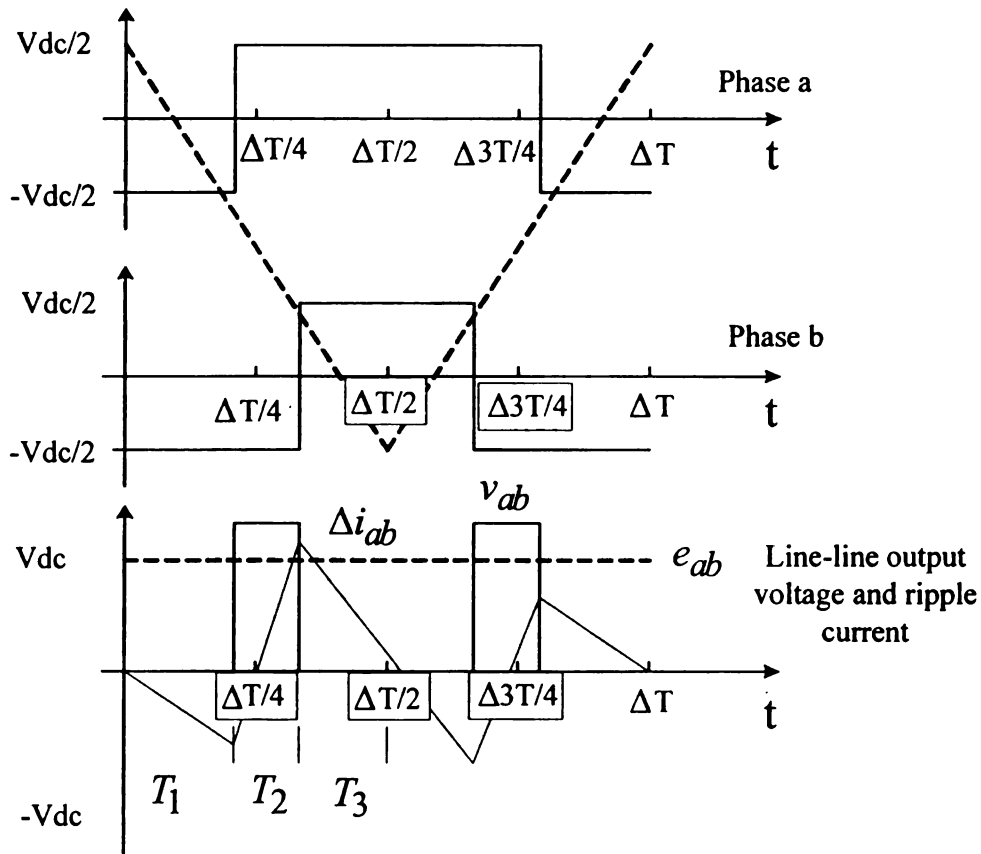


Figure A.1: Ripple current for two phase legs of three-phase inverter.

When  $0 \leq t \leq T_1$ ,

$$\Delta i_{ab} = -\frac{e_{ab}}{L} t \quad (A.1)$$

When  $T_1 \leq t \leq T_1 + T_2$ ,

$$\Delta i_{ab} = \left( \frac{V_{dc} - e_{ab}}{L} \right) (t - T_1) - \frac{e_{ab}}{L} T_1 \quad (\text{A.2})$$

When  $T_1 + T_2 \leq t \leq T_1 + T_2 + T_3$ ,

$$\Delta i_{ab} = \left( \frac{V_{dc} - e_{ab}}{L} \right) T_2 - \frac{e_{ab}}{L} T_1 - \frac{e_{ab}}{L} \left( \frac{\Delta T - T_3}{2} \right) \quad (\text{A.3})$$

Thus, one can obtain

$$\left\langle \Delta i_{ab}^2 \right\rangle = \left( \frac{V_{dc}}{2L} \right)^2 \frac{2}{\Delta T} \left[ \begin{aligned} & \left( \frac{2(e_b - e_a)}{V_{dc}} \right)^2 \int_0^{T_1} t^2 dt + \\ & \left[ \left( \frac{2V_{dc} + 2(e_b - e_a)}{V_{dc}} \right) (t - T_1) \right. \\ & \left. + \left( \frac{2(e_b - e_a)}{V_{dc}} \right) T_1 \right]^2 d(t - T) \\ & \int_0^{T_1} \int_0^{T_2} \left[ \left( \frac{2(e_b - e_a)}{V_{dc}} \right)^2 (t - T_1 - T_2) \right. \\ & \left. + \left( \frac{2V_{dc} + 2(e_b - e_a)}{V_{dc}} \right) T_2 \right. \\ & \left. + \left( \frac{2(e_b - e_a)}{V_{dc}} \right) T_1 \right]^2 d(t - T_1 - T_2) \end{aligned} \right] \quad (\text{A.4})$$

Substitute  $\frac{2e_a}{V_{dc}} = M \cos \theta_0$ ,  $\frac{2e_b}{V_{dc}} = M \cos \left( \theta_0 - \frac{2}{3} \pi \right)$ , thus obtain

$$\Delta i_{ab}^2 = \frac{V_{dc}^2 \Delta T^2}{192L^2} \frac{1}{\pi} \int_{-\pi/3}^{\pi/3} \left\{ \begin{array}{l} \cos^2(\theta + \frac{\pi}{6}) - 3\sqrt{3}M^3 \cos^3(\theta + \frac{\pi}{6}) \\ -\sqrt{3}M^4 \cos(\theta + \frac{\pi}{6}) (\cos^3(\theta - \frac{2\pi}{3})) \\ -\cos^3 \theta \end{array} \right\} d\theta$$

(A.5)

## APPENDIX 2. SOME EXPERIMENT HARDWARES FIGURES



Figure A.2: PV simulator.

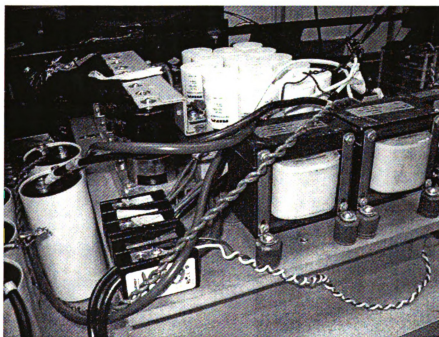


Figure A.3: Z-Source inverter.

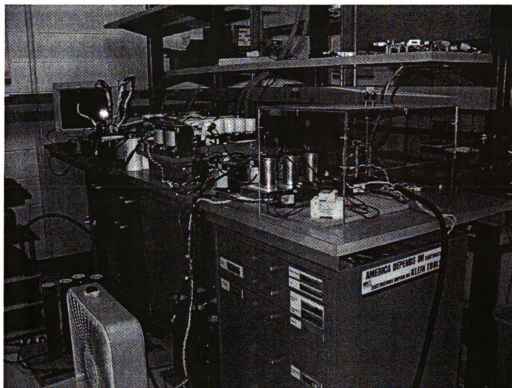


Figure A.4: Part of grid-connected Z-Source inverter with PV simulator system.

## APPENDIX 3. FUNCTIONAL BLOCK DIAGRAM OF 2407A DSP CONTROLLER

Fig. A.5 shows the block diagram of the basic configuration for the LF2407A DSP board. The major interfaces of the board include the target RAM, dual SRAM memory, analog interface, CAN interface, RS 232 interface, 485 interface, SPI data logging interface, analog signals interface, PWM out signal interfaces and other functions.

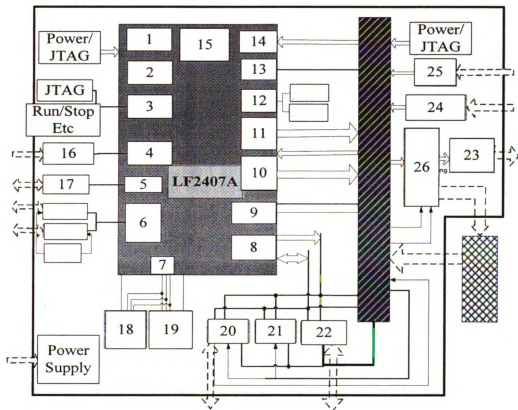


Figure A.5: Functional block diagram of 2407A DSP board

The detailed information is listed below:

1. DRAM 544 Words
2. SRAM 2k Words
3. Other function
4. 10 bit ADC converter
5. Can

6. SCI
7. SPI
8. External memory
9. DSP core
10. Event manager B
11. Event manager A
12. PLL/Reset circuit
13. Other I/O
14. CAP/QEP units
15. Flash/ROM 32k Words
16. Analog signal process units
17. Can transistors
18. SPI flash memory
19. Real time clock
20. Ram 4k
21. Pro/data memory space
22. Extending bus connector
23. Switching signals (Fiber Led)
24. Fault signals (Fiber detector)
25. Frequency signals processing circuit
26. Out PWM signals processing circuit

## REFERENCES

- [1]. R. C. Dugan, T. E. McDermott; "Distributed generation", Industry Applications Magazine, IEEE, Volume: 8 Issue: 2, March-April 2002, pp. 19 –25.
- [2]. Calais, M.; Myrzik, J.; Spooner, T.; Agelidis, V.G. "Inverters for single-phase grid connected photovoltaic systems-an overview"Power Electronics Specialists Conference, 2002. pesc 02. 2002 IEEE 33rd Annual, Volume: 4, 23-27 June 2002 Pages: 1995 – 2000.
- [3]. Wu, T.-F.; Chang, C.-H.; Chen, Y.-K.; "A multi-function photovoltaic power supply system with grid-connection and power factor correction features"Power Electronics Specialists Conference, 2000. PESC 00. 2000 IEEE 31st Annual, Volume: 3, 18-23 June 2000 Pages: 1185 - 1190 vol.3.
- [4]. Jin Wang; Peng, F.Z.; Anderson, J.; Joseph, A.; Buffenbarger, R.; "Low cost fuel cell converter system for residential power generation", Power Electronics, IEEE Transactions on, Volume: 19, Issue: 5, Sept. 2004 Pages: 1315 – 1322.
- [5]. F. Z. Peng, "Z-Source Inverter," IEEE Transactions on Industry Applications, Vol. 39, No. 2, pp. 504-510, March/April 2003.
- [6]. Fang Z. Peng, Miaosen Shen, and Zhaoming Qian, "Maximum Boost Control of the Z-Source Inverter", in Conf. Rec. Power Electronics Specialists Conference, 2004. PESC 04. 2004 IEEE 35rd Annual, Volume: 1 Volume 1, pp: 255-260, Jun. 2004.
- [7]. Y. C. Kuo, T. J. Liang, and J. F. Chen, "Novel Maximum-Power-Point-Tracking Controller for Photovoltaic Energy Conversion System," IEEE Transactions on Industrial Electronics, Vol. 48, No. 3, June 2001, pp. 594-601.
- [8]. Weidong Xiao, William G. Dunford, "A Modified Adaptive Hill Climbing MPPT Method for Photovoltaic Power Systems," 35<sup>th</sup> Annual IEEE Power Electronics Specialists Conference, Aachen, Germany, 2004.
- [9]. K.H.Hussein, I.Muta, T.Hoshino and M.Osakada., "Maximum Photovoltaic Power Tracking: an Algorithm for Rapidly Changing Atmospheric Conditions", IEEE Proceeding Generation, Transmission and Distribution, vol.142, pp.59-64, Jan.1995.

- [10]. E.Koutroulis, K.Kalaitzakis and N.C. Voulgaris, "Development of a microcontroller-based, photovoltaic maximum power point tracking control system", IEEE Trans. power Electronics., vol.16, pp. 46-54, Jan.2001.
- [11]. Shen, M.; Joseph, A.; Wang, J.; Peng, F.Z.; Adams, D.J., "Comparison of traditional inverters and Z-Source inverter", in Conf. Rec. of IEEE Power Electronics Specialist Conference, pp.1692-1698, June, 2005.
- [12]. Reference from <http://www.bigfrogmountain.com/solarhistory.htm>.
- [13]. Solar Electric Power, "The US Photovoltaic Industry Roadmap", Prepared by Energetics, Incorporated, Columbia, Maryland, under contract to Sandia National Laboratories.
- [14]. Arnulf Jager-Waldau, "Status of PV research, solar cell production and market implementation in Japan, USA and the European Union".
- [15]. Tadao ISHIKAWA, "Grid-connected photovoltaic power systems: Survey of inverter and related protection equipments".
- [16]. Muhammad H.Rashid, "Power Electronics Handbook".
- [17]. S.Kumar, S.C. Bhattacharya and M. Augustus Leon, "A survey on PV systems and accessories in ASIA".
- [18]. "IEEE Guide for Terrestrial Photovoltaic Power System Safety", the Institute of Electrical and Electronics Engineers, Inc.
- [19]. Yu Chin Qin, Ned Mohan, Russell Bonn, "Status and Needs of Power Electronics for Photovoltaic Inverters: Summary Document".
- [20]. P.Welter, More, "Better, cheaper-the current market survey: Grid connected inverters "(Mehr, besser, billiger-Die aktuelle Marktübersicht, Wechselrichter zur Netzeinspeisung, in German), PHOTON das Solarstrom-Magazin (German solar electricity magazine), No.3, pp. 60-71, May-June 2000.
- [21]. B.Lindgren, Topology for Decentralised Solar Energy Inverters with a Low Voltage AC-Bus, Proceedings of the 8<sup>th</sup> European Conference on Power Electronics and Applications, Lausanne 1999.

- [22]. R.O.Caceres and I.Barbi, "A boost dc-ac converter: Analysis and experimentation," IEEE Trans. Power Electron., vol. 14, pp. 134-141, Jan.1999.
- [23]. N.Vazquez, J. Alvarez, C. Aguilar, and J.Arau, "Analysis and experimental study of the buck, boost and buck-boost inverters," in Proc. IEEE PESC'99, Charleston, SC, June 27-July1 1999, pp. 801-806.
- [24]. N.kasa, T.lida, and H.Iwamoto, "An inverter using buck-boost type chopper circuits for popular small-scal photovoltaic power system," in Proc. IEEE IECON'99, San Jose, CA, Nov.1999, pp. 185-190.
- [25]. S.B.Kjar and F. Blaabjerg, "A novel single stage inverter for the ac-module with reduced low-frequency ripple penetration," in proc. 10<sup>th</sup> EPE European Conf. Power Electronics and Applications, Toulouse, France, Sep. 2-4,2003.
- [26]. C.M. Wang, "A novel single stage full-bridge buck-boost inverter," in Proc. IEEE APEC'03, Miami Beach, FL, Feb.9-13, 2003.
- [27]. M. Nagao and K. Harada, "Power flow of photovoltaic system using buck-boost PWM power inverter," in Proc. IEEE PEDS'97, Singapore, May 26-29, 1997.
- [28]. M.Kusakawa, H. Nagayoshi, K. Kamisako, and K. Kurokawa, "Further improvement of a transformerless, voltage-boosting inverter for ac modules," Solar Energy Mater. Solar Cells, vol.27, pp.379-387, Mar. 2001.
- [29]. T. Boutot and L. Chang, "Development of a single-phase inverter for small wind turbines," in Proc. IEEE Electrical and Computer Engineering Canadien Conf, Waterloo, ON, Canada, May24-28, 1998, pp. 305-308.
- [30]. S. Saha and V. P. Sundarsingh, "Novel grid-connected photovoltaic inverter." Proc. Inst. Elec. Eng., vol.143, pp. 219-224, Mar. 1996.
- [31]. S.Funabiki, T. Tanaka, and T. Nishi, " A new buck-boost-operation-based sinusoidal inverter circuit," in Proc. IEEE PESC'02, Cairns, Australia, June 23-27, 2002, pp. 1624-1629.
- [32]. T. Shimizu, K. Wada, and N. Nakamura, " A flyback-type single phase utility interactive inverter with low-frequency ripple current reduction on the dc input for an

ac photovoltaic module system,” in Proc. IEEE PESC’02, Cairns, Australia, June 23-27, 2002, pp. 1483-1488.

[33]. B. K. Bose, P. M. Szczesny, and R.L. Steigerwald, “Microcomputer control of a residential photovoltaic power conditioning system,” IEEE Trans. Ind. Applical., vol. IA-21, pp.1182-1191, Sep.1985.

[34]. Soeren Baekhoej Kjaer, John K. Pedersen, and Frede Blaabjerg, “A Review of Single-Phase Grid-Connected Inverters for Photovoltaic Modules”, IEEE trans. On Industry Applications, vol. 41, No.5, Sep/Oct 2005.

[35]. Hang-seok Choi, Y.J.Cho, J.D.Kim and B.H. Cho, Grid-connected Photovoltaic Inverter with Zero-current-switching.

[36]. M.Meinhardt, G. Cramer, B. Burger, and P.Zacharias, Multi-string-converter with reduced specific cost and enhanced functionality, Conference Proceedings of the Eurosun 2000, Kopenhagen, Denmark, June 2000.

[37]. Hudson, R.M.; Behnke, M.R.; West, R.; Gonzalez, S.; Ginn, J.; Design considerations for three-phase grid connected photovoltaic inverters, Photovoltaic Specialists Conference, 2002. Conference Record of the Twenty-Ninth IEEE 19-24 May 2002 Page(s):1396–1401.

[38]. S. Saha and V.P. Sundarsingh, “Grid connected photovoltaic inverter as an industrial product,” Eur. Polymer Fed, pp.46-51, Oct. 1996.

[39]. Beristain, J. Bordonau, A. Gilabert, and G. Velasco, “Synthesis and modulation of a single phase dc/ac converter with high frequency isolation in photovoltaic energy applications”, in Proc. IEEE PESC’03, Aca pulco, Mexico, June 15-19, 2003, pp. 1191-1196.

[40]. Naoto Kikuchi, Souichirou Shigeeda, Hiroshi Watanabe, Tokuo Ohnishi, Fumio Harashima, Single Phase Amplitude Modulation Inverter for Utility interactive Photovoltaic System.

[41]. G. R. Walker, and P.C. Sernia, “Cascaded DC-DC Converter Connection of Photovoltaic Modules.

- [42]. Raymond M. Hudson, Michael R. Behnke, Rick West, Sigifredo Gonzalez and Jerry Ginn, Design Considerations for Three-Phase Grid Connected Photovoltaic Inverters.
- [43]. Source: National renewable Energy Laboratory.
- [44]. Source: [www.Ballard.com](http://www.Ballard.com).
- [45]. Source: [www.beaconpower.com](http://www.beaconpower.com).
- [46]. Source: [www.phoenixtec.com](http://www.phoenixtec.com).
- [47]. Source: [www.fronius.com](http://www.fronius.com).
- [48]. Source: [www.studer.com](http://www.studer.com).
- [49]. Source: [www.sma.com](http://www.sma.com).
- [50]. Source: [www.magnetek.com](http://www.magnetek.com).
- [51]. Source: [www.pvpowered.com](http://www.pvpowered.com).
- [52]. Source: [www.solectrlia.com](http://www.solectrlia.com).
- [53]. Source: [www.xantrex.com](http://www.xantrex.com).
- [54]. Kentaro Hayashi, Takae Shimada, Hiroataka Koizumi, Yasuo Ohashi, A novel cascaded PV inverter by utilizing ready-made Ics for Digital Audio Amplifier.
- [55]. Nobuyuki Kasa, Takahiko Iida, and Liang Chen, Flyback Inverter Controlled by Sensorless Current MPPT for Photovoltaic Power System, IEEE transactions on Industrial Electronics, vol. 52, No. 4, August 2005.
- [56]. Dan Ton, and Ward Bower, Summary Report on the DOE High-tech Inverter Workshop.

- [57]. Thomas Surek, Photovoltaics: energy for the new millennium, National Renewable Energy Laboratory, 1999.
- [58]. R. H. Bonn, Developing a next generation PV inverter, 29<sup>th</sup> IEEE Photovoltaic Specialists Conference, pp. 1352-1355, May 2002.
- [59]. M. E. Ropp, Design issues for grid-connected Photovoltaic systems, Georgia Institute of Technology, 1998.
- [60]. R. West, PV Inverter Products Manufacturing and design Improvements for Cost Reduction and Performance Enhancements, NCPV and Solar program Review Meeting 2003.
- [61]. G. Keller, T.Krieger, M. Viotto, and U. Krengel, Module orientated photovoltaic inverters-a comparison of different circuits, IEEE First World Conference on Photovoltaic Energy Conversion, IEEE Photovoltaic Specialists Conference, pp. 929-932, 1994.
- [62]. S H Lloyd, G A Smith, D G Infield, "Design and construction of a modular electronic photovoltaic simulator", Power Electronics and Variable Speed Drives, the Eighth International Conference, 2000.
- [63]. Hiroshi Nagayshi, "I-V curve simulation by multi-module simulator using I-V magnifier circuit", Solar Energy Materials & Solar Cells 82, pp. 159-167, 2004.
- [64]. Olilla, J., "A medium power PV-array simulator with a robust control strategy", Tampere, Finland, Tampere University of Technology, 1995, IEEE, pp.40.
- [65]. Nagayoshi. H., Orio. S., Kono. Y., Nakajima. H., "Novel PV array/module I-V curve simulator circuit", IEEE 29<sup>th</sup> Photovoltaic Specialists Conference, pp.1535-1538, May 2002.
- [66]. IEEE P929/D11, Draft Recommended Practice for Utility Interface of Photovoltaic (PV) Systems, Nov.1999.
- [67]. T.J. Liang, Y. C. Kou, J. R.Chen, "single-stage photovoltaic energy conversion system," proc. Inst. Elect. Eng., vol. 4, no. 148, pp.339-344, 2001.

- [68]. Wu Libo; Zhao Zhengming; Liu Jianzheng; Liu Shu; Yuan Liqiang; "Modified MPPT strategy applied in single-stage grid-connected photovoltaic system," *Electrical Machines and Systems, ICEMS 2005 Proc. of the Eighth International Conference*, vol. 2, pp. 1027-1030, Sept. 2005.
- [69]. Guo-Kiang Hung; Chih-Chang Chang; Chern-Lin Chen; "Automatic phase-shift method for islanding detection of grid connected photovoltaic inverters," *IEEE Transactions on Energy Conversion*, vol. 18, pp. 169-173, March 2003.
- [70]. J.-M. Kwon, K. H. Nam, B.-H. Kwon, "Photovoltaic Power Conditioning System with Line Connection," *Trans. on Industrial Electronics*, vol. 53, no. 4, pp. 1048- 1054, Aug 2006.
- [71]. S.J. Chiang, K.T. Chang, C.Y. Yen, "Residential photovoltaic energy storage system," *Trans. on Industrial Electronics*, vol. 45, no. 3, pp. 385-394, Jun.1998.
- [72]. Jain, S.; Agarwal, V.; "A Single-stage Grid Connected Inverter Topology for Solar PV Systems with Maximum Power Point Tracking," *IEEE Transactions on Power Electronics*, vol. 22, pp. 1928-1940, Sep. 2007.
- [73]. Liserre, M.; Teodorescu, R.; Blaabjerg, F.; "Stability of photovoltaic and wind turbine grid-connected inverters for a large set of grid impedance values," *IEEE Transactions on Power Electronics*, Volume 21, issue 1, Jan. 2006, pages: 263-272.
- [74]. H. Shokrollah Timorabadi, C. Li, and F. P. Dawson, "Application of a Fast Synchronization Systems in Real Time Power System Monitoring and Control", *Proc. of 22<sup>nd</sup> Biennial Symp. On Communications*, Queen's University, Kingston, Canada, pp. 371-376, May, 2004.
- [75]. K. E. Martin, "Precise timing in electric power systems", *Frequency Control Symp.*, 47<sup>th</sup> proc. of IEEE Int'l, pp. 15-22, June, 1993.
- [76]. G. T. Volpe, "A phase-locked loop control system for a synchronous motor", *IEEE Trans. Automat. Contr.*, vol. AC-15, pp.88-95, Feb. 1970.
- [77]. A. J. Goldstein, "Analysis to the phase controlled loop with a sawtooth comparator", *Bell Syst. Tech.*, pp. 603-633, 1963.
- [78]. J. L. Brown, "A digital phase and frequency-sensitive detector", *Proc. IEEE*, vol. 59, pp. 717, Apr. 1971.

- [79]. R. C. E. Thomas, "Frequency comparator performs double duty", EDN, pp. 29-32, Nov., 1970.
- [80]. Chihchiang Hua, Jongrong Lin, and Chihming Shen, "Implementation of a DSP-Controlled Photovoltaic System with Peak Power Tracking," IEEE Transactions on Industrial Electronics, vol. 45, no.1, pp. 99-107, Feb. 1998.
- [81]. D. P. Hohm, M. E. Ropp, "Comparative study of maximum power point tracking algorithms using an experimental, programmable, maximum power point tracking test bed," IEEE 2000, pp.1699-1702.
- [82]. E. Koutroulis, K.Kalaitzakis and N.C. Voulgaris, "Development of a microcontroller based photovoltaic maximum power point tracking control system", IEEE Trans. Power Electronics, vol. 16, pp.46-54, Jan. 2001.
- [83]. Xuanyuan Wang; Kazerani, M.; "A novel maximum power point tracking method for photovoltaic grid-connected inverters," Industrial Electronics Society, 2003, IECON'03, the 29th Annual Conference of the IEEE, Volume 3, 2-6 Nov. 2003. Pages: 2332-2337.
- [84]. Shen,M.; Jin Wang; Joseph, A.; Peng, F. Z.; Tolbert, L. M.; Adams, D. J.; "Maximum constant boost control of the Z-Source inverter," Industry Applications Conference, 2004. 39th IAS Annual Meeting, Conference Record of the 2004 IEEE, Volume 1, 3-7 Oct. 2004.
- [85]. Boost, M. A.; Ziogas, P.D.; "State of the art carrier PWM techniques: a critical evaluation," IEEE Transactions on Industry Applications, vol. 24, pp. 271-280, March-April 1988.
- [86]. Menniti, D.; Picardi, C.; Pinnarelli, A.; Sgro, D.; "Grid-connected inverters for alternative energy sources with a combine voltage and current control strategy," Clean Electrical Power, 2007, ICCEP'07 International Conference, pp. 223-228, 21-23 May 2007.
- [87]. Arruda, L.N., Sliva, S.M., Filho, B.J.C, "PLL structures for utility connected systems," Industry Applications conference, 2001. Thirty-sixty IAS Annual Meeting. Conference Record of the 2001. Volume. 4, pp. 2655-2660, 2001.
- [88]. Da Silva, Sergio A. Oliveira; Tomozaki, Edgar; Novochadlo, Rhodolfo; Antonia, Ernane; Coelho, Alves; "PLL Structures for Utility Connected Systems

under Distorted Utility Conditions,” IEEE Industrial Electronics, IECON 2006-32nd Annual Conference, pp. 2636-2641, Nov. 2006.

[89]. H. Koizumi, T. Mizuno, T. Kaito, Y. Noda, N. Goshima, M. Kawasaki, K. Nagasaka, K. Kurokawa, “A Novel Microcontroller for Grid-Connected Photovoltaic Systems,” Trans. on Industrial Electronics, vol. 53, no. 6, pp. 1889-1897, Dec 2006.

[90]. Code Composer Studio Development Tools v3.3 Getting Started Guide (Rev. H), [www. TI. com](http://www.ti.com).

[91]. Code Composer Studio’s Command Window, [www.TI.com](http://www.TI.com).

[92]. Programmable power supply ALS150V12A for photovoltaics generator simulation. Technical note 402545-E1 and appendices. Ainelec.

[93]. Elgar Solar Array Simulators. [www.elgar.com](http://www.elgar.com).

[94]. F. G. Shinskey, Feedback Controllers for the Process Industries. New York, McGraw-Hill, 1994.

[95]. M.G.Jaboori, M.M.Saied, and A.A. Hanafy, “ A contribution to the simulation and design of photovoltaic systems”, IEEE Trans.Energy Conv., vol 6, pp.401-406, Sep. 1991.

[96]. Chihchiang Hua, Chihming Shen, “Comparative study of peak power tracking techniques for solar storage system”, Applied Power Electronics Conference and Exposition, 1998. APEC '98. Conference Proceedings 1998., Thirteenth Annual, pp. 679-685., vol.2.

[97]. International Energy Agency. Trends in Photovoltaic Applications: Survey Report of Selected IEA Countries.

[98]. P. D. Maycock, “World PV Cell/Module Production”, PV News, Vol. 24, No. 2, Feb. 2005.

[99]. [http://en.wikipedia.org/wiki/Solar\\_cell](http://en.wikipedia.org/wiki/Solar_cell).

[100]. Renewable energy sources, <http://iamest.jrc.it>.

[101]. <http://www.nextenergynews.com/news1/next-energy-news12.19d.html>.